Master's thesis

NTNU
Norwegian University of Science and Technology
Department of Marine Technology

Ina Anda

Static and Dynamic Response Analysis of Salmar Offshore Aquaculture Cage

Master's thesis in Marine Technology
Supervisor: Bernt Johan Leira
June 2019

NTNU
Kunnskap for en bedre verden

Ina Anda

Static and Dynamic Response Analysis of Salmar Offshore Aquaculture Cage

Master's thesis in Marine Technology
Supervisor: Bernt Johan Leira
June 2019

Norwegian University of Science and Technology
Faculty of Engineering
Department of Marine Technology

NTNU
Norwegian University of
Science and Technology

NTNU
Norwegian University of Science and Technology
Department of Marine Technology

Master Thesis, Spring 2019
for
Master Student Ina Anda

Static and Dynamic Response Analysis of Salmar Offshore Aquaculture Cage

Statisk og Dynamisk Responsanalyse av Salmar Offshore Havbruksanlegg

Traditional cages for the purpose of aquaculture are usually located in more or less sheltered areas. However, there is a continuous trend to move these cages to more exposed areas, which implies that completely new structural concepts are required. A pioneering plant has been developed and completed based on the initiative of the company Salmar, and this plant is presently in operation at an ocean site outside Trondheim.

The objective of the present master thesis is to perform dynamic response analysis of the Salmar cage in order to assess the capacity with respect to extreme loading. Furthermore, results from models test which have been performed at the SINTEF Ocean basin are made available to the candidat. A comparison between the measured and calculated dynamic response levels is accordingly also to be addressed.

The candidate should address the following topics:

1. An overview is to be given of different types of aquaculture plants with particular focus on developments during recent years. A description of the loads which are acting on these structures and methods for both static and dynamic response analysis are to be outlined. Furthermore, application of the computer software SIMO/RIFLEX in relation to such analyses is to be elaborated upon.
2. A numerical model of the Salmar offshore cage is to be implemented in SIMO/RIFLEX. Possible simplifications that are required in relation to the numerical model versus the physical structure are to be discussed. By application of this model, an eigenvalue analysis is to be performed. Furthermore, static and dynamic response analyses are to be performed for a limited set of load cases.
3. As a second main item, the measurements from the ocean basin tests at SINTEF are to be considered. Relevant response quantities for comparison with results from the numerical calculations are to be identified (e.g. static and dynamic offset, accelerations and line tension).
4. A comparison between the calculated and measured response levels is to be made. This is to be seen in the light of possible differences between the numerical and physical models. The effect of variation of relevant analysis parameters for the numerical calculations should also be assessed to the extent that time allows.

The work scope may prove to be larger than initially anticipated. Subject to approval from the supervisor, topics may be deleted from the list above or reduced in extent.

In the thesis the candidate shall present his personal contribution to the resolution of problems within the scope of the thesis work. Theories and conclusions should be based on mathematical derivations and/or logic reasoning identifying the various steps in the deduction.

The candidate should utilise the existing possibilities for obtaining relevant literature.

The thesis should be organised in a rational manner to give a clear exposition of results, assessments, and conclusions. The text should be brief and to the point, with a clear language. Telegraphic language should be avoided.

The thesis shall contain the following elements: A text defining the scope, preface, list of contents, summary, main body of thesis, conclusions with recommendations for further work, list of symbols and acronyms, references and (optional) appendices. All figures, tables and equations shall be numbered.

The supervisor may require that the candidate, in an early stage of the work, presents a written plan for the completion of the work. The original contribution of the candidate and material taken from other sources shall be clearly defined. Work from other sources shall be properly referenced using an acknowledged referencing system.

Supervisor: Professor Bernt J. Leira

Start-up: January 15th, 2019

Deadline: June 12th, 2019

Preface

The following work is a master's thesis in marine structural engineering, written at the Department of Marine Technology at the Norwegian University of Science and Technology. The work was carried out during the spring of 2019.

The objective of the thesis is modelling and analysis of aquaculture structures in exposed environments. The offshore fish farm concept Ocean Farm 1 has been modelled and analyzed. Parts of the background information and theory presented are widely based on the work conducted by the author throughout the project thesis during the fall of 2018.

I would like to thank my supervisor Professor Bernt Johan Leira for the guidance and help provided throughout the thesis. I would also like to express my greatest appreciation to the PhD candidates Thomas Hansen Viuff and Carlos Eduardo Silva de Souza for the many hours spent helping me troubleshooting throughout the modelling process.

Abstract

The Norwegian aquaculture industry has reached a state where further growth of the industry is not considered as sustainable. At the same time, the aquaculture industry is expected to produce larger quantities to feed the ever growing population. Driven by acreage, environmental and economical challenges, the industry is now forced to find new and innovative solutions, ensuring that more food can be produced in a more environment-friendly manner. Closed cage systems and offshore fish farming have proven to be feasible alternatives, and several concepts for these purposes have been suggested. Offshore fish farming will be the focus area of the thesis.

Moving the fish farms offshore requires new solutions in terms of design. Conventional fish farms are built for sheltered environments, and hence are not suited for the harsh environments at exposed locations. By combining technologies from the aquaculture and offshore industries, several concepts for offshore fish farming have been developed. Ocean Farm 1, the first offshore fish farm in Norwegian waters will be the concept evaluated throughout the thesis.

The fish farm is modelled as a coupled SIMO-RIFLEX model in SIMA. The pontoons are initially modelled using the Sesam software GeniE and HydroD, before imported to SIMA as SIMO-bodies. A static, dynamic and eigenvalue analysis have been performed. The results obtained were compared to model tests performed by MARINTEK. Direct comparison of the results proved to be difficult as the design was updated since the execution of the model tests. However, similar characteristics were found for most areas, whereas some revealed larger differences.

The static analysis revealed that the structural components of the hull experience small forces and moments with reference to the critical buckling stress and yield stress, respectively. Implying that fatigue might be the most relevant failure mode for the structure.

The dynamic analysis shows that the system allows for large horizontal offsets. The resulting maximum mooring line tensions were found to be good within the design criteria even for extreme environmental conditions. Vertical and transverse displacements and accelerations were generally small, coinciding well with expected characteristics of the semisubmersible structure.

The eigenvalue analysis revealed that the dominating mode shapes are excited by long wave periods, way outside the the range of typical wave frequencies. This implies limited wave-induced motions and that nonlinear effects caused by difference-frequencies are of importance to the dynamic response.

Sammendrag

Den norske havbruksnæringen har nådd et punkt der videre vekst av næringen ikke lenger ansees som bærekraftig. Samtidig er næringen forventet å produsere større kvanta for å mate den stadig voksende verdensbefolkningen. Som en konsekvens av mangel på tilgjengelige områder egnet til oppdrett, samt økonomi- og miljøutfordringer har havbruksnæringen sett seg nødt til å finne nye, innovative løsninger for å kunne forsikre en bærekraftig vekst av næringen. Lukkede merder og offshore oppdrettsanlegg er to av alternativene som blir stadig mer utredet, og er konsepter som ser ut til å kunne løse flere av utfordringene næringen står ovenfor. Offshore oppdrettsanlegg vil være hovedfokuset for oppgaven.

Når anleggene flyttes til mer eksponerte lokaliteter dukker flere utfordringer opp når det gjelder krav til utforming av anleggene. De tradisjonelle anleggene vi i dag finner i norske fjorder er utformet på bakgrunn av designkrav for små miljølaster. Konstruksjonene er dermed ikke dimensjonert for lastene man opplever offshore. Løsningen har vært å kombinere kunnskap og teknologi fra både havbruks- og offshorenæringen, og flere slike konsepter er i dag under utvikling. Norges første offshore oppdrettsanlegg, Ocean Farm 1, vil være temaet for oppgaven.

Oppdrettsanlegget er laget som en koblet SIMO-RIFLEX modell i SIMA. Pontongene blir først laget ved hjelp av Sesam-programmene GeniE og HydroD, før de importeres til SIMA som SIMO-kropper. I SIMA kjøres en statisk-, dynamisk- og egenverdianalyse. Resultatene blir sammenlignet med resultater fra modelltester utført av MARINTEK. Det skulle vise seg å bli vanskelig å gjøre en direkte sammenligning av resultatene, da designet har blitt oppdatert etter modelltestene ble utført. Like tendenser ble likevel funnet for begge konstruksjonene på de fleste områder, mens forskjellene ble større enn forventet på noen områder.

Den statiske analysen viser at komponentene i konstruksjonen generelt opplever små krefter og momenter sammenlignet med kritisk knekkspenning og materialets flytspenning. Dette tyder på at utmatting på sikt kan bli den viktigste årsaken til brudd.

Den dynamiske analysen viser at systemet tillater store horisontale forskyvninger. Det resulterende maksimale ankerlinestrekket var godt innenfor designkravene selv for ekstreme værtilstander. Forskyvninger og akselerasjoner i y- og z-retning var generelt små. Denne karakteristikken sammenfaller bra med hva som er forventet fra den halvt nedsenkbare konstruksjonen.

Egenverdianalysen viser at svingeformenene som dominerer den dynamiske responsen blir trigget av svært lange bølgeperioder, langt utenfor spennet som inkluderer typiske bølgeperioder. Konstruksjonen vil dermed oppleve lite respons trigget av førsteordens effekter (bølgefrekvenser). De høye egenperiodene tilsier derimot at andreordens effekter trigget av differansefrekvenser vil være viktig for den dynamiske responsen.

Contents

List of Figures

List of Tables

Nomenclature

Matrices and Vectors

$\mathbf{A}$	Added mass matrix
$\mathbf{C}$	Damping matrix
$\mathbf{C}^h$	Hydrodynamic damping matrix
$\mathbf{C}^s$	Structural damping matrix
$\mathbf{F}$	Excitation force
$\mathbf{H}(\omega)$	Frequency response function
$\mathbf{i}$	Unit vector along x-axis
$\mathbf{j}$	Unit vector along y-axis
$\mathbf{K}$	Global stiffness matrix
$\mathbf{k}$	Unit vector along z-axis
$\mathbf{K}(r)$	Secant stiffness matrix
$\mathbf{K}_I$	Incremental stiffness matrix
$\mathbf{M}$	Mass matrix
$\mathbf{M}^h$	Hydrodynamic mass matrix
$\mathbf{M}^s$	Structural mass matrix
$\mathbf{Q}$	External load vector

$\mathbf{R}$	Global load vector
$\mathbf{r}$	Nodal displacement vector
$\mathbf{R}_{int}$	Internal load vector
$\mathbf{X}$	Complex load vector
$\mathbf{x}$	Complex response vector

Greek Symbols

α	Angle between net normal and flow direction
α_1	Mass proportional damping coefficient
α_2	Stiffness proportional damping coefficient
β	Direction of wave propagation
Δ	Measure of roughness
η_i	Rigid body mode i
λ	Mesh size of net
λ	Wave length
λ_i	Modal damping ratio of mode i
ω	Wave frequency
ω_i	Eigenfrequency of mode i
ϕ	Velocity potential
ϕ_i	Eigenvector of mode i
ψ_ζ	Phase angle
ρ	Sea water density
ρ_a	Mass density of air
σ_{cr}	Critical buckling stress
ε	Phase angle in the surface elevation
ζ	Wave elevation

ζ_a Wave amplitude

Roman Symbols

A Area of net panel

a_i Acceleration in direction i

A_{wp} Waterplane area

C Current coefficient

C Shape coefficient

C_A Added mass coefficient

C_D Drag force coefficient

D Duration of sea state

D Twine diameter

F_D Mean drag force on net panel

F_k Radiation load

F_L Mean lift force on net panel

g Acceleration of gravity

H Horizontal tension of mooring line

h Water depth

H_{m0} Estimate of significant wave height, calculated from the wave spectra

H_{max} Estimate of largest wave height in a sea state

H_s Significant wave height

k Wave number

KC Keulegan-Carpenter number

m_n Spectral moment

N Number of waves in a sea state

n_i Normal vector to the body surface

p	Undisturbed pressure field
P_{cr}	Critical buckling load
q	Basic wind pressure
r	Velocity reduction factor
Re	Reynolds number
S	Projected area of surface/member normal to the direction of the force
S	Wet surface
$S(\omega, \theta)$	Directional wave spectrum
s_i	Suspended length of mooring line component i
Sn	Solidity ratio
T	Wave period
T_{ni}	Natural period
T_p	Peak period
T_z	Zero crossing period
u	Wake velocity
V_{ib}	Vertical tension at bottom of mooring line component i
V_{it}	Vertical tension at top of mooring line component i
w_i	Submerged weight of mooring line component i
F_W	Wind force normal to the member axis/surface
U_∞	Incident flow velocity
U_C	Current velocity
$\mathrm{U}_{T,z}$	Wind velocity averaged over time interval T at reference height z

Chapter 1

Introduction

1.1 Motivation and Background

The world's population is expected to reach a total of 9 billion by 2050 [1]. Whilst meeting the needs of a rapidly growing population, the world faces grate challenges in producing enough food in a sustainable and environment-friendly manner. More food must be produced using less resources and with minimal environmental impact.

With an annual growth rate of 5.8 percent during the period 2001-2016, the aquaculture industry has grown faster than other major food-producing industries. By 2016, the aquaculture industry accounted for a total of 53 percent of all fish used for human consumption [2]. The World Bank projects that this will increase to 62 percent by 2030 [1], demonstrating that the aquaculture industry is expected a further growth to contribute in meeting the future needs of the ever growing population. The Norwegian aquaculture industry will play an important role in meeting these goals, and has experienced a steady growth over the last decades as illustrated in Figure 1.2.

Traditionally, fish farms have been placed at sheltered coastal areas. The Norwegian coastline with it's many inlets and islands has proven to have excellent conditions for fish farming, making the aquaculture industry one of the major industries along the coastal areas of Norway. However, driven by acreage and environmental challenges, the Norwegian Directorate of Fisheries (NDF) no longer recognize further expansion of the industry as sustainable. Therefore, they now encourage companies to look towards the open sea as future production sites.

To motivate this change, the Norwegian Directorate of Fisheries in 2015 invited the industry to apply for free development licenses for concepts showing innovative solutions to the challenges facing today's industry. Ocean Farming AS, with it's ocean cage concept, Ocean Farm 1, was one of the applicants getting their concept approved by the NDF.

During September of 2017, Ocean Farm 1 arrived it's location at Frohavet, north-west of Trondheim, becoming the first offshore fish farm in Norwegian waters. A map indicating the location of the farming site is shown in Figure 1.1. As of today,

> Ocean Farm 1 is a full-scale pilot facility for testing, learning, research and development [...]. Aiming to reduce environmental footprints, improve fish welfare and answer acreage challenges, the learning and new solutions from the project could represent a new era in sustainable seafood production [3].

Figure 1.1: The location of Ocean Farm 1 at Frohavet indicated by the red pin [4]

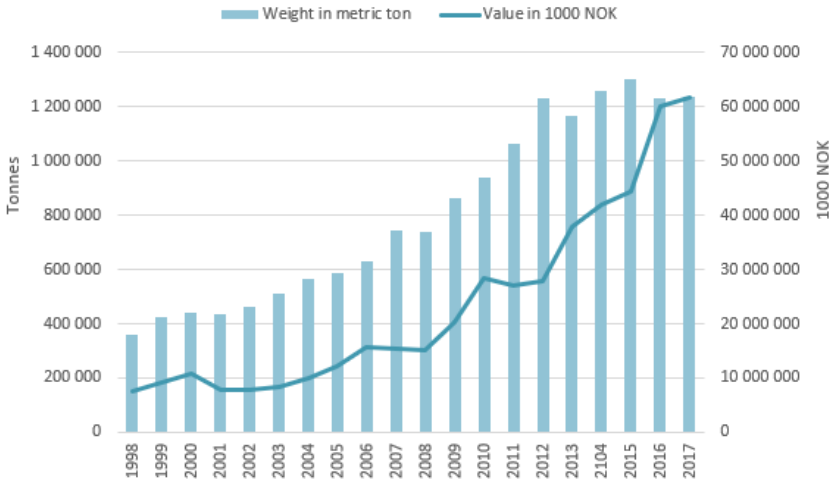

Figure 1.2: Sale of slaughtered salmon from the Norwegian aquaculture industry. Based on statistics from the Directorate of Fisheries [5]

1.2 Objective

The objective of the thesis is to illustrate the modelling and analysis process undergone in design of aquaculture structures by performing a global response analysis on an offshore fish farm model. The capacity with respect to extreme loading is to be found. The fish farm is to be modelled as a coupled SIMO-RIFLEX model in SIMA. The analyses to be included are a static, a dynamic and an eigenvalue analysis. The results obtained will be compared to results from model tests performed by MARINTEK at the SINTEF Ocean basin.

1.3 Limitations

Several limitations relating the modelling and analysis process were introduced throughout the work conducted in the thesis. Some of the more significant limitations discovered will be presented and briefly discussed throughout this section.

The information available relating dimensions, mass contributions, properties, etc. in the design of Ocean Farm 1 was limited to the information found in Bore and Fossan's master thesis, *Ultimate- and Fatigue Limit State Analysis of a Rigid Offshore Aquaculture Structure*, from 2015 [6].

In addition, the MARINTEK *reference report* [7] was introduced at a late stage in the process. It was then discovered that the design had been updated since the model tests were performed, and hence the results obtained could not be compared directly. The results from the model tests could therefore only be used as a guideline to what magnitude the results should be in.

The fish net cross section used in the SIMA model limited the dynamic analyses to regular waves and quite short time duration. This occurred as a consequence of limitations discovered in the software. Realistic implementation of the environmental conditions could therefore not be tested. Consequences of this will be further elaborated later on in the thesis.

1.4 Structure of Thesis

- Chapter 1 includes an introduction to the background and motivation for choosing the specific topic for the thesis. The objective and limitations for the thesis are also presented.
- Chapter 2 gives an insight in the current state of the aquaculture industry and the challenges facing the industry as it is today. An introduction to different offshore fish farming concepts and a brief presentation of rules and regulations in design of these structures will also be given.

- Chapter 3 describes the relevant theory of which the work conducted throughout the thesis is based on.
- Chapter 4 presents the Ocean Farm 1 concept. This includes a description of the concept in addition to dimensions, properties and drawings of which the SIMO-RIFLEX model is based on.
- Chapter 5 describes the modelling process undergone in the thesis.
- Chapter 6 includes a presentation and discussion of the results obtained from the analyses conducted.
- Chapter 7 includes a final discussion on drawbacks in the modelling and analysis approach used in the thesis.
- Chapter 8 presents the final conclusions.
- Chapter 9 presents recommendations for further work.

Chapter 2

Traditional Fish Farming and Offshore Fish Farm Concepts

2.1 Traditional Fish Farming

The Norwegian aquaculture industry had it's early breakthrough in the 1970's as the first sea cage for fish farming was constructed [8]. Since then, the industry has come a long way, and has with increased knowledge and improved technologies developed into a major industry along the coastal areas of Norway.

Today, the most common fish farms are built up by a number of circular or rectangular cages connected to a floater, where one single cage can carry up to 200 000 fish. Examples of such systems are plastic fish cages and rigid steel cages. These are systems designed to resist and dissipate environmental forces [9]. Figure 2.1 shows an illustration of a typical traditional fish farm, here illustrated by a plastic gravity type cage.

Other systems such as submersible cages, submerged cages and single point mooring cages also exist, but are not as commonly used as the former two mentioned. These systems are designed to avoid the environmental forces by submerging the cages below the surface [9]. Submerging the cages comes with grate advantages, however, to this day there are too many challenges relating fish welfare and operation of such systems, making them a less used alternative.

The fish farms are located at sheltered areas along the Norwegian coast. The farming sites are chosen based on considerations concerning fish welfare, cage system and legal/logistics criteria [11]. This includes water temperature, salinity, environmental conditions (wave, wind and current), bottom topology and distance to other fish farms.

Figure 2.1: Illustration of a traditional fish farm [10]

2.1.1 Challenges in Traditional Fish Farming

Conventional fish farming is facing several challenges preventing a sustainable growth of the industry. In the following sections, some of the most pronounced challenges will be presented, and whether moving the fish farms to more exposed locations will solve these challenges will be discussed.

Location

Due to the rapid growth of the aquaculture industry, in addition to competition with other coastal-based industries, one of the problems emerging is the lack of available locations for future plants. By looking at the possibility of moving out of the fjords, utilizing the open sea as production sites, the number of suitable locations increase tremendously.

Environmental Impact

Near the production site, there will be a great concentration of waste in the water column. This emerges from feeding particles, feces, medicine and chemicals used in the production. This effects both the waters near the fish farms as well as the sea bed. Moving the fish farms offshore will ensure less impact on the nearby areas as the environmental conditions at exposed locations ensures a more rapid dispersal of the waste.

Escapes

Escapes presents a huge threat to the environment as it enables farmed fish to interfere with the wild stock. This can cause a spread in diseases, competition for food and interbreeding between the species. Figure 2.2 shows the number of escaped salmon in the time period 2001-2018. The real number is expected to be higher than what is presented here as many

incidents do not get reported. The graph shows that even though the number of escapes is reduced over the past years, the problem is not yet resolved.

Moving the fish farms out of the fjords will increase the distance between the farmed fish and the wild stock, making it less probable for them to cross paths if escapes were to happen. In addition, with the introduction to harsher environments the need for innovating thinking in the design process arises. As new concepts are created, there are possibilities of integrating new solutions with focus on preventing escapes.

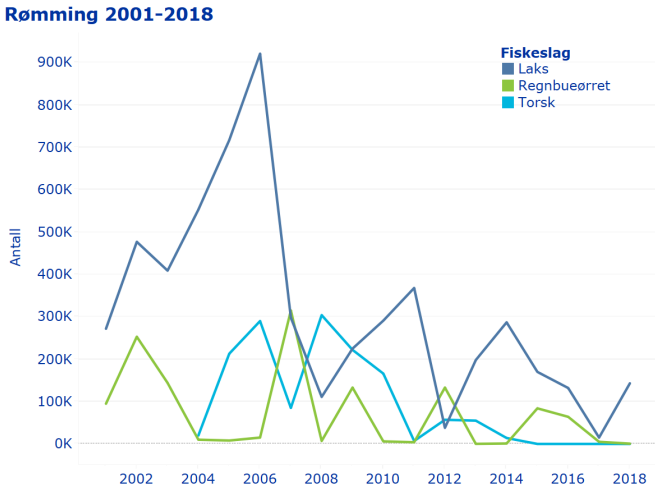

Figure 2.2: The reported number of escaped fish from the Norwegian aquaculture industry in the time period 2001-2018. The dark blue line represents escaped salmon. [12]

Sea Lice

Sea lice is one of the major challenges facing today's aquaculture industry, causing big economic losses. The fish farms has a dens fish population, holding a large number of "hosts" at the same location over a long time period. This shows to be ideal conditions for development of sea lice [13]. Another concern is that sea lice can travel up to 30 kilometers, transmitting sea lice from the farmed fish to the wild stock [14].

Whether moving the fish farms offshore will solve these challenges is not yet known. However, companies working on offshore fish farming concepts are putting great efforts into inventing new solutions to meet these challenges. This includes solutions such as closed cage systems, submersed systems and steel louse skirts. All mentioned solutions exploit the fact that the sea lice primarily lives in the top layers of the water column.

2.2 Offshore Fish Farming Concepts

Several companies are now looking at the possibility of moving fish farming out of the fjords, looking towards the open sea as future production sites. By utilizing well known technologies from both the aquaculture and offshore industries, together with new innovative technology, the goal is to address the major challenges facing today's aquaculture industry.

In the following sections, a selection of different design concepts will be presented. These concepts have all been approved by the Norwegian Directorate of Fisheries, and assigned development licenses to further develop and realize their concepts. As of now, all concepts discussed below are still in a conceptual phase with exception of Ocean Farm 1.

2.2.1 Havfarm

The offshore fish farm concept "Havfarm" is designed by NSK Ship Design on behalf of Nordlaks. The frame of the structure is designed as a vessel with hydrodynamic properties similar to a semi-submersible platform. It is designed to withstand significant wave heights up to 10 meters.

The structure has a total length of 430 meters and width of 54 meters. Further, the structure consists of six cages of 50 x 50 meters at the surface, with nets reaching down to 60 meters below the surface. One Havfarm is designed to hold up to 10 000 tons of salmon, corresponding to over two million salmons [15].

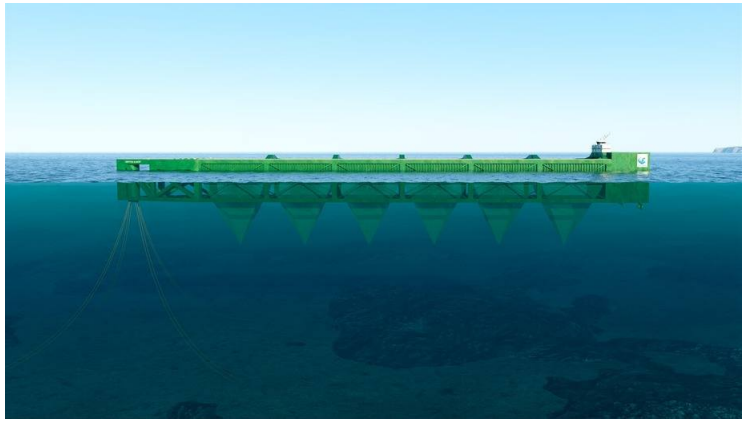

Figure 2.3: Illustration picture of the stationary Havfarm from a cross section view [16]

The design comes in three variants, differing in the way of anchoring the structure. This includes the stationary, the dynamic and the movable Havfarm. The different designs ensures that optimal solutions are available for different types of farming sites. Figure 2.3 shows the conceptual design of the stationary Havfarm with a single-point mooring system.

2.2.2 Arctic Offshore Farming

Arctic Offshore Farming is a concept developed by Norway Royal Salmon in cooperation with Aker and Aker solutions. The design is a semi-submersible fish farming system, holding up to 3000 tons in one cage [17]. Preliminary estimates suggest that the fish farm is to be up and running during the summer of 2020 [18].

The semi-submersible structure is designed for harsh environments with significant wave heights up to 15 meters. During operational conditions, the fish farm will be submerged so that the top of the net is located 10 meters below the surface. This provides limited exposure to environmental loads and sea lice. For the salmon to be able to live at this sea level over longer time periods, air pockets are integrated in the structure creating an artificial air surface.

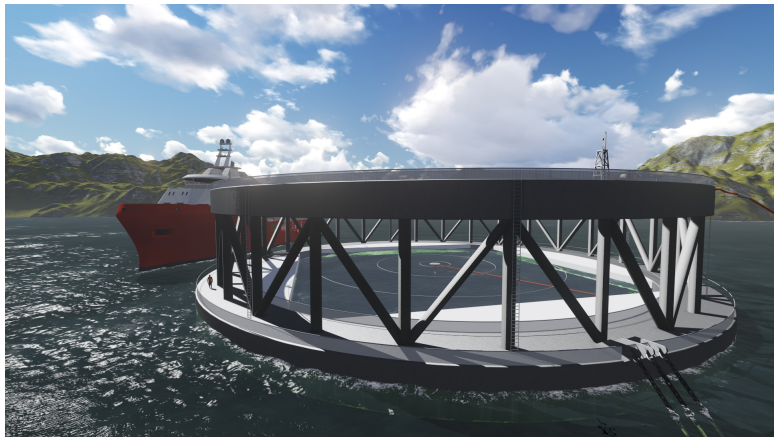

Figure 2.4: Illustration of the Arctic Offshore Farming concept [17]

2.2.3 The Egg

The Egg is a closed cage fish farm developed by Hauge Aqua for Marine Harvest. The structure is 44 meters tall and 33 meters wide, holding up to 1000 fish in one egg. By use of a robust closed cage system one avoids sea lice entering the fish farm while at the same time preventing escapes. In addition, it reduces the requirements to choice of location, as it no longer depends on strong currents for dispersal of waste and circulation of water [19]. Figure 2.5 shows an illustration of the Egg concept.

Unlike the other concepts presented, the egg is a fjord-based system. However, it is included as it shows innovative solutions addressing the challenges facing the industry without moving the operations offshore.

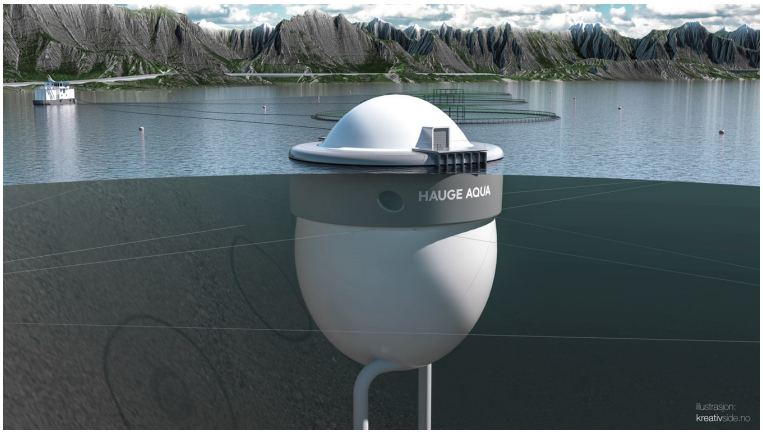

Figure 2.5: Illustration of The Egg [19]

2.2.4 Ocean Farm 1

Ocean Farm 1 is a semi-submersible offshore fish farm designed by Global Maritime on behalf of Ocean Farming AS - a subsidiary of the SalMar Group. The structure has a total height of 68 meters and diameter of 110 meters, holding up to 1.6 million salmon. The structure is designed to withstand significant wave heights up to 5 meters - a sea state including a maximum wave height of about 10 meters.

Figure 2.6: Ocean Farm 1 towing operation [20]

Figure 2.6 shows Ocean Farm 1 during transportation to it's production site north-west of Trondheim where it is currently working as a pilot-facility. The design concept of Ocean Farm 1 will be discussed in further detail in Chapter 4.

2.3 Rules and Regulations

Compared to the offshore industry, there are few rules and regulations to follow when designing a fish farm. This might be caused by the fact that the fish farms has up until now been located at sheltered environments, yielding relatively safe work environments and little structural damage caused by the environments.The offshore industry has on the other hand experienced several major accidents where structural damage has lead to loss of human lives. Such accidents has lead to further development of rules and regulations in design of offshore structures with the focus of preventing similar accidents.

The rules and regulations for design of fish farms in Norwegian waters mainly include NYTEK [21] and NS-9415 [22]. NYTEK is a national regulation for certification and inspection of floating fish farms developed by the Norwegian Directorate of Fisheries. The purpose of the regulation is to prevent escapes by assuring technical standard on the plants. NS-9415 is an accreditation body to NYTEK, providing requirements for site survey, risk analyses, design, dimensioning, production, installation and operation [21].

When moving fish farming to offshore environments the need for new rules and regulations arises. In July 2017, DNV GL issued a new set of rules for classification of offshore fish farming units and installations, DNVGL-RP-OU-0503 [23]. These includes requirements on material, stability, structural design, mooring and towing, surveys and different types of equipment and systems. However, as these regulations were issued, Ocean Farm 1 was already under construction. In design of Ocean Farm 1, it was therefore necessary to combine regulations from the aquaculture industry, such as NYTEK and NS9415, with rules and regulations from the offshore industry, including NORSOK and DNVGL-RP-C205.

Chapter 3

Theoretical Background

This chapter presents the essential theory of which the work conducted throughout the thesis is based on. This includes wave theory, a description of different environmental loads and forces acting on aquaculture structures. In addition, the basis for the static, dynamic and eiegenvalue analysis will be given. The theory is seen in light of the computer programs used in the thesis, mainly how the general concepts presented in the chapter are implemented in the different software.

3.1 Environmental Loads

For structures located at sea the environmental conditions of interest are waves, winds and currents. The following section will therefore introduce how one can estimate the related loads induced by these conditions.

3.1.1 Wind Loads

Wind induced loads acting on structures are characterized as dynamic loads as the wind speed fluctuates with time. The wind speed also varies depending on the height above the sea surface. It is therefore necessary to specify the averaging time for the wind speeds and the reference height of which the wind speed is measured [24]. According to DNV-RP-C205, typical averaging times are 1 minute, 10 minutes and 1 hour, and the most commonly used reference height is 10 meters above the mean water level.

By DNV's recommended practice, the basic wind pressure can be defined as

$$q = \frac{1}{2}\rho_a \, \mathrm{U}_{T,z}^2 \tag{3.1}$$

Where ρ_a is the mass density of air and $U_{T,z}$ the wind velocity averaged over a time interval T at a height z above the mean water level. The wind force on a structural member/surface acting normal to the member axis/surface may be expressed as

$$F_W = C\,q\,S\,sin\alpha \tag{3.2}$$

Where C is the shape coefficient, S the projected area of the surface or structural member normal to the direction of the force and α is the angle between the wind direction and the axis of the member/surface.

3.1.2 Current Loads

Current loads are considered as static forces arising from the constant flow of water passing through the structure. For moored structures such as the one discussed in the thesis, current forces are of great importance as it causes large steady excursions and slow drift motions. It also contributes to increased drag and lift forces and phenomena such as VIV [24].

By DNV's recommended practice, the steady current load can be defined as

$$F = C\,U_c^2 \tag{3.3}$$

Where U_c is the current velocity and C the current coefficient, usually determined empirically. For slender structures, as is assumed for all parts of the fish farm with exception of the pontoons, the current forces can be calculated as the drag force term in Morison's equation.

$$F_D = \frac{1}{2}\,\rho_w\,C_D\,A\,U_\infty \tag{3.4}$$

Where C_D is the drag coefficient, A the projected area perpendicular to the current and U_∞ the incident flow velocity.

3.1.3 Regular Waves

The sine (or cosine) function is mathematically describing a smooth periodic oscillation and defines what is called a regular wave. Generally, regular waves are characterized by a given wave amplitude, ζ_a, it's wavelength, λ, and its wave period, T. In RIFLEX, regular waves are modelled by two alternative methods; Airy linear wave theory and Stokes' 5th order wave theory. Both theories describes regular, long crested waves propagating in an arbitrary direction and can be expressed as

$$\zeta = \zeta_a sin(\omega t - kx\,cos\beta - ky\,sin\beta - \phi) \tag{3.5}$$

Where β represents the direction of wave propagation, ϕ the phase angle, $k = \frac{2\pi}{\lambda}$ the wave number and $\omega = \frac{2\pi}{T}$ the wave frequency.

The velocity potential for long crested regular waves can by Airy theory be expressed as

$$\phi = \frac{\zeta_a g}{\omega} \frac{cosh\big(k(h+z)\big)}{cosh(kh)} cos(-\omega t + kxcos\beta + kysin\beta + \psi_\zeta) \tag{3.6}$$

Where g is the acceleration of gravity, h the water depth and ψ_ζ the phase angle lag.

The disperison relationship relates the wavelength to the wave frequency and is defined as

$$\omega^2 = kg \cdot tanh(kh) \tag{3.7}$$

Behind the expressions presented above lies the assumption of finite water depths. Assuming deep waters, $h \to \infty$, one can approximate

$$\frac{cosh\, k(z+h)}{cosh\, kh} \to e^{kz} \tag{3.8}$$

$$tanh(kh) \to 1 \tag{3.9}$$

By use of these approximations, the velocity potential and dispersion relation for infinite water depths can be written as

$$\phi = \frac{g\zeta_a}{\omega} e^{kz}\, cos(\omega t - kx\, cos\beta + ky\, sin\beta + \psi_\zeta) \tag{3.10}$$

$$\omega^2 = kg \tag{3.11}$$

This approximation is assumed to be valid for water depths $h > \frac{\lambda}{2}$ [25].

3.1.4 Irregular Waves

Observing an actual sea state one can easily see that regular waves do not represent the reality. The wave pattern appears random and chaotic. This is called an irregular sea state, and is described by a statistical model based on the theory of stochastic processes. By this theory, irregular waves are approximated as a superposition of regular, long crested waves with I different wave frequencies and J directions. This is expressed as

$$\zeta(x,y,t) = \sum_{i=1}^{I} \sum_{j=1}^{J} \zeta_{Aij}\, cos(\omega_i t - k_i xcos(\theta_j) - k_i ysin(\theta_j) + \varepsilon_{ij}) \tag{3.12}$$

For wave component ij

- ζ_{Aij} is the wave amplitude
- ω_i is the wave frequency
- k_i is the wave number
- θ_j is the direction of the wave propagation
- ε_{ij} is the phase angle, uniformly distributed between 0 and 2π

It is here assumed that the wave process is *stationary* and *ergodic*, meaning that the mean value and variance is constant within a short time interval (20 minutes to 3 hours), and that one single realization is representative for the entire wave process. It is further assumed that the wave elevation is *uniformly distributed* with mean value of zero and variance σ^2 [26]. Assuming linear waves, the energy per unit area in the frequency interval $\Delta\omega$ and the direction interval $\Delta\theta$ can be expressed as

$$\Delta E_{ij} = \frac{1}{2}\rho g \zeta_{Aij}^2 \tag{3.13}$$

The total energy in a sea state is then defined as a sum of the energy of I wave frequencies and J directions.

$$\frac{E}{\rho g} = \sum_{i=1}^{I}\sum_{j=1}^{J}\frac{1}{2}\zeta_{Aij}^2 = \sum_{i=1}^{I}\sum_{j=1}^{J} S(\omega_i,\theta_j)\Delta\omega\Delta\theta \tag{3.14}$$

In the last equality above, the wave spectra $S(\omega,\theta)$ is introduced. This is defined such that the area inside a small frequency interval $\Delta\omega$ equals the energy of all wave components inside this frequency interval. By assuming $i,j \to \infty$, such that $\Delta\omega$, $\Delta\theta \to 0$, the wave elevation can be expressed by the wave spectrum as

$$\zeta_{Aij} = \sqrt{2S(\omega_i,\theta_j)\Delta\omega\Delta\theta} \tag{3.15}$$

Inserted into Equation 3.12, the surface elevation can now be rewritten as

$$\zeta(x,y,t) = \sum_{i=1}^{I}\sum_{j=1}^{J}\sqrt{2S(\omega_i,\theta_j)\Delta\omega\Delta\theta}\,cos(\omega_i t - k_i x cos(\theta_j) - k_i y sin(\theta_j) + \varepsilon_{ij}) \tag{3.16}$$

The wave spectrum can now be used to derive relations between different wave parameters. Typical wave parameters of interest are the significant wave height, H_s, and the peak period, T_p. These can be expressed in terms of moments of the wave spectrum and is defined as

$$m_n = \int_0^\infty \omega^n S(\omega) d\omega, \; n = 1, 2, 3... \tag{3.17}$$

The significant wave height is an estimate of the average value of the 1/3 largest wave heights measured in a time series. If calculated from the wave spectrum it is denoted H_{m0} and can be estimated using m_0 as

$$H_s = H_{m0} = 4\sqrt{m_0} \tag{3.18}$$

The most probable largest wave height for a given sea state can now be estimated using H_{m0}.

$$H_{max} = H_{m0}\sqrt{\frac{\ln N}{2}} \quad \text{for large N} \tag{3.19}$$

Where N is the number of waves in the given sea state and is the largest uncertainty in the estimation above. In order to estimate the number of waves in a sea state the duration, D, of the sea state and the mean zero upcrossing period, T_z, must be known.

$$N = \frac{D}{T_z} \tag{3.20}$$

Where

$$D = 164\, H_s^{-1.87} \text{ (hours)} \tag{3.21}$$

The duration of a sea state estimated from the significant wave height is based on data from the winter season at Haltenbanken, north west of Trondheim. As this is not far from Frohavet, where Ocean Farm 1 is located, this estimation is assumed to be valid in the thesis.

3.2 Wave Induced Forces

This section provides a description of wave induced forces in regular waves. The theory presented is based on literature written by Faltinsen [27]. Only regular waves are considered as wave induced forces in irregular waves can be found by superimposing results from regular wave components. The theory assumes regular waves of small wave steepness and steady state condition.

Looking at wave induced forces in regular waves, the problem can be divided in two subproblems, often referred to as the *diffraction problem* and the *radiation problem*. These are in turn cause of two categories of wave induced forces; wave excitation loads and added mass, damping and restoring loads. These loads will be further elaborated in the following sections.

3.2.1 Wave Excitation Loads

Wave excitation loads appears as the structure is fixed, hence restrained from oscillating, while exposed to incident waves. The hydrodynamic loads appearing can then be divided in two components; Froude-Kriloff loads and diffraction loads. The former is connected to the undisturbed pressure field of the undisturbed waves, whereas the latter is connected to changes in the pressure field caused by the presence of the structure. The velocity potential solving the diffraction problem is defined as

$$\phi(x,y,z,t) = \underbrace{\phi_0(x,y,z,t)}_{\text{incident wave}} + \underbrace{\phi_D(x,y,z,t)}_{\text{diffraction}} \tag{3.22}$$

The total excitation loads are obtained by integrating the incident wave dynamic pressure and the diffraction pressure along the mean wetted surface of the body. The excitation loads can then be expressed as

$$\mathbf{F} = \mathbf{i}\,\mathrm{F}_1 + \mathbf{j}\,\mathrm{F}_2 + \mathbf{k}\,\mathrm{F}_3 \tag{3.23}$$

Where

$$\mathrm{F_i} = \underbrace{-\iint_s p\, n_i\, ds}_{\text{Froude-Kriloff}} + \underbrace{A_{i1}a_1 + A_{i2}a_2 + A_{i3}a_3}_{\text{diffraction}} \tag{3.24}$$

Where p denotes the undisturbed pressure field, n_i the normal vector normal to the body surface, S the wet surface and a_i the acceleration in direction i. A_{ij} is read as the added mass in direction i due to a force in direction j, this term will be further discussed in Section 3.2.2. The undisturbed pressure and accelerations are found using the velocity potential defined in Equation 3.22.

$$p = -\rho\frac{\partial\phi}{\partial t} \qquad a_1 = \frac{\partial\phi^2}{\partial x\partial t} \qquad a_2 = \frac{\partial\phi^2}{\partial y\partial t} \qquad a_3 = \frac{\partial\phi^2}{\partial z\partial t} \tag{3.25}$$

3.2.2 Added Mass, Damping and Restoring Loads

The added mass, damping and restoring terms appears as the structure is forced to oscillate in its six degrees of freedom with the wave excitation frequency, ω. There are no incident waves. The oscillations of the body generates waves (radiation waves) and causes an oscillating fluid pressure on the body surface. The added mass and damping loads are caused by this dynamic pressure and are hence classified as hydrodynamic loads. The restoring loads are on the other hand connected to the hydrostatic pressure due to variation of buoyancy as the body moves, and are therefore classified as hydrostatic loads. Summing

up the hydrodynamic and hydrostatic loads, the total radiation loads due to the harmonic motion mode η_j can be expressed as

$$F_k = -A_{kj}\frac{d^2\eta_j}{dt^2} - B_{kj}\frac{d\eta_j}{dt} - C_{kj}\eta_j \tag{3.26}$$

Where A_{kj}, B_{kj} and C_{kj} denotes the added mass, damping and restoring coefficients, respectively. The subscripts j and k should be read as force/coefficient in k due to a motion mode in direction j. η_1, η_2 and η_3 then refers to the transnational rigid body modes surge, sway and heave, respectively. Whereas η_4, η_5 and η_6 refers to the rotational rigid body modes roll, pitch and yaw. To better understand the physical meaning of the added mass, damping and restoring loads, a brief description of each load component will be given.

Added Mass

Added mass is the additional mass an objects appears to have when being accelerated in a surrounding fluid [28]. As the object moves, so must the fluid surrounding it. As the fluid has an inertia, an additional force is required to accelerate the fluid. This is called the added mass force, and is proportional to the acceleration.

Damping

> Damping designates the ability of a structure to dissipate kinetic energy, i.e. transform it into other types of energy such as heat or radiation (of water waves, sound waves etc) [29].

There are several sources contributing to damping of floating structures. Commonly, the different sources of damping are divided in two main categories, namely the hydrodynamic and structural damping. The hydrodynamic damping accounts for diffraction effects for floating, partly submerged elements [30]. It is mainly composed by two terms, one of them being the linear viscous damping term arising as kinetic energy is transformed to wave energy. The other term is the nonlinear drag damping arising due to vortex shedding and viscous effects [29]. Structural damping is on the other hand accounting for energy dissipation in the structure itself. In RIFLEX, structural damping is implemented using the global Rayleigh damping model. The damping is then expressed as a linear combination of the mass and stiffness matrices.

$$\mathbf{C} = \alpha_1\mathbf{M} + \alpha_2\mathbf{K} \tag{3.27}$$

Where α_1 and α_2 are the mass- and stiffness-proportional damping coefficients related to the modal damping ratio, λ_i, through

$$\lambda_i = \frac{1}{2}\left(\frac{\alpha_1}{\omega_i} + \alpha_2\omega_i\right) \tag{3.28}$$

This formulation is useful as the damping matrix gets the same orthogonal properties as **M** and **K**. The equation of motion can then be rewritten as n decoupled equations that can be solved independently. For known modal damping ratios and frequencies, Equation 3.28 is used to determine α_1 and α_2 as

$$\alpha_1 = \frac{2\omega_1\omega_2}{\omega_2^2 - \omega_1^2}(\lambda_1\omega_2 - \lambda_2\omega_1) \tag{3.29}$$

$$\alpha_2 = \frac{2(\omega_2\lambda_2 - \omega_1\lambda_1)}{\omega_2^2 - \omega_1^2} \tag{3.30}$$

Restoring

For a freely floating body, restoring forces will appear as a consequence of hydrostatic and mass considerations [27]. It is connected to the specific gravity and buoyancy forces, which will vary as the body moves. For the restoring coefficients , C_{ij}, the only non-zero terms for a body with x-z symmetry plane will be

$$\begin{aligned} C_{33} &= \rho g A_{wp} \\ C_{35} &= C_{53} = -\rho g \iint_{A_{wp}} x\, ds \\ C_{44} &= \rho g V \overline{GM}_T \\ C_{55} &= \rho g V \overline{GM}_L \end{aligned} \tag{3.31}$$

Where A_{wp} is the waterplane area and V the displaced volume of water. $\overline{GM}_T$ and $\overline{GM}_L$ are the transverse and longitudinal metacentric heights, respectively.

Frequency Dependency

The added mass and damping shows strong dependence of the frequency. This arises due to the fact that the added mass and damping depends on the motion mode [27]. One can say that the wave frequency affects the body's capability of generating waves, at the same time, the added mass and damping originates from the generated waves, creating a circular dependency. Numerical calculations shows that the difference in the added mass and damping terms are especially strong as $\omega \to 0$ and $\omega \to \infty$.

3.3 Hydrodynamics of Net Cages

In order to analyze net structures exposed to waves and currents, a structural model and a hydrodynamic model is needed. The hydrodynamic force models can be divided in two

main categories; Morison models and screen models [31]. The Morison models represents the net as a system of twines or trusses and calculates the drag forces on each twine individually. The screen models assumes the net can be divided into a number of net panels, calculating the total drag- and lift forces on the panel as a whole. The *current force model* developed by Løland in 1991 [32] is an example of a screen model. This model is used in the modelling of the net panel in the thesis and will therefore be further derived in the following sections.

3.3.1 Current Forces

The main assumption by the current force model is that the net cages can be divided into several net panels, neglecting structural compatibility between the different net panels [32]. The total force on the net cage is then found as the sum of the forces acting on each panel individually. Based on empirical data and results obtained from model tests, Løland formulated expressions for the drag and lift force coefficients for net panels. These expressions are commonly known as Løland's formula.

> The current force model is constructed in such way that it takes into account the most important effects such as the net solidity, weights of sinkers, shielding, initial geometry and deformation of the net cages [32].

The total force on each net panel will consist of a drag force and a lift force contribution. The drag force is defined as the force in the direction of the flow, and the lift force is the force normal to the flow direction. The method is now based on assuming that the mean drag and lift force on a given net panel can be expressed as

$$F_D = \frac{1}{2}\rho\, C_D(\alpha) \mathrm{A}\, \mathrm{U}^2 \tag{3.32}$$

$$F_L = \frac{1}{2}\rho\, C_L(\alpha) \mathrm{A}\, \mathrm{U}^2 \tag{3.33}$$

Where α denotes the angle between the flow direction and net normal vector in the direction of the flow, C_D the panel drag coefficient, C_L the panel lift coefficient, A is the area of the net panel and U the current velocity. By Løland's formula one can now present the following relationship

$$C_D = 0.04 + (-0.04 + 0.33Sn + 6.54Sn^2 - 4.88Sn^3)\, cos\alpha \tag{3.34}$$

$$C_L = (-0.05Sn + 2.3Sn^2 - 1.76Sn^3)\, sin(2\alpha) \tag{3.35}$$

Sn is called the solidity ratio, and is defined as the ratio between the area covered by the threads and the total area of the net panel [32].

$$Sn = \frac{2D}{\lambda} - \left(\frac{D}{\lambda}\right)^2 \tag{3.36}$$

Where D denotes the twine diameter and λ the mesh size of the net as illustrated in Figure 3.1 below.

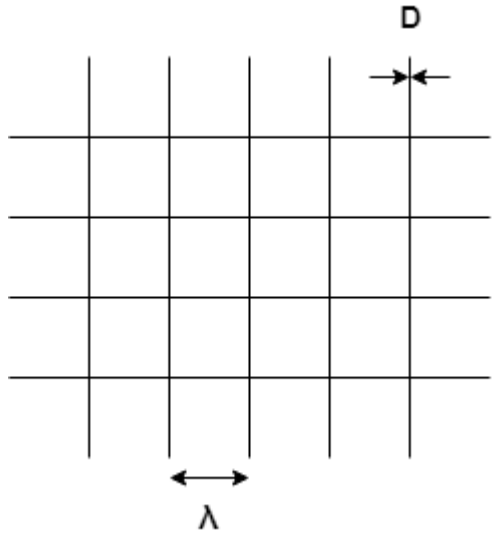

Figure 3.1: Definition of net mesh variables

3.3.2 Velocity Reduction Factor

As shown in Equations 3.32 and 3.33, the current forces on a net cage are functions of the squared current velocity. It is therefore important to describe the velocity profile within and around the net as correctly as possible. A net cage is a permeable structure, and hence it will alter the flow field of the current passing the structure. The permeability of the net leads to a flow pattern where parts of the flow is forced to go around the structure, while the rest of the fluid flows through the net at a lower speed [32]. The reduced velocity in the wake of the net is called the wake velocity and is defined as

$$u = r\mathrm{U} \tag{3.37}$$

$$r = 1 - 0.46C_D \tag{3.38}$$

Where U is the velocity of the free flow and r the velocity reduction factor. By the current force model, the velocity reduction factor is defined as in Equation 3.38 and is based on model test results performed by Løland [32]. Figure 3.2 shows the correlation between the drag coefficient, C_D, and the velocity reduction factor, r, as a function of the solidity ratio Sn.

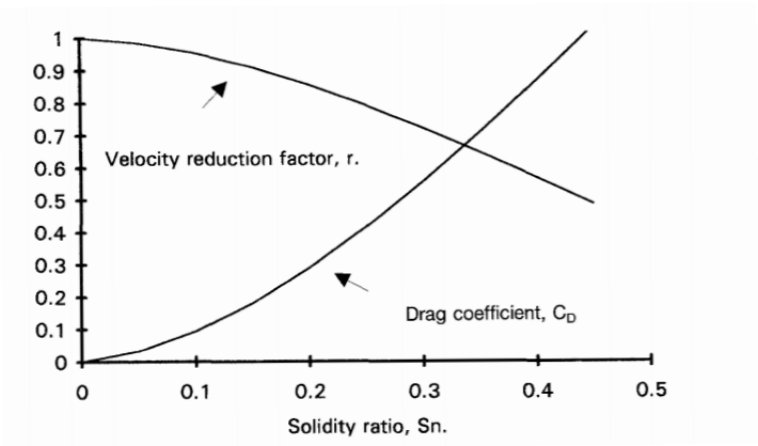

Figure 3.2: Drag coefficient and velocity reduction factor as a function of solidity ratio [33]

3.4 Static Analysis

Throughout the following section, the methods used for obtaining the static response will be presented. The theory presented is widely based on definitions from the RIFLEX *Theory Manual* [30] and Chapter 12 of Moan's compendium *Finite Element Modelling and Analysis of Marine Structures* [34].

3.4.1 Linear Analysis

A static response analysis is conducted in order to determine the nodal displacements so that the complete system is in static equilibrium. The principles of which a static structural analysis is based on can be expressed as

- equilibrium of all parts of the structure
- kinematic compatibility in the material
- stress-strain relationship

For the linear case we assume small displacements and linear elastic material behavior. The global nodal displacements are then found by solving the linear set of equations expressed as

$$\mathbf{Kr} = \mathbf{R} \tag{3.39}$$

Where $\mathbf{K}$ is the global stiffness matrix, $\mathbf{R}$ is the global load vector and $\mathbf{r}$ the global nodal displacement vector.

3.4.2 Non-Linear Analysis

For the non-linear case the assumptions of small deflections and linear elastic material behavior are no longer valid. Non-linearities are introduced through change in geometry, non-linear material behavior and boundary conditions due to contact problems [34]. This results in a stiffness dependent on the displacement, and the stiffness relationship is rewritten as

$$\mathbf{K}(r)\mathbf{r} = \mathbf{R} \tag{3.40}$$

Generally, Equation 3.40 can not be solved analytically, and iterative and/or incremental methods must be used [34]. For these purposes Equation 3.40 is written on differential form as

$$\mathbf{K}_I(r)d\mathbf{r} = d\mathbf{R} \tag{3.41}$$

Where $\mathbf{K}_I$ is the incremental stiffness consisting of a linear stiffness term and a non-linear geometric stiffness term due to change in geometry. RIFLEX solves this by use of an incremental-iterative procedure based on a combination of the Euler-Cauchy incrementation and the Newton-Raphson iteration [30].

Euler-Cauchy Method

Euler-Cauchy is a load incremental method for solving of non-linear problems by a stepwise application of the external loading, starting from the initial condition $\mathbf{r}_0 = \mathbf{0}$. At each step, the displacement increment is determined by Equation 3.41. By adding the displacement increments the total displacement is obtained [34].

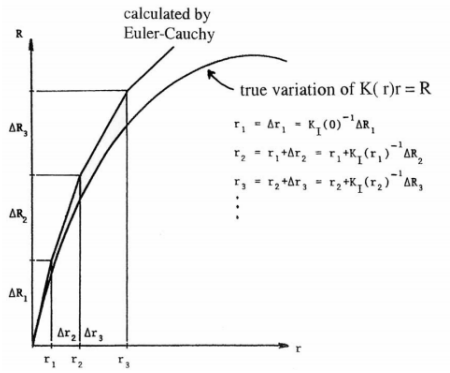

Figure 3.3: Euler-Cauchy incrementing for a single degree of freedom system [34]

As seen from Figure 3.3, the approximation used by Euler-Cauchy leads to a slight deviation from the exact solution. This arises as the equation for total equilibrium, $\mathbf{R} = \mathbf{R}_{int}$ is not fulfilled. By reducing the size of the load increments the accuracy is increased.

Improvements to the Euler-Cauchy method can also be implemented by introducing a correction to the equilibrium equation. The residual forces are added to the next load increment, hence reducing the external loads so that global equilibrium is restored. This is shown in Figure 3.4.

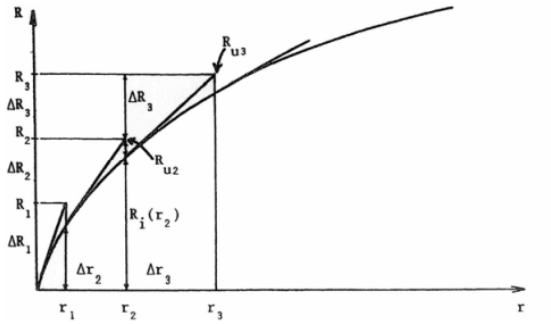

Figure 3.4: Euler-Cauchy incrementing with equilibrium correction [34]

Newton-Raphson Method

Newton-Raphson is an iterative method for solving of structural non-linear problems by formulating Equation 3.41 by the iterative formula as given in Equation 3.42. Figure 3.5 shows an illustration of the procedure.

$$\mathbf{r}_{n+1} = \mathbf{r}_n - \mathbf{K}_I^{-1}(\mathbf{r}_n)(\mathbf{R}_{int} - \mathbf{R}) \tag{3.42}$$

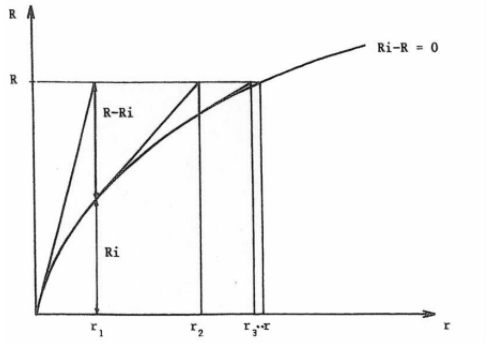

Figure 3.5: Newton-Raphson iteration for a single degree of freedom system [34]

This procedure is adopted in RIFLEX due to it's quadratic convergence rate. However, the approach requires recomputation of $\mathbf{K}_I$ for each iteration cycle. As this is quite time-consuming, RIFLEX offers the option of using a modified version of the Newton-Raphson method by keeping $\mathbf{K}_I$ constant during several iterations. The convergence rate will be somewhat slower, but the computational time is significantly reduced [30].

Combined Method

In RIFLEX, static equilibrium is obtained by a combination of the Euler-Cauchy and Newton-Raphson method. External loads are applied in a number of small load increments, whereas the static configuration at each step is found by iteration [30]. This procedure is illustrated using a modified Newton-Raphson method in Figure 3.6.

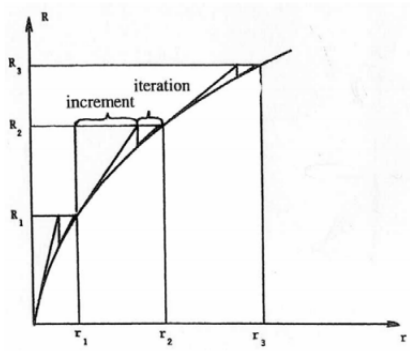

Figure 3.6: Combined incremental and iterative methods [34]

RIFLEX recommends using the true Newton-Raphson iteration scheme, with number of iterations selected to be somewhere in the range of 5-15, and accuracy of the displacement in the range of $10^{-4} - 10^{-6}$ [30].

3.5 Dynamic Analysis

Unlike the static analysis, the dynamic analysis implies a time dependent solution. This is because the structure is subjected to a dynamic (time-varying) loading, causing inertia forces, damping forces and external time dependent forces. By application of Newton's 2^{nd} law, d'Alembert's principle and the principle of virtual work, the dynamic equilibrium equation can be expressed as

$$\mathbf{M}\ddot{\mathbf{r}} + \mathbf{C}\dot{\mathbf{r}} + \mathbf{K}\mathbf{r} = \mathbf{Q}(t) \tag{3.43}$$

Where **M**, **C** and **K** are the mass, damping and stiffness matrices, respectively. **Q**(t) denotes the time dependent external load vector, and $\mathbf{r}$, $\dot{\mathbf{r}}$ and $\ddot{\mathbf{r}}$ represents the structural dis-

placement, velocity and acceleration vectors, respectively. For floating, partly submerged structures, the damping matrix is divided in the following terms

$$\mathbf{C} = \mathbf{C}^s + \mathbf{C}^h \tag{3.44}$$

Where $\mathbf{C}^s$ is the structural damping and $\mathbf{C}^h$ the hydrodynamic damping. Similarly, the mass matrix is divided in the terms

$$\mathbf{M} = \mathbf{M}^s + \mathbf{M}^h \tag{3.45}$$

Where $\mathbf{M}^s$ represents the structural mass and $\mathbf{M}^h$ the hydrodynamic mass, commonly known as the added mass.

3.5.1 Frequency Domain Analysis

Introducing the expressions

$$\mathbf{Q}(t) = \mathbf{X}e^{i\omega t} \tag{3.46}$$

$$\mathbf{r} = \mathbf{x}e^{i\omega t} \tag{3.47}$$

The dynamic equation of motion can be written in the frequency domain as

$$\left[-\omega^2\mathbf{M} + i\omega\mathbf{C} + \mathbf{K}\right]\mathbf{x} = \mathbf{X} \tag{3.48}$$

This gives a solution on the form

$$\mathbf{x}(\omega) = \frac{\mathbf{X}}{-\omega^2\mathbf{M} + i\omega\mathbf{C} + \mathbf{K}} = \mathbf{X}(\omega)\mathbf{H}(\omega) \tag{3.49}$$

Where $\mathbf{H}(\omega)$ is called the frequency response function, expressing the frequency domain relationship between an input and an output of a linear, time-invariant system. $\mathbf{x}$ and $\mathbf{X}$ here denotes the complex response and load vectors, respectively.

Solving the dynamic analysis in the frequency domain one can easily express the sensitivity of a structure to the load frequency [29]. This is especially useful for structures with frequency-dependent mass, damping or stiffness matrices. Advantages with this approach is that it gives physical insight, and is a relatively fast algorithm compared to the dynamic analysis performed in the time domain. However, nonlinearities can not be fully captured, and only the steady state solution is included [35]. Figure 3.7 illustrates how a dynamic analysis in the frequency domain may look.

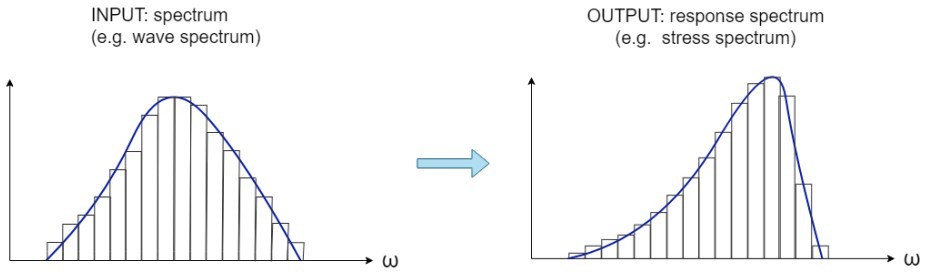

Figure 3.7: Illustration of a frequency domain analysis (Based on [35])

3.5.2 Time Domain Analysis

The dynamic equation of motion as defined in Equation 3.43 is a function solved at particular values of time, t. One can then say the dynamic analysis is performed in the time domain. The result comes as a time history, and is useful as it resembles the reality and can fully capture nonlinearities [35]. Figure 3.8 shows how a time domain analysis may look.

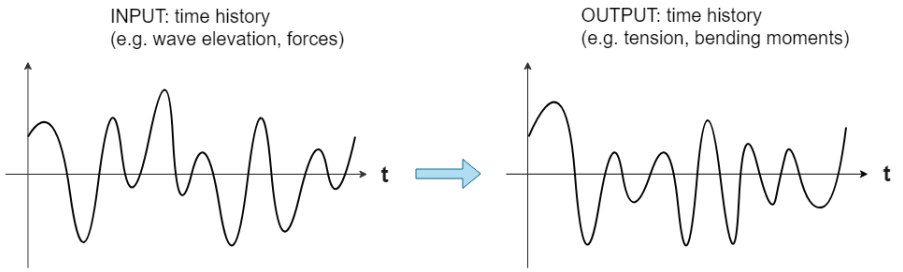

Figure 3.8: Illustration of a time domain analysis (Based on [35]

The time domain analysis includes both the transient and steady state response. The transient state decays due to damping, leaving only the steady state response left after some period of time. Usually, one assumes the wave environment has been present long enough for the transient state to have fully dissipated.

3.6 Eigenvalue Analysis

An eigenvalue analysis is performed in order to determine the eigenfrequencies and the corresponding mode shapes of the system. The eigenvalue analysis is of great importance in dynamic analysis as the loads acting on the structure can oscillate with frequencies coinciding with the eigenfrequencies, causing large dynamic amplifications and possibly structural damage or failure.

There are uncertainties related to how the eigenvalue analysis is performed in RIFLEX as this is not included in the theory manual. The following section will therefore give a general approach on how to solve the general eigenvalue problem.

3.6.1 The General Eigenvalue Problem

The eigenvalues and corresponding mode shapes are determined by solving the general eigenvalue problem. The general eigenvalue problem is derived from the dynamic equation of motion

$$\mathbf{M}\ddot{\mathbf{r}} + \mathbf{C}\dot{\mathbf{r}} + \mathbf{K}\mathbf{r} = \mathbf{Q}(t) \tag{3.50}$$

By studying the case of free undamped vibrations, the following assumptions are applied

$$\mathbf{C} = \mathbf{0} \tag{3.51}$$
$$\mathbf{Q}(t) = \mathbf{0} \tag{3.52}$$

The dynamic equation of motion is then reduced to

$$\mathbf{M}\ddot{\mathbf{r}} + \mathbf{K}\mathbf{r} = \mathbf{0} \tag{3.53}$$

By assuming harmonic vibrations, the nodal displacements and accelerations can be expressed as

$$\mathbf{r} = \phi sin(\omega t) \tag{3.54}$$
$$\ddot{\mathbf{r}} = -\omega^2 \phi sin(\omega t) \tag{3.55}$$

Where ϕ denotes the eigenvector and ω represents the circular frequency. The reduced equation of motion can now be expressed as the eigenvalue problem on the general form

$$(\mathbf{K} - \omega^2 \mathbf{M})\phi = \mathbf{0} \tag{3.56}$$

By solving of Equation 3.56 one obtains a set of eigenvectors ϕ_i. Each eigenvector is associated with an eigenvalue ω_i^2, where ω_i is the eigenfrequency of mode i [29]. The lower eigenfrequencies and corresponding mode shapes will be of most importance as these are the ones dominating the dynamic response of the system. It is however important to note that the mode shapes originate from scaled eigenvectors, implying that the magnitude of the mode shapes are arbitrary. The mode shapes must hence be read as an indication of the behavior for the given frequency and should not be read as actual displacements.

Chapter 4

Ocean Farm 1 Concept

This chapter will provide a detailed description of the Ocean Farm 1 concept and gives the basis for the modelling process undergone in the thesis. The concept presented is based on drawings, dimensions and properties found in Bore and Fossan's master thesis; *Ultimate- and Fatigue Limit State Analysis of a Rigid Offshore Aquaculture Structure* [6] and the MARINTEK *reference report* [7]. Some alterations has been made to the design since the publication of [6] and hence the model made is not identical to the actual structure. However, it gives a presentable representation of the structure for the purposes of the thesis.

4.1 Design Concept

The concept behind Ocean Farm 1 is to create a robust structure able to withstand the harsh environments at exposed locations, whilst still ensuring fish welfare and safe operations. During the design process, emphasis has been put into making the structure as escape- and sea lice-proof as possible, as these are two of the major concerns presented by the Norwegian Directorate of Fisheries. As a pilot facility, the fish farm is made fully-automated in order to minimize the need of service vessels and outside equipment, making operations more environment-friendly. A fully-automated facility also reduces the need for crew on board, and the entire facility is operated by a crew of only two to four people [36].

The structure is designed as a semi-submersible cage, much like semi-submersible structures used for offshore operations. Important for the semi-submersibles are the good stability and seakeeping characteristics, making it suitable for the purposes of offshore fish farming. The good seakeeping characteristics arises from the structure being designed with a small waterplane area, hence large natural periods, T_n, defined as

$$T_{ni} = 2\pi\sqrt{\frac{M_{ii} + A_{ii}}{C_{ii}}} \tag{4.1}$$

Where M denotes the structural mass, A the added mass of the system and C the system stiffness. High natural periods yields little wave-induced motions as most wave periods are significantly lower than the natural periods of the structure. The fish farm is therefore defined as an inertia dominated system as illustrated in Figure 4.1. For inertia dominated systems, the inertia is too large for the displacements to be large enough to mobilize any significant restring forces [37]. Hence, the structure is very stable, even with harsh environments acting on it. This is key for safe operations and fish welfare in exposed environments.

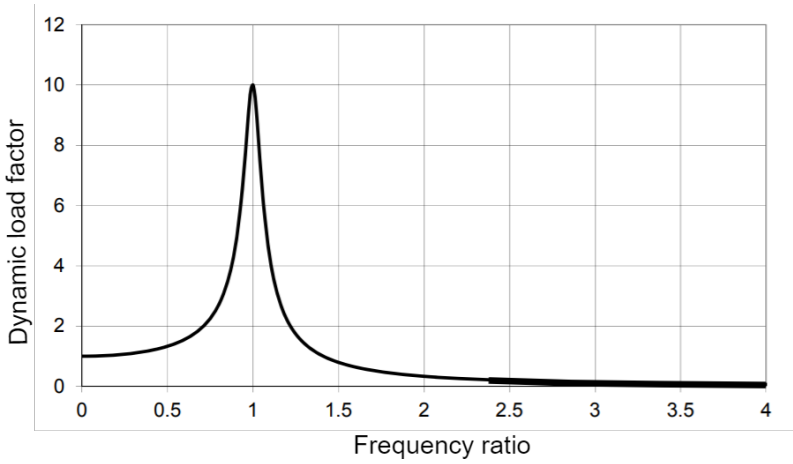

Figure 4.1: Inertia dominated region [37]

4.2 Coordinate System

The global coordinate system and rigid body motion modes used throughout the thesis are defined as in Figure 4.2. The origin of the global coordinate system is placed at the waterplane area of the centre column, hence at the location of the free surface when the structure is in equilibrium position in calm water. Waves, winds and currents are defined with an incoming angle which is zero when in the direction of the positive x-axis, moving counter clockwise as shown in Figure 4.2b.

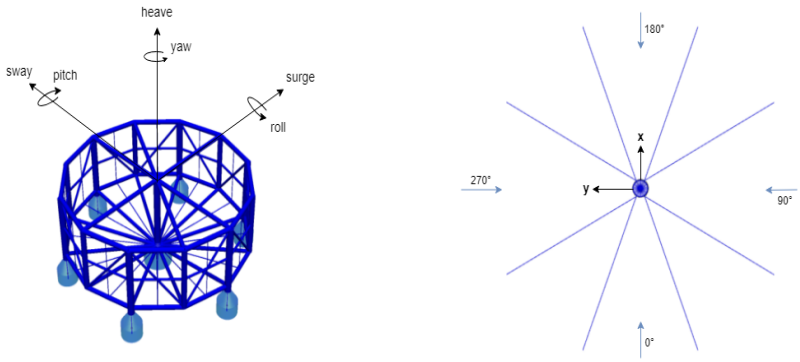

(a) Vessel degrees of freedom **(b)** Wave directions

Figure 4.2: Definition of the rigid body motion modes and global coordinate system

4.3 Main dimensions

Ocean Farm 1 is designed as a 12 edged cylinder frame consisting of twelve vertical columns along the periphery and one vertical column at the centre of the frame. The hull is internally equipped with a circular collar for the net, which is stretched along the sides and bottom of the frame. Buoyancy is obtained by submerged pontoons at the bottom of the structure. The draft of the structure can then be adjusted by altering the water level in the pontoons. There are a total of seven pontoons, six of them placed along the periphery of the structure, and one at the centre column. Figure 4.3 shows the structure at the transit draft. An overview of the main dimensions of the structure is found in Table 4.1.

Figure 4.3: Ocean Farm 1 at transit draft [3]

Table 4.1: Main dimensions of the Ocean Farm 1 concept

Dimension	Value	Unit
Diameter	110	m
Circumference	341.6	m
Height (including topside)	68	m
Height of vertical side columns	33	m
Height of vertical mid column	37	m
Height of periphery pontoons	13	m
Height of centre pontoon	7	m
Diameter of periphery pontoons	12	m
Diameter of centre pontoon	17	m
Operation draft	43	m
Transit draft	8.8	m
Net volume	245 000	m^3

4.4 Hull Structure

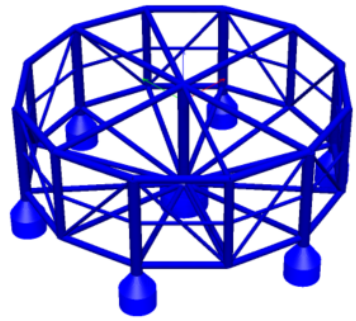

Figure 4.4: Snapshot of the hull structure modelled in RIFLEX

The hull structure includes all columns, braces, beams and pontoons as shown in Figure 4.4. The material used is NV-36 steel with material properties as given in Table 4.2.

Table 4.2: Material properties of NV-36 steel

Property	Value	Unit
Modulus of elasticity	210	GPa
Yield strength	355	MPa
Density	7850	kg/m^3
Poisson ratio	0.3	-

The details of the hull dimensions used in the modelling process are listed in Table 4.3 and should be seen in context with the structural drawing found in Appendix A.3. As seen from the table, different diameters and thicknesses are used across the segments. These are set so that the dimensions of the elements facing the joints are correct, which is important to obtain the correct stresses at these especially vulnerable locations. The midspan is given dimensions ensuring the segments has the correct total weight. This is to include the weight contribution of the ring stiffeners present in the segments [6].

Table 4.3: Hull dimensions used in the RIFLEX model

Member	D_{mid}	D_{end}	t_{mid}	t_{end}	L
Centre column	3.56	3.58[1]	32	40[1]	37
Periphery columns above pont.	3.56	3.58	34	40	33
Periphery intermediate columns	2.80	2.83	30	40	33
Bottom radial beams	1.75	1.75	23	23	55.4
Bottom ring beams	2.05	2.05	24	24	28.5
Top cross beams	2.05	2.08	18	40	55
Top ring beams	2.29	2.33	18	40	28.5
Middle ring beams	1.00	1.00	15	15	28.5
Diagonal supports	1.00	1.00	15	30	43.6
Centre pontoon cylinder	17.0	17.0	137	137	7
Centre pontoon cone	8.0 - 3.56	8.0 - 3.56	137	137	5
Periphery pontoons cylinder	12.0	12.0	62	62	7
Periphery pontoons cone	12.0 - 3.58	12.0 - 3.58	62	62	6
Dimension	m	m	mm	mm	m

[1] Only at the top end

4.4.1 Bulkheads

The hull is equipped with two fixed bulkheads and one movable bulkhead. These are highlighted in the structural drawing found in Appendix A.2. The fixed bulkheads goes from the centre column to columns C10 and C11. The movable bulkhead goes from the centre column to column C5 when in the parked position, which will be the position used throughout the modelling process. For the movable bulkhead, the outer end is connected to a circular collar inside the 12 edged frame. This way it can easily be moved along the collar for separation of fish. The dimensions used in the modelling of the bulkheads are listed in Table 4.4. The diameter and thickness for the movable bulkhead are set to preserve the total weight of the bulkhead.

Table 4.4: Bulkhead dimensions used in the RIFLEX model

Member	L [m]	D [m]	t [mm]
Fixed Bulkheads	55	2.05	64
Movable bulkhead	55	1.5	78

4.5 Mooring system

The structure is kept in place by a mooring configuration of eight catenary mooring lines equally spread around the cylinder. The mooring lines are connected to the structure in pairs at the top of given pontoons, where the pontoons are named by what column they are connected to. Table 4.5 shows the numbering of the mooring lines and what pontoon the given mooring line is connected to. The numbering should be seen in context with the structural drawing shown in Figure 4.5. As the spread is symmetric, there is an angle of 45° between each line, with line 1 starting at 22.5° moving clockwise from the positive x-axis through C1.

Table 4.5: Mooring line numbering

Mooring line	1	2	3	4	5	6	7	8
Pontoon	C2	C2	C6	C6	C8	C8	C12	C12

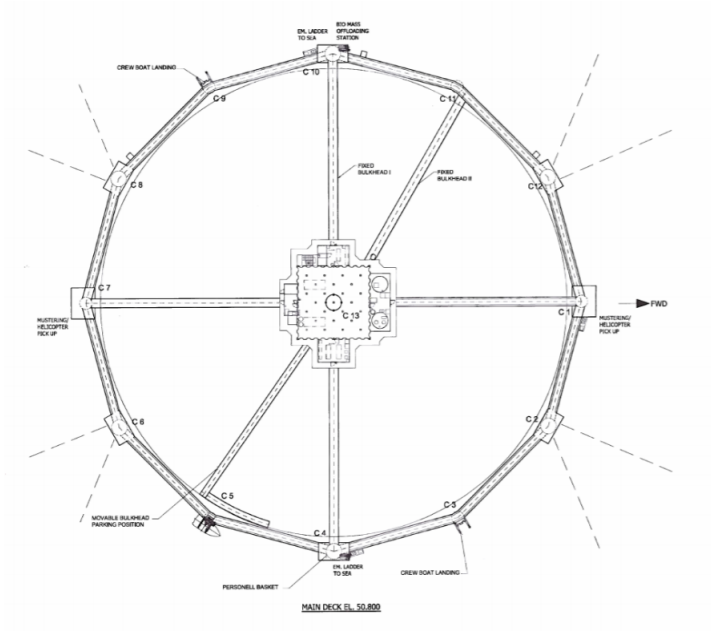

Figure 4.5: Structural drawing of Ocean Farm 1 from a top view

For a catenary configuration, the restoring force preventing horizontal offset is provided by the line weight of the mooring line. The mooring line chosen for the Ocean Farm concept is a multi-component cable composed of studless chain and fibre rope. The properties of the mooring line components are shown in Table 4.6. By use of a combination of the two materials, it is possible to obtain sufficient stiffness for a smaller total weight. The chain

section is used at the bottom part of the mooring line, and is necessary to increase the line's wear resistance and to avoid fatigue failure due to combined bending and tensile actions [38]. The fibre rope is connected to the fairlead in order to reduce the total dead weight of the mooring line.

Table 4.6: Mooring line properties

	Chain	Fibre rope	Unit
Length	1000	100	m
Diameter	88	160	mm
Axial stiffness	680.81	235.44	MN
Minimum breaking load	7051.4	8122.7	kN
Submerged weight	147	4	kg/m
Top tension	196.2		kN
Water depth	150		m

When modelling the mooring lines in SIMA, one can not properly model the cross sections of the mooring line components. Instead, the mooring lines are modelled using the axisymmetric pipe cross section. The dimensions of the mooring line components are then altered to best match the properties of the actual mooring line. The diameter, thickness and density are given values so that the cross-sectional area and submerged weight remains the same as for the original concept. Similarly, the modulus of elasticity is set to give the same axial stiffness (EA) as is the original concept, whereas the minimum breaking load (MBL) is kept from the original concept and can directly be inserted as input in SIMA. Table 4.7 lists the modified mooring line properties as implemented in SIMA.

Table 4.7: Modified mooring line properties used as input in RIFLEX

	Chain	Fibre	Unit
Diameter	124.5	160.0	mm
Thickness	61.2	79.0	mm
Modulus of elasticity	60.0	11.7	GPa
Minimum breaking load	7051.4	8122.7	kN
Material density	13 110	1224	kg/m3

4.6 Fish Net

The fish is kept inside the fish farm by a net stretched over the sides and bottom of the structure. In the design of Ocean Farm 1, emphasis has been put into making the fish farm escape-proof, and the choice of net type and design is an important contribution to this. Where conventional fish farms typically uses nets of fibre material, Ocean Farm 1 uses a polyethylene terephthalate (PET) net called EcoNet. PET is a strong and lightweight

material with a semi-rigid structure. The semi-rigid structure of the net makes it better suited for exposed environments as deformation of the net due to the environments is significantly reduced compared to conventional net types. In addition, it ensures that the mesh will remain intact even with a single wire being cut off, helping to prevent escapes if damage of the net were to happen.

The EcoNet design comes in three sizes; small, large and super large. For the Ocean Farm concept, the small size is used. The net dimensions are listed in Table 4.8 and should be seen in context with Figure 4.6, giving an illustration of the EcoNet mesh and it's design parameters.

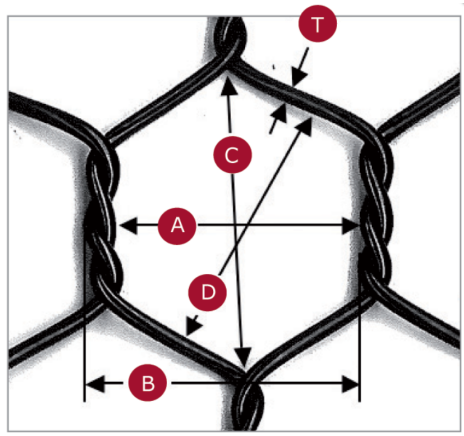

Figure 4.6: Illustration of EcoNet design and dimensions [39]

Table 4.8: EcoNet dimensions/properties

Parameter	Symbol	Value	Unit
Wire thickness	T	2.5	mm
Mesh width	A	30	mm
Mesh pitch	B	40	mm
Mesh height	C	43	mm
Mesh diagonal	D	37	mm
Weight	w	570	g/m^2
Solidity ratio	Sn	0.157	-

4.7 Mass Contributions

The structural mass of the members building up the hull will not provide sufficient mass to obtain the actual operational draft and motion characteristics of the structure. For the real structure, several contributions will add to the total weight, such as equipment, tanks,

handrails, ladders etc. A rough estimation of weight contributions found in [6], provided by Global Maritime are listed in Table4.9.

Table 4.9: Estimate of weight contributions

Contribution	Weight [kg]
Fish feed	600 000
Main deck	350 496
Marine growth	50 000
Ice/Snow	109 000
Aquaculture equipment	151 141
Marine systems and equipment	140 163
Walkways, handrails and ladders	150 870
Foundations	129 961
Deck plates and bulkheads	72 138
Brackets	100 000
Anodes	15 000
Paint, welds and corrosion allowance	329 856
Fixed bulkheads	172 001
Structure in connection with movable bulkhead	195 706
Oil, water, ensile and fuel oil tanks	93 600

Chapter 5

Modelling

This chapter will give a description of the entire modelling process undergone in the thesis. A brief introduction to the different software used in the modelling process is also given. Emphasis has been made on making the model as realistic and correct as possible based on the drawings, dimensions and information available.

5.1 Pontoons

The pontoons were implemented in SIMA as SIMO bodies. The SIMO bodies were made using the Sesam software GeniE and HydroD. Figure 5.1 shows a flowchart of the modelling process. Each step of the process will be further elaborated in the following sections.

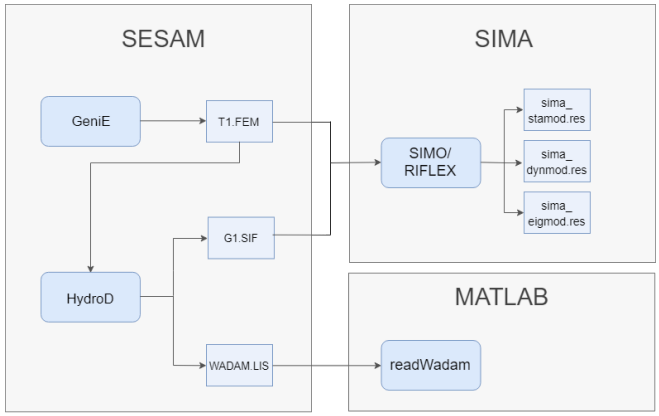

Figure 5.1: Flowchart of the modelling process of the pontoons

5.1.1 GeniE

The first step in the modelling of the pontoons was to create panel models of the pontoons. Two panel models were made - one for the centre pontoon and one for the 6 periphery pontoons. The panel models were made using GeniE, a Sesam software for design and analysis of ships and offshore structures developed by DNV GL [40].

The panel models were made by modeling one quarter of the outer skin of the pontoons. Only one quarter was needed as both Wadam and SIMO has the option of utilizing the double symmetry of the panel models. This contributes in reduced computational time and need of storage capacity. The panel models were made using the dimensions given in Table 4.3.

As the geometry is made, wet sides are defined and a dummy hydrodynamic pressure is applied. As the pontoons are fully submerged, all sides are defined as wet sides, with exception of the top lid as this will be connected to the hull. Lastly, the model is meshed and exported as a FEM file. This file is later imported into the Wadam module in HydroD. Figure 5.2 shows the meshed panel models made in GeniE.

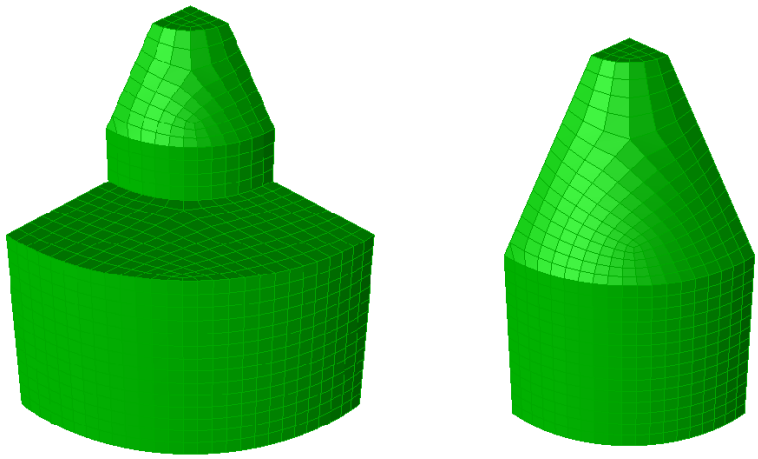

Figure 5.2: Panel model of the centre pontoon (left) and periphery pontoons (right) with mesh size 0.5 m x 0.5 m made in GeniE

5.1.2 HydroD

The hydrodynamic analysis of the panel models was performed using the Wadam wizard in HydroD. HydroD is a Sesam software for computation of hydrostatics, stability, wave loads and motion response for ships and offshore structures [41]. The wave loads and motions are computed by Wadam (Wave Analysis by Diffraction and Morison Theory), which is a program for calculation of wave-structure interaction [42].

The analysis is performed in the frequency domain with frequencies corresponding to periods in the range of 0.5 to 40 seconds. The interval is set to 0.5 seconds. The wave propagation directions are set to vary from 0 to 90 degrees with an interval of 5 degrees. Only values from the first quadrant is chosen due to the double symmetry of the model.

The pontoons are analysed at the operational draft, hence fully submerged at about 30 meters below the free surface. To account for the effect of the columns that the pontoons will be connected to in the SIMO-RIFLEX model, an *additional restoring matrix* is added. The diagonal elements, C_{ii}, with i varying from 1 to 6, are all set to a high value to create an artificial stiff connection to the hull.

Drift forces are included by both pressure integration in all six degrees of freedom and far field integration. This is included to account for slow-drift motions, which are important for moored structures like the one considered in the thesis.

From the hydrodynamic analysis executed in Wadam, the hydrodynamic results were saved as a formatted sequential file (SIF) which will later be the basis for the SIMO bodies in SIMA. Also, the Wadam print file (LIS) was saved in order to perform a mesh convergence study of the hydrodynamic results in MATLAB. The results from the convergence analysis are presented and discussed in Section 6.1.

5.1.3 Implementation in SIMA

The SIF- and FEM-files are imported into SIMA in order to create SIMO bodies of the pontoons. The FEM file includes information about the body geometry, whereas the SIF file includes all the hydrodynamic properties as found from the hydrodynamic analysis in Wadam. When imported into SIMA, the SIMO bodies contains the following properties:

- Structural mass data
- Linear damping matrix
- Hydrostatic stiffness data
- First order motion transfer functions
- First order wave force transfer functions
- Wave drift force
- Frequency dependent added mass, damping and retardation functions
- Added mass matrix at zero- and infinite frequency

In order to assure correct modelling of the pontoons in connection with the hull, some additional features must be added to the bodies, and modifications must be made to some of the data imported from Wadam. This will be further discussed through Sections 5.1.4-5.1.7, before the final SIMO properties will be presented in Section 5.1.8.

5.1.4 Buoyancy

As a default setting in SIMA, a body is assumed to be neutrally buoyant. It is therefore necessary to specify that gravity and buoyancy forces are to be included. While gravity can be included directly inside the body data, buoyancy must be calculated and added manually. Buoyancy is hence included by applying a *specified force* with magnitude of the buoyancy force in the pontoon's vertical centre of buoyancy. The force is given a magnitude equal to the weight of the fluid displaced by the body as expressed in Equation 5.1 below.

$$F_B = \rho g V \tag{5.1}$$

5.1.5 Ballast

Ballast was added to the pontoons by altering the structural mass data of the SIMO bodies. The data being modified included structural mass, moments of inertia and centre of gravity. Ballast was added until the specified operational draft was achieved. The filling ratios used in the SIMA model are given in Table 5.1. From the table one can observe that the filling ratios are somewhat higher than the ones specified by Global Maritime. It is assumed that this occurs as Global Maritime has a better overview of all weight contributions, whereas these weights are compensated for with ballast water in the SIMA model.

Table 5.1: Pontoon filling ratios for the SIMA model compared to the Global Maritime model

Pontoon	Filling ratio SIMA [%]	Filling ratio GM [%]
C2	95.6	88.6
C4	93.9	88.6
C6	95.0	88.6
C8	97.6	89.2
C10	93.7	82.9
C12	99.2	83.9
C13	78.7	37.7

5.1.6 Hydrostatic Stiffness

The hydrostatic stiffness matrix obtained from Wadam included a stiffness contribution in heave, roll and pitch.

> A fully submerged body presents a special case. Firstly there is no waterplane and therefore no metacentre. The forces of weight and displacement will always act vertically through G and B respectively [43].

Looking at the expressions for the restoring forces as defined in Equation 3.31 together with the statement presented above, the restoring coefficients C_{ij} will all become zero for the pontoons. The non-zero entries was therefore set to zero and hence the entire stiffness matrix consist of zero entries only.

5.1.7 Retardation Functions

The retardation functions are used as a way of including frequency dependent added mass and damping in the time domain analyses [44]. In the equation of motion, the frequency dependent added mass and damping are then rewritten as

$$\begin{aligned} \mathbf{A}(\omega) &= \mathbf{A}_\infty + \mathbf{a}(\omega) \\ \mathbf{C}(\omega) &= \underbrace{\mathbf{C}_\infty}_{=0} + \mathbf{c}(\omega) \end{aligned} \tag{5.2}$$

Where $\mathbf{a}(\omega)$ and $\mathbf{c}(\omega)$ are inverse Fourier transforms of the retardation function. The frequency dependent added mass and damping will hence not be used directly in the time domain analysis and are consequently removed from the SIMO body properties.

In order to assure retardation functions that can properly account for the frequency dependency of the hydrodynamic properties, a proper time step and cut factor must be determined. Small time steps and large cut factors leads to increased accuracy, but require longer computational time. The magnitude of the time step is determined such that it is smaller than the time step used in the time domain analysis, whereas the cut factor must be set high enough for the motion to have dissipated to zero. The resulting surge - surge retardation function for the periphery pontoons is shown in Figure 5.3, illustrating good characteristics for retardation functions.

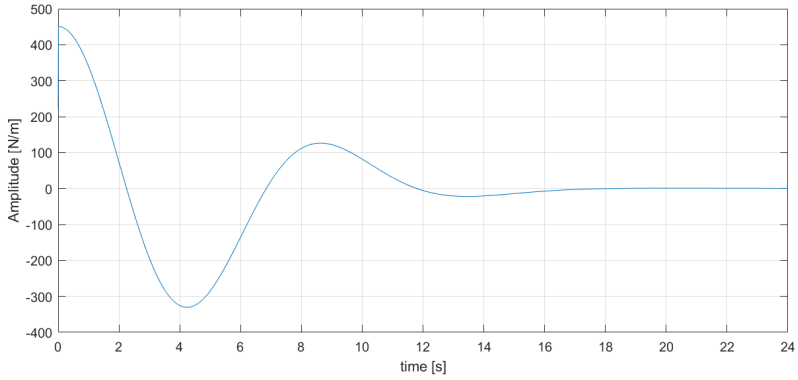

Figure 5.3: Retardation function for surge - surge, time step: 0.01 seconds

5.1.8 Final SIMO Properties

The final SIMO body properties as defined for the pontoons are summarized below.

- Modified structural mass data
- Linear damping matrix
- Modified hydrostatic stiffness matrix
- First order wave force transfer functions
- Wave drift force
- Added mass at infinite frequency and retardation functions

5.2 Hull Structure

The hull structure is modelled as a coupled SIMO-RIFLEX model. All parts of the hull with exception of the pontoons are made as tubular beams in RIFLEX using axisymmetric pipe cross sections with dimensions as given in Table 4.3. The RIFLEX slender elements are shown in Figure 5.4 as the green parts of the figure, whereas the blue parts illustrate the SIMO-bodies. More detailed information regarding different aspects of modelling the RIFLEX parts of the hull will be further discussed in the following sections.

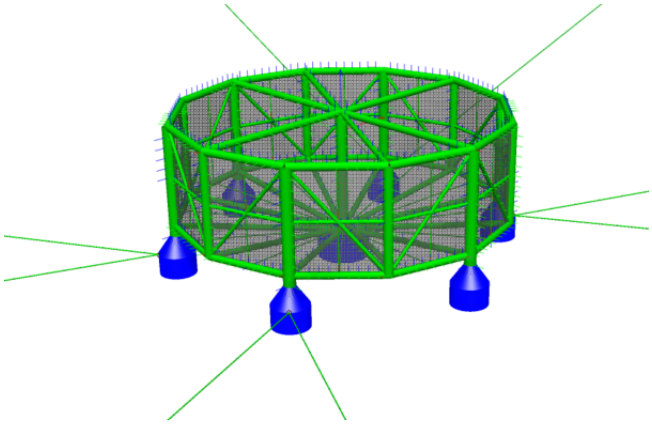

Figure 5.4: Coupled SIMO-RIFLEX model

5.2.1 Movable Bulkhead

As discussed in Section 4.4.1, the hull consists of a movable bulkhead. The movable bulkhead is attached to the centre column and has the possibility of moving the outer end to different locations along the cylindrical shape of the hull. In modelling of the movable

bulkhead, it was considered whether to keep the outer end free or fixed in the location of the parked position. It was decided to fix the outer end to the parked position, which might give a slightly stiffer solution than when the bulkhead is placed at other locations along the cylindrical frame. However, it is not considered to be of much importance for the global dynamic response or structural analysis of the hull.

5.2.2 Mass Contributions

The weight contributions given in Table 4.9 are added to the SIMA model as nodal bodies and external wrappings. A *nodal body* is in RIFLEX defined as a body directly attached to a nodal point with no motion degrees of freedom itself [45]. The component is used to add concentrated masses, weight or buoyancy forces to the system, here represented by tanks for various purposes and the topside structure. An *external wrapping* is a component used to model additional weight or buoyancy to a segment [45] and is here used to model the remaining weights as distributed masses at given parts of the hull. The weight contributions as implemented in RIFLEX are listed in Table 5.2.

Table 5.2: Weight contributions applied as external wrappings and nodal bodies in RIFLEX

Member	Distributed mass [kg/m]
Centre column	758.08
Periphery & intermediate columns	1414.94
Top ring beams & top cross beams	1068.54
Bottom ring beams & bottom radial beams	216.44
Middle ring beams & diagonal supports	110.16
Location	**Concentrated mass [kg]**
Top node of centre column, C13	953 496
TopCrossBeam13_10, 11 meters out from C13	18 600
TopCrossBeam13_7, 22 meters out from C13	22 000
TopCrossBeam13_1, 11 meters out from C13	50 000

5.2.3 Structural Damping

The mass- and stiffness-proportional damping coefficients α_1 and α_2 can be determined using the Rayleigh damping model as described in Section 3.2.2. This requires known damping ratios for at least two frequencies. As this information was not available, typical values for steel structures were used. The chosen values and the resulting mass- and stiffness-proportional damping coefficients are given in Table 5.3. Higher damping levels were chosen for the mooring lines than for the hull as the individual links in the chain component is assumed to give significant friction, contributing to higher damping levels for the mooring lines [6].

Table 5.3: Selected damping levels and corresponding Rayleigh damping coefficients

Property	Hull structure	Mooring lines
λ_1	0.05	0.07
λ_2	0.02	0.05
ω_1	0.0628	0.0628
ω_2	2.094	2.094
α_1	0.0062	0.0086
α_2	0.0177	0.0458

The resulting Rayleigh damping as included in the RIFLEX model is found in Figure 5.5. The plots shows that for waves within the typical wave regime (T = 5-20 s), the structural damping for the hull is within 1-2 %, whereas the mooring lines has damping ratios in the range of 2-4%.

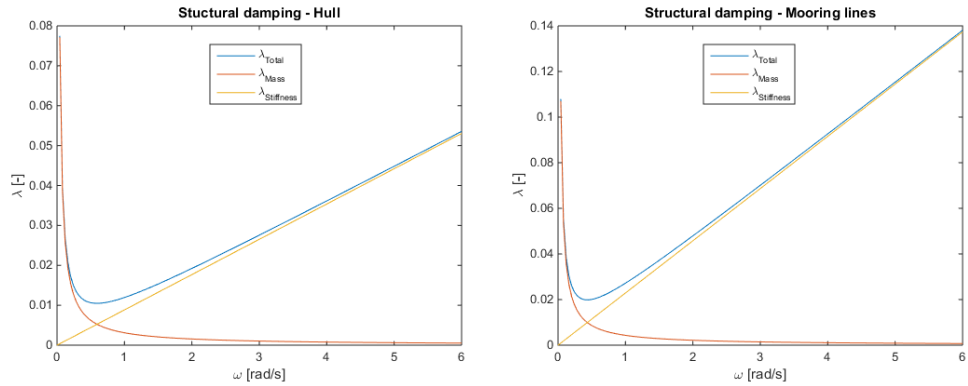

Figure 5.5: Rayleigh damping as included in the RIFLEX model

5.3 Mooring System

5.3.1 Determination of Mooring Line Profile

Catenary equations for elastic, multi-component cables were used in order to determine the mooring line profile. Figure 5.6 shows the schematics of a multi-component cable of three components. For the mooring line used in this thesis, component 1 represents the chain component and component 2 the fibre rope.

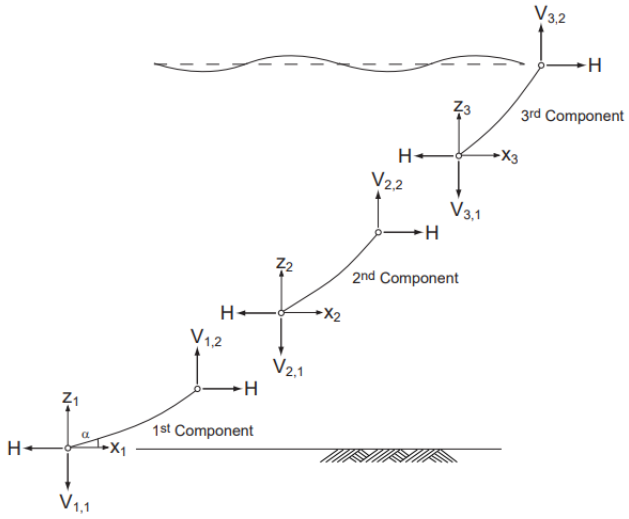

Figure 5.6: Schematic of a multi-component cable [38]

Chain Component

For the chain component, the bottom boundary conditions are defined as

$$\begin{aligned} V_{1,1} &= V_{seabed} \\ x_{1,1} &= 0 \\ z_{1,1} &= 0 \end{aligned} \tag{5.3}$$

As the catenary configuration is horizontal at the touchdown, the vertical force at touchdown, V_{seabed}, is zero. The top boundary conditions for the chain component can now be expressed as

$$V_{1,2} = V_{1,1} + w_1 s_1 \tag{5.4}$$

$$x_{1,2} = \frac{H}{w_1}\left[sinh^{-1}\left(\frac{V_{1,2}}{H}\right) - sinh^{-1}\left(\frac{V_{1,1}}{H}\right)\right] + \frac{Hs_1}{AE_1} \tag{5.5}$$

$$z_{1,2} = \frac{H}{w_1}\left[\sqrt{1+\left(\frac{V_{1,2}}{H}\right)^2} - \sqrt{1+\left(\frac{V_{1,1}}{H}\right)^2}\right] + \frac{Hs_1}{AE_1}\left[\left(\frac{V_{1,1}}{H}\right) + \frac{w_1 s_1}{2H}\right] \tag{5.6}$$

Where s represents the suspended length of the component and w the submerged weight given in N/m.

Fibre Rope Component

For the fibre rope component, the following conditions applies to the bottom boundary

$$\begin{aligned} V_{2,1} &= V_{1,2} \\ z_{2,1} &= z_{1,2} \\ x_{2,1} &= x_{1,2} \end{aligned} \tag{5.7}$$

The top boundary is determined in the same way as in Equations 5.4-5.6. With known top tension, hence known H and $V_{2,2}$, it is possible to solve the system of equations above. The mooring profile obtained is shown in Figure 5.7.

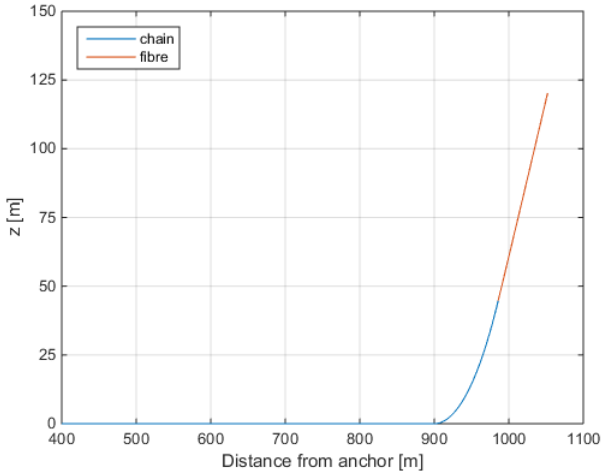

Figure 5.7: Mooring line profile

To find the correct coordinates for the anchor point of each mooring line, the mooring profile was translated to their respective fairlead coordinates and rotated in their given directions. The coordinates obtained for the anchor points are found in Table 5.4. Figure 5.8 shows an illustration of the mooring spread.

Table 5.4: Anchor coordinates

Mooring line	x-coordinate	y-coordinate
1	1019.6	-430.1
2	450.2	-999.4
3	-450.2	-999.4
4	-1019.6	-430.1
5	-1019.6	430.1
6	-450.2	999.4
7	450.2	999.4
8	1019.6	430.1

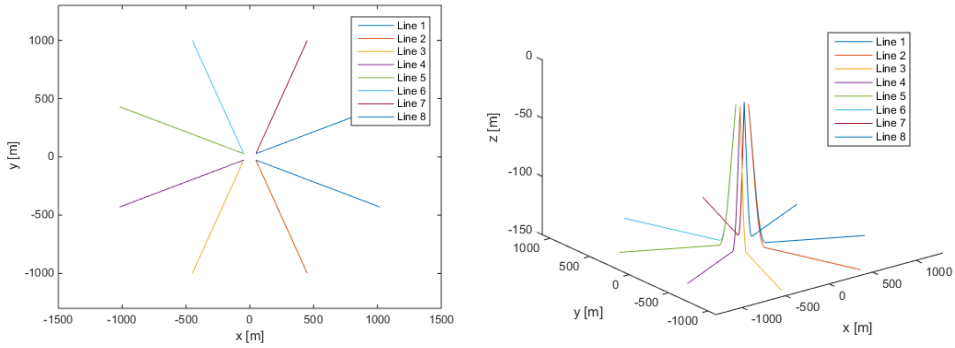

(a) Top view

(b) Side view

Figure 5.8: Mooring spread

5.3.2 Implementation in RIFLEX

The mooring lines are modelled as axisymmetric pipe cross sections with dimensions and anchor coordinates as given in Table 4.6 and 5.4, respectively. Pretension is accounted for by applying the constraint *fixed or prescribed* for the anchor nodes. The mooring lines are then first defined as stress-free straight lines, before the anchor node is fixed at the anchor location during the static analysis. When accounting for volume forces and specified displacements in the static analysis the mooring lines will fall into place with pretension as given in Table 4.6. Figure 5.9 shows the prescribed configuration as modelled in SIMA.

DNVGL's offshore standard for position mooring [46] and OrcaFlex chain properties [47] were used in order to determine the hydrodynamic force coefficients for the mooring line components. The drag force and added mass coefficients as implemented in SIMA are listed in Table 5.5.

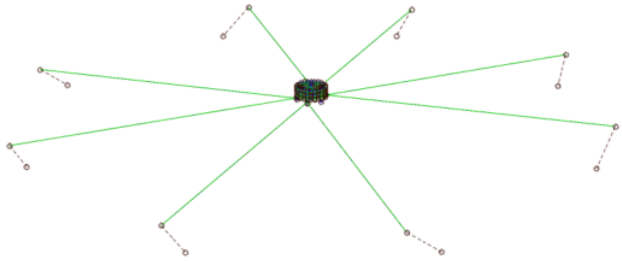

Figure 5.9: Illustration of the mooring lines as modelled in SIMA

Table 5.5: Hydrodynamic force coefficients as implemented in RIFLEX

	Chain	Fibre rope
$C_{D,\,\text{transverse}}$	2.4	1.6
$C_{D,\,\text{longitudinal}}$	1.15	-
$C_{A,\,\text{transverse}}$	1.0	1.0
$C_{A,\,\text{longitudinal}}$	0.5	1.0

5.4 Net

Due to the twelve sided cylinder shape of the hull, Ocean Farm 1 consists of 24 net panels; 12 rectangular side panels and 12 triangular bottom panels. The net is modelled in RIFLEX using slender lines with a fish net cross section at each of the 24 panels. By use of the fish net cross section instead of other alternative methods of modelling the net, the damping due to the net is easily included in the model. This is important to the global response of the fish farm as the net gives a significant damping contribution.

In order to acquire the input for the fish nets in RIFLEX, the equations listed below are used. n here represents the total number of twines of the net panel, $n_{vertical}$ the number of twines in the vertical direction, A_{twine} the twine area and A_{net} the area of the given net panel [48]. Finally, the axial stiffness, k can be calculated.

$$n = \frac{L}{d} \cdot Sn \qquad n_{vertical} = \frac{L}{\lambda} \tag{5.8}$$

$$A_{twine} = \frac{\pi}{4} d^2 \qquad A_{net} = A_{twine} \cdot n \tag{5.9}$$

$$k = E \cdot A_{twine} \cdot n_{vertical} \tag{5.10}$$

By use of the current force model as described in Section 3.3, each net is assigned their respective velocity reduction factor, r, based on the net panel drag coefficient for each net panel. This is summarized in Table 5.6. Net 4-9 are assigned a velocity reduction factor equal to 1, hence no velocity reduction as these will experience the full current velocity. The remaining nets will on the other hand experience a reduced velocity as they are placed in the wake of the nets in front. These values are based on an incoming current in the direction of the positive x-axis, hence $\theta = 0°$. This is kept constant through all analyses, while the incoming direction of the waves may differ. α is then defined as the angle between the x-axis and the net normal in the direction of the flow.

Table 5.6: Drag force coefficients and velocity reduction factor of the side and bottom net panels

Net no.	$\pm\alpha$	C_D	r
1, 12	15	0.1889	0.9131
2, 11	45	0.149	0.9315
3, 10	75	0.0799	0.9632

The added mass coefficients for the net cross sections are assumed to be equal 1.0. This assumption is based on assuming the threads of the fish net can be seen as circular cylinders in potential flow [49].

5.5 Environmental Conditions

The environmental conditions applied in the analyses are based on the reference report from model tests performed by MARINTEK. This sea state is again based on the 100-year contour line. The 100-year environment will in this report be referred to as Load Case 1 and can be summarized as

- Waves: H = 5 m, T = 11 s
- Wind: U_w = 30 m/s, $\theta = 0°$
- Current: U_c = 0.75 m/s, $\theta = 0°$

The model tests are performed using irregular waves with the input parameters as listed in Load Case 1. For the thesis, only regular waves will be used as SIMA does not support irregular waves for models including fish net cross sections. To account for the fact that an irregular sea state with H_s = 5 m includes wave heights much larger than 5 meters, the conversion from irregular to regular waves as described in Section 3.1.4 is used. The conversion makes it possible to estimate the largest probable wave height in an irregular sea state, and hence one can run the analysis using regular waves with H = H_{max}. This sea state is referred to as Load Case 2 and can be summarized as

- Waves: H = 9.9 m, T = 11 s
- Wind: U_w = 30 m/s, $\theta = 0°$

- Current: $U_c = 0.75$ m/s, $\theta = 0^\circ$

Based on the reference report, the wind is defined by the NPD wind spectrum, with a reference height of 10 meters above the mean water level. The current is placed at a water depth of 15 meters below the free surface.

Chapter 6

Results

Throughout the following chapter, the results obtained from the analyses conducted will be presented. This includes a convergence study in addition to a static, a dynamic and an eigenvalue analysis. Some results will be compared to the MARINTEK *reference report* [7]. However, as previously mentioned the design characteristics of which the SIMA model is based on correspond to an updated version of the model made for the ocean basin tests. Results can therefore not be compared directly. The model test results will hence be used as an indication of whether or not the results obtained are within the correct magnitudes.

When referring to the reference report, keep in mind that the coordinate system is defined in the opposite direction of what is defined in the thesis. Waves, winds and currents are hence applied in the opposite direction in the model tests than in the thesis.

6.1 Convergence Study

A convergence study of the hydrodynamic results obtained from HydroD is conducted in order to determine what mesh size to use for the pontoon panel models. The choice of mesh size is made as a compromise between desired accuracy and computational time and is important in order to ensure as realistic results as possible. Reduced mesh size yields increased computational time and use of storage capacity. It is therefore preferable to keep the mesh size as large as possible while still ensuring sufficient accuracy in the results.

The convergence analysis was carried out by considering the frequency dependent hydrodynamic properties of the panel models, hence the added mass, radiation damping and the first order wave force transfer functions. These were plotted for all mesh sizes in all six degrees of freedom. The mesh size was initially set to 1.5 m x 1.5 m, decreasing the mesh

by 0.25 meters per step. A selection of the results obtained for the panel model of the periphery pontoons are shown in Figure 6.1 and 6.2.

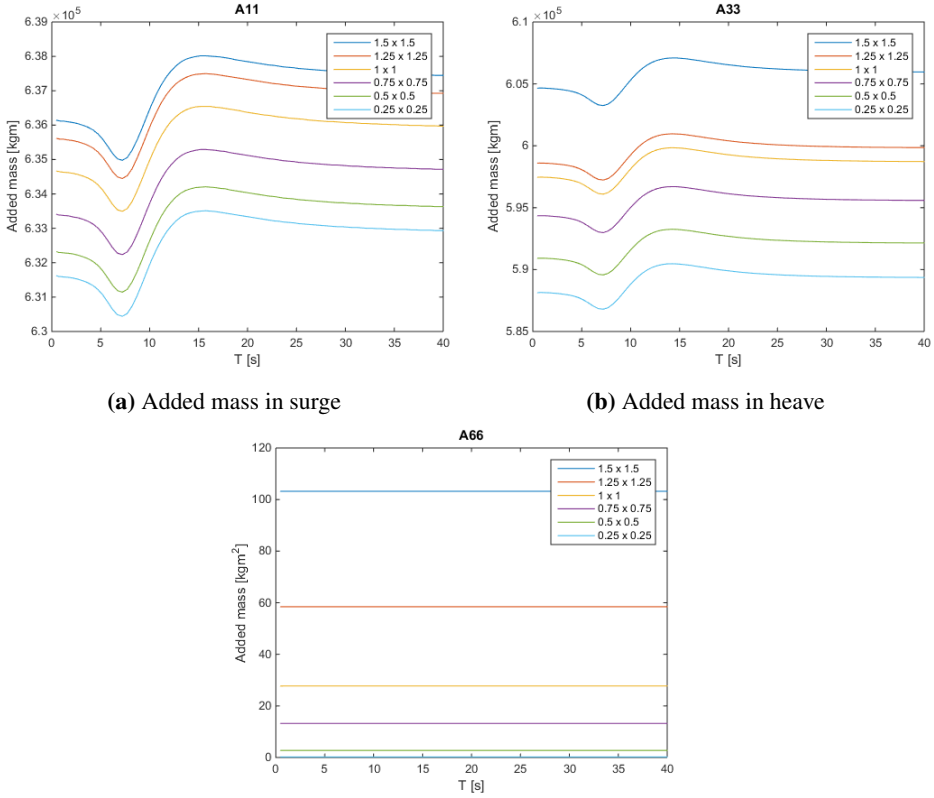

(a) Added mass in surge

(b) Added mass in heave

(c) Added mass in yaw

Figure 6.1: Convergence of added mass in surge, heave and yaw for the periphery pontoon panel model

For the first five degrees of freedom, the results obtained for all hydrodynamic properties seem to converge already at relatively coarse mesh sizes. For these degrees of freedom, the largest difference between the results obtained for the coarsest and finest mesh size was found to be 20 %, which was found for the first order wave force transfer function in heave. As for the added mass, the plots do not immediately seem to converge. However, the largest difference between the results obtained for the coarsest and finest mesh size is here between 0.7-2.8 %, with the largest differences found in heave. Similarly, the differences between the results for the coarsest and finest mesh size for the radiation damping lies in the range of 0.2-3.9 %, also here with the largest differences found in the heave direction.

The convergence of the hydrodynamic properties in the yaw direction do not show the same tendencies as for the five other directions. The results are converging at a slower

rate, showing that the coarser mesh sizes gives quite bad accuracy. Based on these considerations, a mesh size of 0.5 m x 0.5 m was chosen for the panel models. At this mesh size the results in the yaw direction seem to achieve a sufficient level of accuracy. Similar tendencies are found for the hydrodynamic properties for the centre pontoon, and the same mesh size is therefore chosen for both models. The hydrodynamic results obtained for the chosen mesh size for the centre pontoon and periphery pontoon panel models are found in Appendix B.

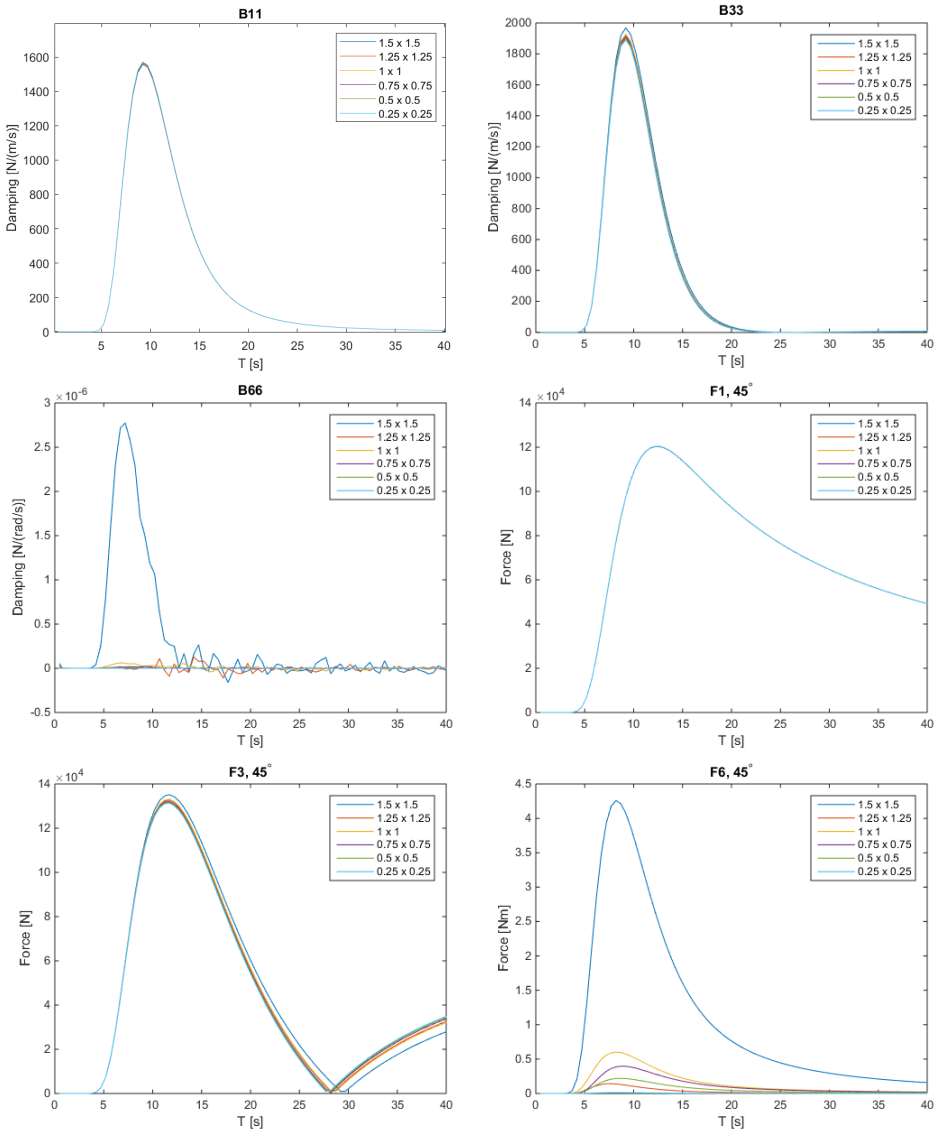

Figure 6.2: Convergence of radiation damping and first order wave force transfer functions (wave propagation angle of 45 °) in surge, heave and yaw for the periphery pontoon panel model

6.2 Static Response

This section provides the results obtained from the static analysis conducted in SIMA. Emphasis has been put on making the static configuration as correct as possible with reference to the specified operational draft before adding the static current load to the system. Further, static forces and bending moments for selected members of the hull will be presented and discussed.

6.2.1 Global Displacements

The first step of the static analysis is performed without the static force of the current acting on the structure. By this approach the static analysis finds the static configuration of the structure in still water, only accounting for self-weight and buoyancy. Figure 6.3 shows a snapshot from SIMA illustrating the static configuration obtained from the initial static analysis.

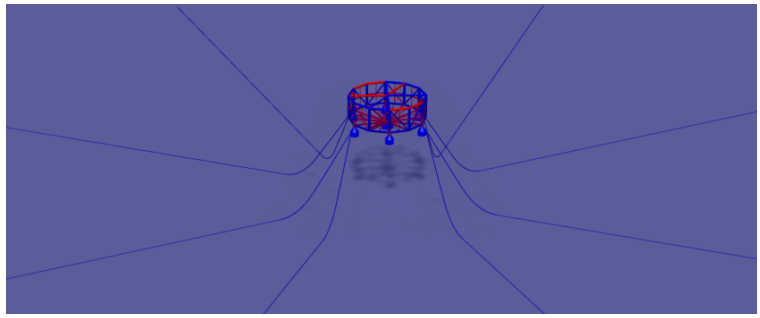

Figure 6.3: Snapshot of the static configuration in SIMA

The coordinates along the centre column, C13, is extracted and plotted against the initial configuration for comparison. This is illustrated in Figure 6.4a. The initial configuration corresponds to the centre column being placed at the origin of the defined coordinate system, with z-coordinates corresponding to the specified operational draft of the design. It is observed that the deviation in all directions is within 4 cm, which is considered small considering the large dimensions of the structure. It is also observed a slight deviation along the column length in all directions, suggesting that there is a slight initial heeling angle. Again, considering the large dimensions of the structure, this is not considered to be of any importance for further results.

The mooring line coordinates from the static configuration was also extracted and plotted against the profile found using catenary equations as explained in Section 5.3. Figure 6.4b shows what is referred to as mooring line 4 for both solutions. The deviation is largest near the fairlead and touchdown locations. This is caused by the fairlead being moved somewhat further down on the pontoons in the RIFLEX model than initially intended when finding the mooring profile. However, overall the mooring line profiles are considered quite similar considering that approximations have been made in both solutions.

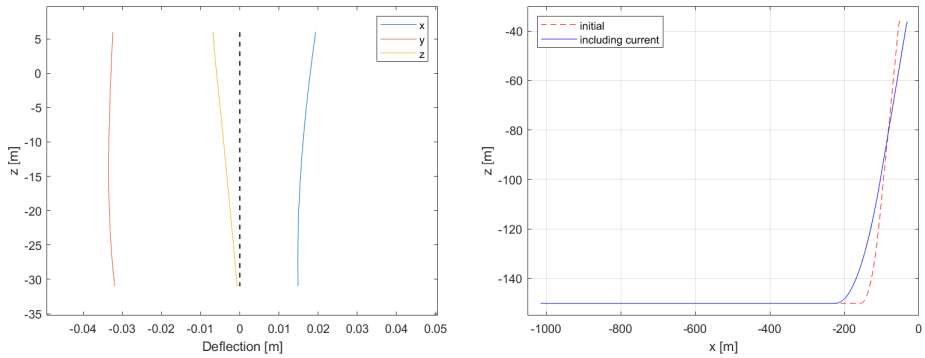

(a) Deviation from initial configuration along C13 **(b)** Deviation along line 4

Figure 6.4: Comparison of initial and static configuration

6.2.2 Current Calibration Test

In the model tests performed by MARINTEK, a current load test was performed by applying three different current velocities at 15 meters water depth, with an incoming angle of 180 degrees. A similar test was executed in SIMA in order to tune the drag coefficients for the structural members of the hull. For the tests performed in SIMA, the current is given an incoming angle of 0 degrees, hence in the opposite direction of the model tests. It is however assumed that the results are comparable due to the symmetry of the structure. The results obtained from both tests are summarized in Table 6.1.

Table 6.1: Current calibration test

U_c [m/s]	X-offset MARINTEK [m]	X-offset SIMA [m]
0.5	-8.53	7.0
0.68	-15.97	15.7
0.82	-22.43	23.2

The results show that for low current velocities, the SIMA model gives a somewhat smaller offset than what was recorded in the model tests, whereas the opposite applies to higher velocities. For the current velocity of 0.68 m/s, the two mooring line designs give quite similar offsets. Considering the fact that the mooring systems compared are based on different designs, the results are not expected to fully follow each other for all current velocities. However, an important observation made is that the SIMA model give offsets of the same magnitude as what was measured in the model tests, implying that further results in terms of displacements can be expected to be in good agreement with the recorded results from the model tests.

6.2.3 Global Displacements Due to Current Forces

The estimated 100-year current velocity $U_{C,100}$ = 0.75 m/s is now applied as part of the static analysis with an income angle of zero degrees. As one can observe from Figure 6.5, the current load causes the structure to move sideways along the x-axis. The offset in the x-direction is found to be 19.6 meters. Comparing with the surge offsets presented in the current calibration test in the previous section, an offset of 19.6 meters for a current velocity of 0.75 m/s seems reasonable. In addition, the current load causes the structure to obtain a slight heeling angle, corresponding to a pitch angle of 0.13 degrees. Lastly, the current causes the structure to be dragged somewhat downwards, such that the air gap is reduced by 36 cm at the top node of the centre column.

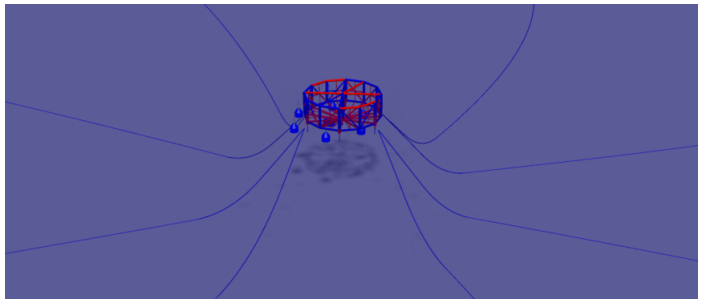

Figure 6.5: Snapshot of the static configuration including current in SIMA

Figure 6.6 shows the new mooring line profile of what is referred to as mooring line 4 compared to the profile obtained without current forces applied to the system. It is observed that the current load causes line 4 to be more lifted from the sea bed, moving the touchdown by 45 meters in the negative x-direction.

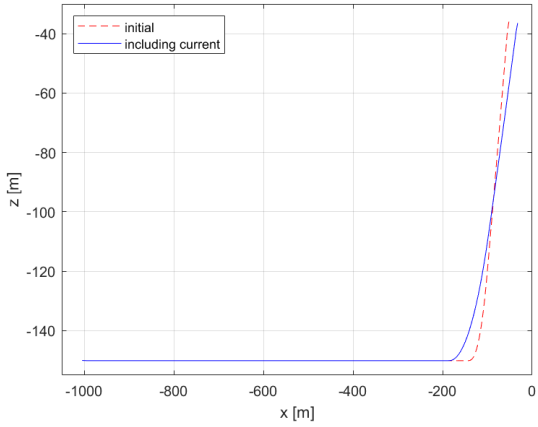

Figure 6.6: Comparison of mooring profile with and without current forces for mooring line 4

6.2.4 Forces and Moments

Each of the twelve frames of the 12 sided hull are built up by the following structural members

- Two vertical columns
- Three horizontal columns referred to as the top, mid and bottom ring beams, these are connecting the two vertical columns horizontally
- One diagonal support
- Two bottom radial beams connecting the vertical columns to the centre column

Frame 1 is then located between column C1 and C2, frame 2 between C2 and C3 and so on. When reading the resulting maximum forces and moments from the static analysis, the maximum value in each of the twelve vertical columns were extracted and compared to each other in order to see which column experiences the largest forces and moments. This procedure is repeated for all structural members listed above.

Bending Moments

Figure 6.7 shows the resulting maximum bending moments for the different structural components of the hull and in what frame they are located. In order to make the measured bending moments in the different parts of the hull comparable, the bending stresses over the different cross section areas are calculated. The maximum bending moments measured in the different parts of the hull and the corresponding maximum bending stresses are summarized in Table 6.2. The maximum bending stresses are generally small, with the largest utilization with reference to the yield strength of the material being 25.21 %. This occurs for the top ring beam located in frame 11.

Table 6.2: Maximum bending stresses for the structural components of the hull

Members	M_{tot} [kN]	σ_b [MPa]	% of σ_y [%]
C13	2009	5.16	1.45
C11	9141	37.9	10.68
Diagonal support 11	130.5	6.06	1.71
Mid ring beam 12	219.4	19.5	5.49
Top ring beam 11	11480	89.5	25.21
Bottom ring beams 7	2299	23.2	6.53
Bottom radial beams 7	4689	88.2	24.84

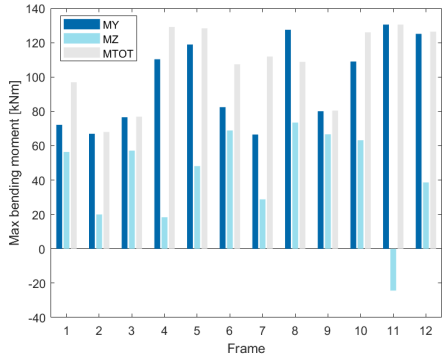

(a) Diagonal supports

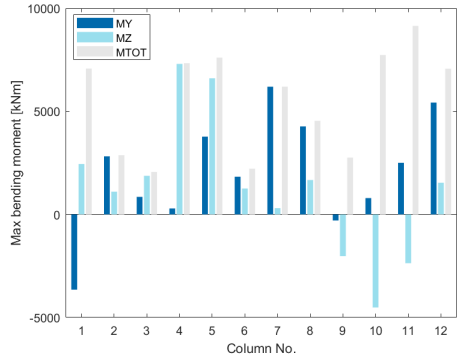

(b) Vertical columns

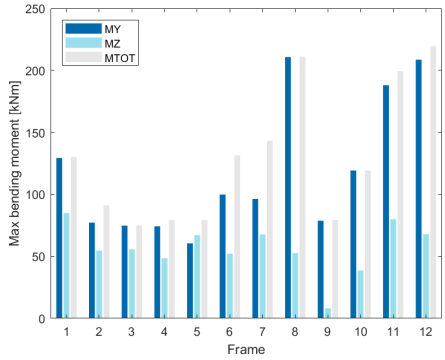

(c) Mid ring beams

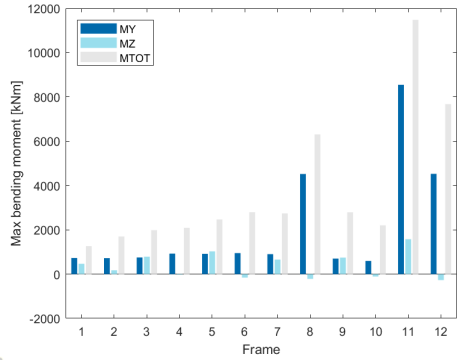

(d) Top ring beams

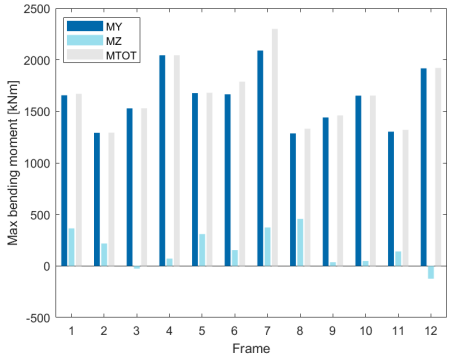

(e) Bottom ring beams

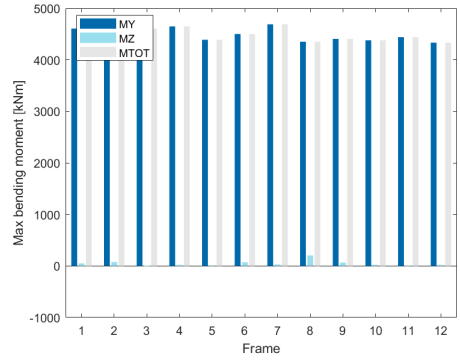

(f) Bottom radial beams

Figure 6.7: Maximum bending moments for the different structural members of the hull

Effective Tensions

Figure 6.8 shows the resulting maximum effective tensions for the different structural components of the hull. It is observed that all bottom ring beams have their maximum value in compression, implying that the columns must be checked for vulnerability to buckling. The same applies to several of the vertical columns, diagonal supports and top ring beams. Dividing by the structural components respective cross sectional areas, the axial stresses of the members are obtained. For the members in compression, the axial stresses are compared to the Euler buckling stress defined as

$$\sigma_{cr} = \frac{P_{cr}}{A} = \frac{\pi^2 EI}{A\, l_k^2} \tag{6.1}$$

Where E is the modulus of elasticity, I is the moment of inertia, A is the cross section area and l_k is the buckling length. Table 6.3 lists the structural components experiencing the largest effective tensions and their corresponding axial stresses. If the maximum tension is found in compression, a comparison to the critical buckling stresses of the respective components is given.

Table 6.3: Maximum axial stresses for the structural components of the hull

Members	P_{max} [kN]	σ_a [MPa]	% of σ_{cr} [%]
C13	-11666	-25.98	1.11
C11	-2253.9	-6.44	0.09
Diagonal support 8	-1348.4	-14.75	2.87
Mid ring beam 11	1693.8	36.5	-
Top ring beam 11	-561.14	-1.95	0.04
Bottom ring beam 10	-32860	-26.29	0.28
Bottom radial beam 8	1802.5	11.78	-

It is observed that the mid ring beam located in frame 11 experiences the largest axial stress among the hull components, whereas the bottom ring beam located in frame 10 experiences the largest compressive axial stress. One can also observe that all structural members are far from buckling as the largest utilization with reference to the critical buckling stress is found to be 2.87 %. This occurs for the diagonal support located in frame 8.

Comparing the critical buckling stresses of the hull components with the yield strength of the material one can assume that yielding is likely to occur long before buckling takes place. Bending moments will therefore be of greater importance compared to the axial forces for the structural components of the hull.

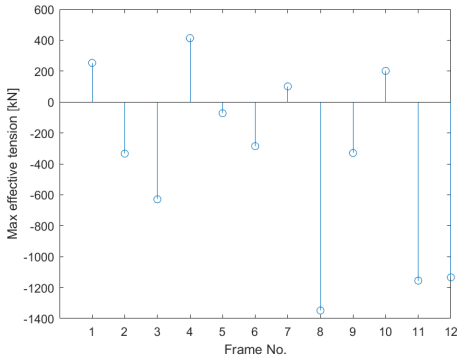

(a) Diagonal supports

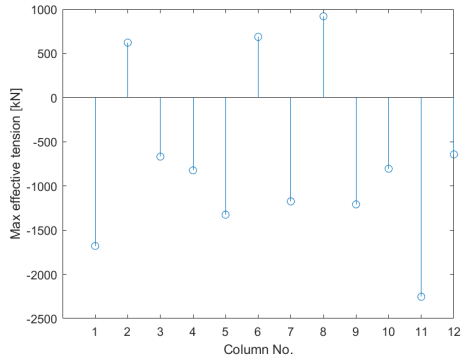

(b) Vertical columns

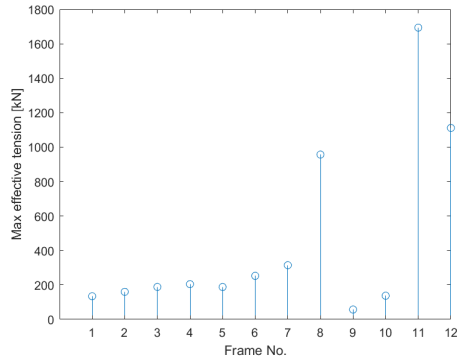

(c) Mid ring beams

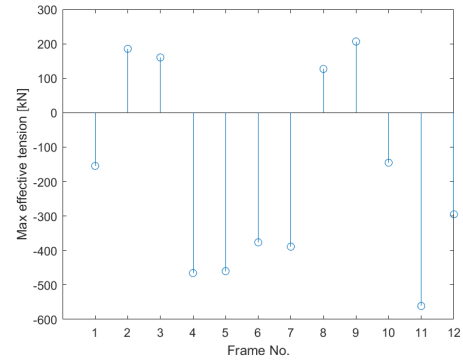

(d) Top ring beams

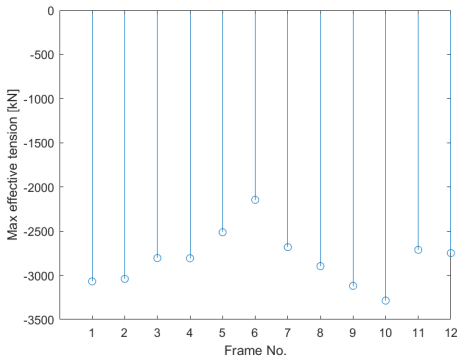

(e) Bottom ring beams

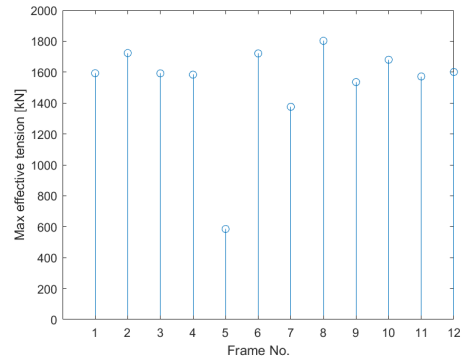

(f) Bottom radial beams

Figure 6.8: Maximum effective tensions for the different structural members of the hull

Mooring Line Tensions

Figure 6.9 shows the effective tension along the mooring lines. The maximum tensions are found for line 3 and 6. This occurs as a consequence of the excursion caused by the current forces, where line 3 and 6 are the lines with the largest distance from the fairlead to the touchdown locations. A larger portion of these mooring lines are hence lifted from the sea bed compared to the remaining mooring lines. Consequently, line 1 and 8 experience the smallest tensions as these have the smallest distance from the touchdown to the fairlead locations. A larger portion of the line length is hence extended along the sea bed.

Generally, it is observed for all mooring lines that the effective tension is nearly constant along the length of the fibre rope component, with the peak value located at the fairlead. For the chain component the effective tension is at it's highest at the transition to the fibre rope component. From the top end to the touchdown location the effective tension decreases.

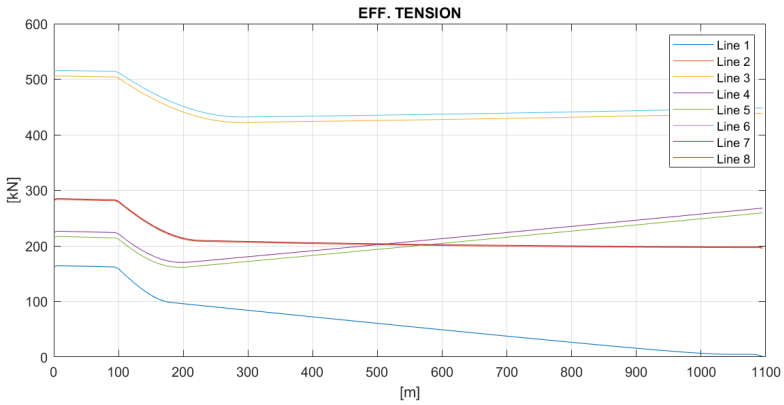

Figure 6.9: Effective tension along length of the mooring lines

6.3 Dynamic Response

6.3.1 Load Case 1

The following section will present the global response of the fish farm in regular waves with environmental conditions as defined for Load Case 1. The wave propagation direction will vary between 0, 45 and 90 degrees, whereas the wave height of 5 meters and wave period of 11 seconds are kept constant through all analyses. See Section 5.5 for further details relating the environmental conditions defined for the load case.

Pontoons Motions

In order to assess some important characteristics of the dynamic response of the hull structure, the pontoon motions will be briefly discussed. Figure 6.10 shows the vertical displacements of the pontoons as a function of time for the in-line direction, hence $\theta = 0°$.

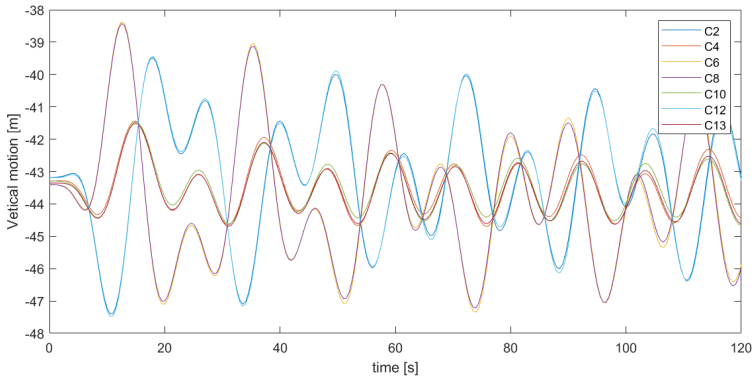

Figure 6.10: Vertical pontoon motions for H = 5 m, T = 11 s, $\theta = 0°$

It is observed that for a wave direction parallel to the positive x-axis, the pontoons located $\pm$ 22.5° relative to the wave direction experiences the largest vertical motions. These are the pontoons named C2, C6, C8 and C12 as seen from the structural drawing found in Appendix A.1. As expected, the centre pontoon has the smallest vertical motions. It is also observed that the pontoons C6 and C8 move out of phase with the pontoons C2 and C12, implying that the hull structure behaves like a rigid structure.

The vertical displacements are largest as the first wave passes the structure. As more waves passes, the pontoon motions starts to stabilize. A slight decrease in the vertical motions are still occurring for each new wave at t = 121 seconds, implying that the transient state has not fully dissipated after 11 wave periods.

Displacements

The displacements at the top node of the centre column were extracted and plotted for comparison with the displacements obtained from the model tests. Figure 6.11 shows the displacements in the x-, y- and z-directions. As mentioned in the preface of this chapter, the values are not directly comparable. They will however be used as a guideline as to what magnitude the results should be in.

The largest recorded surge offset is found for $\theta = 0°$, with an offset of 38.23 meters from the origin, about 18.6 meters from the initial static configuration due to the current forces. The mean offset is found to be 32.93 meters. The maximum surge offset obtained in the model tests was found to be 36.8 meters, with a mean value of 28.4 meters.

The sway motions were generally small for all wave directions, with a maximum offset of 7.659 meters for $\theta = 90°$. For the in-line wave direction, $\theta = 0°$, displacements in the transverse direction were almost not present, with a maximum displacement of 34 cm. For the model tests, the largest recorded sway offset is only given for the in-line wave direction, where the maximum value was found to be 4.524 meters. The large difference obtained is assumed to occur partly as a consequence of the dynamic analysis being performed in regular waves, causing little transverse motions compared to a dynamic analysis under irregular waves.

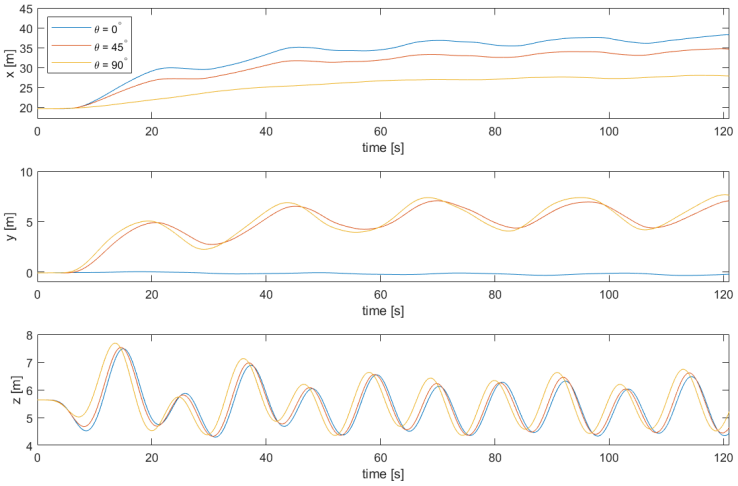

Figure 6.11: Displacements for the top node of the centre column for Load Case 1

Comparing the x-displacements obtained for a wave direction of 0 degrees with the y-displacements for a wave direction of 90 degrees, the offsets are generally much larger for the in-line direction. This suggests that the mooring system gives higher restoring forces for the transverse direction than for the in-line direction, coinciding well with the behaviour observed from the model tests.

The largest recorded heave motions were found for $\theta = 90°$, with a value of 2.05 meters from the initial position of z = 5.64 meters. This occurred for the first wave passing the structure. However, the vertical motions stabilizes around $\pm$ 1 meter from the initial position for the second half of the analysis. The maximum recorded heave motion for the model tests was found to be 0.95 meters. The difference in maximum recorded heave motions could suggest some lack of damping in the SIMA model resulting in larger dynamic responses. It can also partly be due to the changes made to the design.

Accelerations

The nodal displacements for the top node of the centre column were differentiated twice in order to obtain the nodal accelerations. Accelerations at this location are of interest as

they give an indication of the level of the accelerations experienced at the topside of the fish farm. Accelerations should be small in order to assure safe operations and welfare both for the fish and the crew on board. Table 6.4 lists the maximum nodal accelerations obtained from the dynamic analysis in SIMA and for what wave direction it occurred. The maximum accelerations measured in the model tests are also given.

Table 6.4: Global accelerations for the top node of the centre column for Load Case 1

	Max SIMA [m/s^2]	Wave Direction [deg]	Max MARINTEK [m/s^2]
a_x	0.8649	0	0.4728
a_y	0.6304	90	0.1196
a_z	-0.8267	90	0.4728

The largest acceleration in the y- and z-directions were found for a wave direction of 90 degrees, whereas the largest acceleration in the x-direction was obtained for a wave direction of 0 degrees. The accelerations recorded were generally small in all directions, but are much higher than the accelerations measured in the model tests. This is as expected since larger displacements were recorded for the SIMA model than for the model tests, and hence the accelerations will consequently also be larger.

Figure 6.12 shows the nodal accelerations for the different wave directions as a function of time. Compared to the displacement plots given in Figure 6.11, one can observe a strong correlation between the magnitude of the accelerations and displacements measured for the different wave directions. For example, for a wave direction of 0 degrees the y-displacements were extremely small, resulting in accelerations in the y-direction close to zero m/s^2.

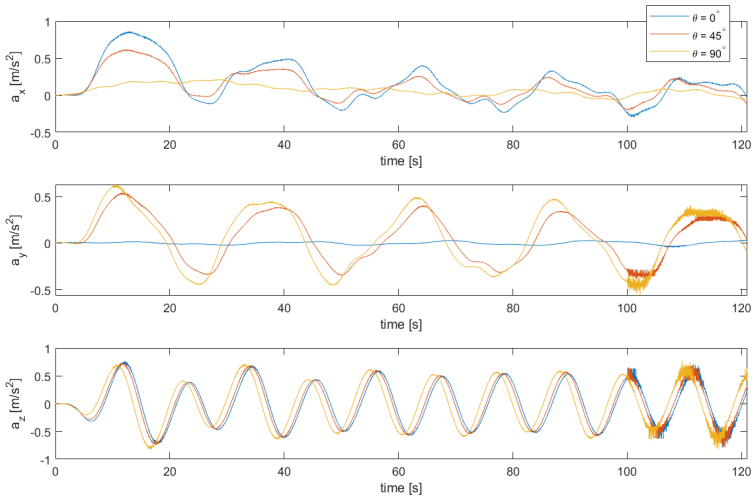

Figure 6.12: Accelerations for the top node of the centre column for Load Case 1

Mooring Line Tensions

Figure 6.13 shows the maximum effective tensions for the mooring lines for different wave directions. As for the static configuration, the mooring lines experiencing the largest tensions are line 3 and 6, with the maximum value found in line 3.

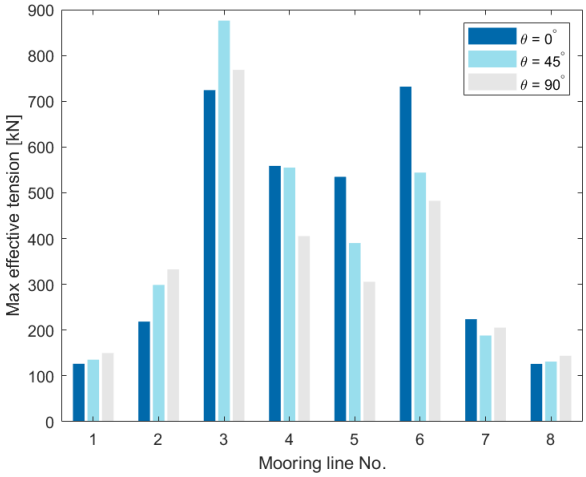

Figure 6.13: Maximum mooring line tensions for different wave directions

The highest recorded line tension for Load Case 1 is 876.2 kN. This gives a safety factor of 9.27 for the fibre rope component with a minimum breaking load of 8122.7 kN. Compared to the reference report, the largest line tension recorded was 1944 kN. This occurred for the largest recorded surge motion of 36.8 meters. For the mooring line used in the model tests, this gave a safety factor of 2.61 as the minimum breaking load for the mooring line was significantly smaller for this concept.

6.3.2 Load Case 2

The following section will present the global response of the fish farm in regular waves with environmental conditions as defined for Load Case 2. The sea state is based on using the significant wave height of the 100-year environment to estimate the most probable largest wave height and is therefore considered as an extreme environmental condition. For this condition the relative wave heights may exceed the still water airgap. See Section 5.5 for further details relating the environmental conditions defined for the load case.

Only the in-line condition will be presented, hence $\theta = 0°$. The results obtained will be compared with results from similar simulations using wave heights of 3, 5 and 7 meters. One can then compare the effect of increasing wave heights on the different aspects of the dynamic response.

Displacements

Figure 6.14 shows the displacements in the x-, y- and z-directions for increasing wave heights. The displacements caused by the regular waves shows tendencies of regular response time histories. Generally, increasing wave heights results in increasing dynamic responses. The exception is found for the vertical displacements for the second half of the time domain analysis. Here, the vertical displacement stabilizes at about the same magnitude for all wave heights. The largest wave height is then not necessarily causing the largest vertical motions.

The largest surge offset recorded for Load Case 2 is 55.14 meters, about 35 meters from the initial position due to the static current load. This is a quite large offset, illustrating that the mooring system modelled may be too soft as the model test results did not show the same increase in surge motions for tests with increasing significant wave heights.

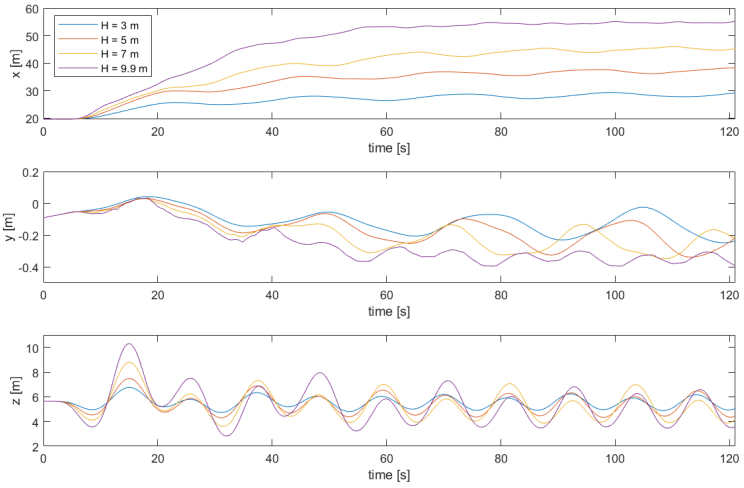

Figure 6.14: Displacements for the top node of the centre column for Load Case 2

Accelerations

Figure 6.15 shows the nodal accelerations at the top node of the centre column for increasing wave heights. The maximum accelerations recorded are 1.34 m/s^2 in the lateral direction and 1.797 m/s^2 in the vertical direction. In the transverse direction, accelerations were generally small for all wave heights, with a maximum value of -0.0397 m/s^2. All maximum accelerations were found for the extreme environmental condition, H = 9.9 meters.

Generally, it is observed that for the first half of the analysis, larger wave heights yields larger accelerations. However, during the second half of the analysis, the differences in ac-

celerations for increasing wave heights even out. With time, it is therefore not necessarily the largest wave heights are causing the largest accelerations.

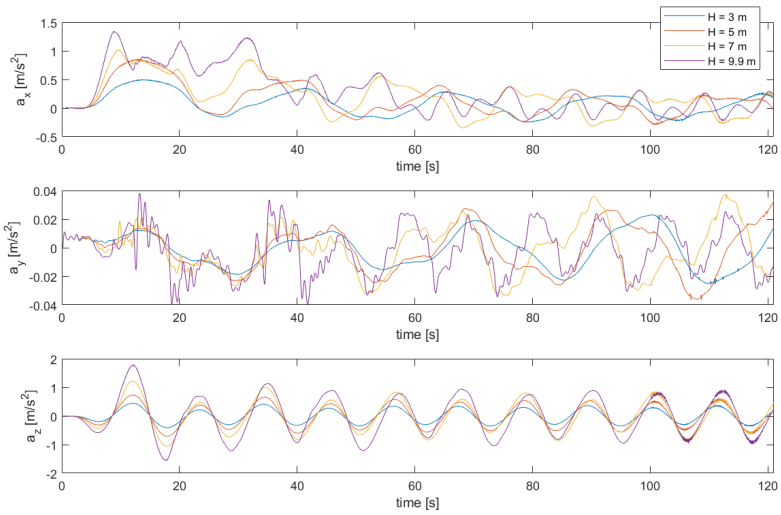

Figure 6.15: Accelerations for the top node of the centre column for Load Case 2

Mooring Line Tensions

Figure 6.13 shows the maximum effective tensions for the mooring lines for increasing wave heights. It is observed that line 3-6 experience increasing line tensions for increasing wave heights. This occurs as the mooring lines are lifted from the sea bed due to the increasing excursion for increasing wave heights. At the same time, line 1,2,7 and 8 will have more of the chain component laid down along the sea bed as the surge offset increases, yielding decreasing mooring line tensions for increasing wave heights.

The highest recorded line tension for Load Case 2 is 1868 kN, giving a safety factor of 4.35 for the fibre rope component. This occurs for line 4 during the extreme environmental condition with wave height H = 9.9 meters. The high safety factor illustrates that the mooring system is safe even for extreme conditions as much higher line tensions are needed in order to reach the minimum breaking load.

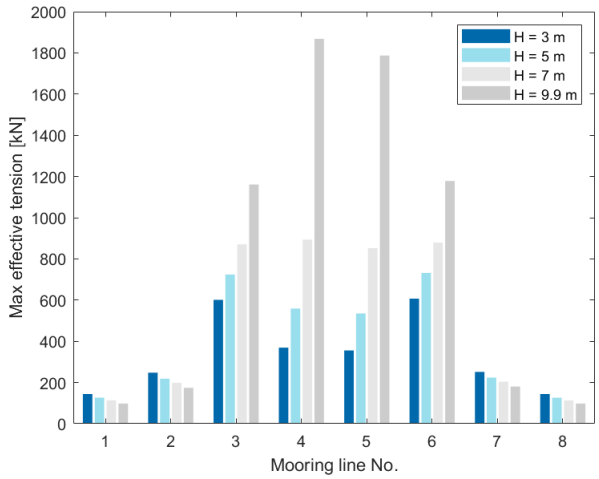

Figure 6.16: Maximum mooring line tensions for different wave heights

6.4 Eigenvalue Analysis

For the eigenvalue analysis, a number of 100 eigenvectors and corresponding eigenvalues were calculated per element. Throughout the following sections, the most important findings from the eigenvalue analysis will be presented and discussed.

6.4.1 Frequencies

Figure 6.17 shows the range of eigenfrequencies obtained from the eigenvalue analysis. It is observed that the eigenfrequencies for the system lie within a range of 0-0.1650 Hz. The eigenvalues obtained at 0.0 Hz imply that parts of the structure might be under-constrained, allowing parts of the structure to move in a free and rigid body manner [50].

As explained in Section 3.6, the lower eigenfrequencies and corresponding mode shapes are those of most importance as they are dominating the dynamic response. The first 36 modes are located in a frequency range of 0.0039-0.0491 Hz, corresponding to wave periods in the range of 20-256 seconds. Normal wave periods are typically in the range of 5-20 seconds, and hence none of the 36 first mode shapes will be excited due to first order loading. This implies that the structure will experience little wave-induced motions. This coincides with typical characteristics for semisubmersibles, where slow-drift motions excited by low frequencies are of importance, exciting resonance motions in surge, sway and yaw [27]. This is a nonlinear effect caused by difference-frequencies, and hence can not be excited by a single regular wave frequency as applied in the thesis.

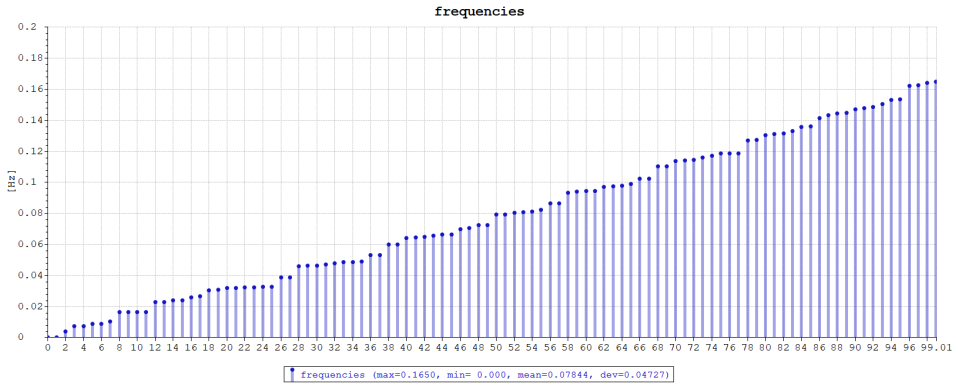

Figure 6.17: Range of eigenfrequencies obtained from the eigenvalue analysis

Mode 37-100 will be excited for wave periods in the range of 6-19 seconds, hence for periods in typical wave regimes. As previously mentioned, these will not be dominating the global response, but can be of importance for local response. Either way, it illustrates that both first order (wave frequencies) and second order (difference-frequencies) dynamic response must be assessed in order to fully describe the global response. The 10 first modes obtained are summarized in Table 6.5.

Table 6.5: Eigenfrequencies for mode 1-10

Mode	Frequency [Hz]	Period [s]	Angular frequency [rad/s]
1	0.0039	256.4	0.0245
2	0.0072	138.9	0.0452
3	0.0075	133.3	0.0471
4	0.0088	113.6	0.0553
5	0.0088	113.6	0.0553
6	0.0106	94.3	0.0666
7	0.0000	-	0.0000
8	0.0000	-	0.0000
9	0.0163	61.3	0.1024
10	0.0164	61.0	0.1030

The first eigenperiod of 256 seconds should correspond to the natural period in surge. In the model tests, this was found to be 175 seconds. When investigating possible reasons causing the large differences in the surge natural period, it was discovered that not only the mooring design was changed in the updated design, but also the diameter of the periphery pontoons was increased by 1 meter. This leads to a significantly higher displacement for the SIMA model than for the model made for the model tests. In addition, it is observed in the dynamic analyses that the mooring system may lack some stiffness, which will also lead to an increase in natural periods.

6.4.2 Mode Shapes

Investigating the mode shapes for the entire system (hull structure and mooring lines) it is discovered that the 27 first frequencies mainly excite displacements for the hull structure, whereas the remaining frequencies excite little to none displacements for the hull, and hence mainly excite displacements for the mooring lines.

Selected mode shapes for mooring line 4 are shown in Figure 6.18. The left and right end corresponds to the fairlead and anchor locations, respectively. As mentioned in Section 3.6, the magnitude of the displacements are arbitrary as they originate from scaled eigenvectors. They do however illustrate the displacement patterns that can be excited by the respective frequencies. All of the 100 eigenvalues and corresponding mode shapes for mooring line 4 can be found in Appendix C.

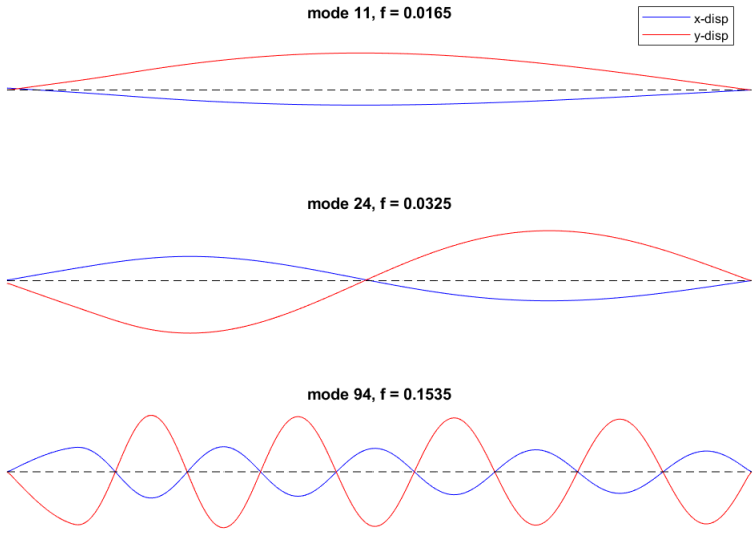

Figure 6.18: Selected mode shapes for mooring line 4

Chapter 7

Discussion

From the results obtained it is clear that neither the modelling nor the analyses have been carried out ideally throughout the thesis. Simplifications have been made both as a consequence of limitations discovered in the software and due to the limited time available. Some of the aspects considered as drawbacks with the modelling and analysis approach in the thesis will be discussed, and suggestions for improvements will be given.

The dynamic analyses conducted in the thesis were all set to run for a duration of 11 wave periods, corresponding to a time period of 121 seconds. Ideally, a time domain analysis should last longer than that, allowing the transient state to fully dissipate. However, when including the fish net cross section in the model, the dynamic analysis required a significant increase with respect to number of time steps in order to run. The drastic increase in number of time steps made the analyses quite time consuming, and it was necessary to keep the duration of the analyses shorter than initially intended.

The fish net also limited the dynamic analysis to regular waves as SIMA does not support irregular waves for models including fish net cross sections. Nonlinear effects caused by sum-frequencies (HF) and difference-frequencies (LF) could hence not be investigated in the dynamic response as they require at least two different frequencies in order to be represented.

For further work it is therefore suggested to create a model including the net structure and the associated hydrodynamic properties of the net without using the fish net cross section directly. It is then especially important to properly account for the damping contribution due to the net as this is a significant contribution to the total damping of the system. Excluding the fish net cross section hence opens the possibility of implementing more realistic environmental conditions and to account for nonlinear effects such as for example slow-drift motions.

Initially, the eigenvalue analysis was intended for investigating which eigenfrequencies excited which rigid body modes. The respective eigenperiods could then be compared

to the natural periods obtained from the model tests. However, it was discovered that it was quite difficult to determine which of the 100 eigenfrequencies corresponded to pure translations and rotations corresponding to the rigid body modes. This was discovered at a late stage in the process. It was therefore no time to perform decay tests instead.

Several aspects could have been investigated from the dynamic analyses conducted in the thesis. However, it was decided to focus on results available from the model tests, such that a comparison could be made. This included displacements, accelerations and mooring line tensions. A structural analysis of the hull structure from the dynamic analysis was therefore not considered at this stage. It would however be interesting to investigate the utilization of the structural components of the hull, in addition to assessments of fatigue and accidental loads.

Chapter 8

Conclusion

During the modelling and analysis process, several limitations were discovered that will have an effect on the accuracy of the results. In addition, the MARINTEK reference report was introduced at a late stage in the process. It then became clear that the model made for the model tests was based on an earlier version of the concept than the model made for the thesis. Several differences in the design have been discovered, making the results difficult to compare directly. However, the work conducted throughout the thesis has been good for illustration of different aspects relating the modelling and analysis processes. Some concluding remarks from the results obtained will now be presented.

The static analysis revealed that the structural components of the hull experience small bending moments and axial forces with reference to the yield stress and the critical buckling stress, respectively. This suggests that fatigue might be the most important failure mode for the hull members.

For regular waves with the 100-year environment, the vertical and transverse motions were generally small for all wave directions considered in the thesis. The maximum lateral motions recorded was about 38 meters. This was found for the in-line case, with waves, wind and current all coming from the same direction. This resulted in a maximum mooring tension of 876.2 kN.

For the extreme environmental condition it became clear that the mooring system modelled allowed large offsets compared to the model tests, illustrating that the mooring lines modelled may lack some stiffness. The maximum surge offset recorded was 55 meters, resulting in a maximum mooring line tension of 1868 kN. This corresponds to a safety factor of 4.35 with reference to the minimum breaking load. The high safety factor illustrates that the mooring lines are safe to operate even for extreme environmental conditions.

The eigenvalue analysis revealed that the most important mode shapes with reference to the dynamic response will be excited for long wave periods, way outside the typical range of wave frequencies. This implies that limited wave-induced motions are expected, and that

nonlinear effects can lead to resonance of slow-drift motions. The characteristics observed from the eigenvalue analysis coincides well with typical characteristics of semisubmersibles.

Chapter 9

Further Work

As already discussed in previous chapters, several aspects in the modelling and analysis approach can be further improved in order to achieve more realistic results. The following chapter will present a list of recommendations for further work. Some of the suggestions have already been discussed in further detail in Chapter 7, whereas others will be presented for the first time.

Modelling

- The topside has only been modelled as a point mass in the thesis. The volume of the topside should also be modelled in order to fully assess the effect of wind loads.
- Mass contributions should be modelled in more detail to better match the weights of the actual structure. Lack of mass contributions is here compensated for by adding ballast water to the pontoons, causing differences in the center of gravity and hence the dynamic response.
- The pontoon panel models should be given more optimized meshes in order to better capture the hydrodynamic properties of the pontoons. It is proposed to use the HydroMesh module in HydroD to create the meshed panel models rather than GeniE.
- Alternative methods of modelling the net should be investigated. Alternatively, the model could be made using other software capable of analysing fish net cross sections under irregular waves.
- Investigations should be made on how to better model the geometry and properties of the mooring line components.

Analysis

- The dynamic analysis should be performed using a more realistic implementation of the environmental conditions. This includes irregular waves from multiple directions, swell waves, wind and current. Full 3-hour simulations should be performed.
- Decay tests should be performed in order to determine the natural periods of the system. This can be done by performing 6 dynamic analyses with impulse nodal loads in the respective transnational and rotational degrees of freedom.
- Structural loads during the dynamic analysis should be assessed. This includes ultimate limit state (ULS), fatigue limit state (FLS) and accidental limit state (ALS) analyses.

Bibliography

[1] World Bank. “Fish to 2030: Prospects for Fisheries and Aquaculture”. In: *Agriculture and environmental services discussion paper* 3 (2013).

[2] Food and Agriculture Organization of the United Nations. *The State of World Fisheries and Aquaculture*. Available from: http://www.fao.org/3/CA0191EN/CA0191EN.pdf. 2018.

[3] SalMar. *Offshore Fish Farming [Internet]*. Available from: https://www.salmar.no/en/offshore-fish-farming-a-new-era/.

[4] Norgeskart. *Map of Frohavet [Internet]*. Available from: https://www.norgeskart.no/. 2019.

[5] Directorate of Fisheries. *Statistics Aquaculture (time series)*. Available from: https://www.fiskeridir.no/Akvakultur/Statistikk-akvakultur/Akvakulturstatistikk-tidsserier. 2018.

[6] Bore, P.T. and Fossan, P.A. “Ultimate- and Fatigue Limit State Analysis of a Rigid Offshore Aquaculture Structure”. Master Thesis. Department of Marine Technology, NTNU, 2015.

[7] MARINTEK. “Ocean Fish Farm. Model Tests”. Unpublished report. 2014.

[8] Food and Agriculture Organization of the United Nations. *National Aquaculture Sector Overview. Norway*. Available from: http://www.fao.org/fishery/countrysector/naso_norway/en. 2005.

[9] Shainee, M., Ellingsen, H., Leira, B.J. and Fredheim, A. “An optimum design concept for offshore cage culture”. In: *Ocean Space Utilization; Ocean Renewable Energy* 7 (2012).

[10] Hvalpsund Net. *Gravity cage [Image on the internet]*. Available from: http://fishfarmsolution.com/fish-farming-solutions-en/.

[11] Cardia, F. and Lovatelli, A. “Aquaculture operations in floating HDPE cages - a field handbook”. In: *FAO Fishieries and aquaculture technical paper 593* (2015), pp. 2–6.

[12] Directorate of Fisheries. *Escape Statistics 2001-2018 [Image on the internet]*. Available from: https://www.fiskeridir.no/Akvakultur/Statistikk-akvakultur/Roemmingsstatistikk. 2019.

[13] Costello, M.J. "How sea lice from salmon farms may cause wild salmonid declines in Europe and North America and be a threat to fishes elsewhere". In: *Proceedings of the Royal Society of London B: Biological Sciences* (2009).

[14] Krkošek, M., Lewis, M.A., Volpe, J.P. and Morton, A. "Fish Farms and Sea Lice Infestations of Wild Juvenile Salmon in the Broughton Archipelago". In: *Reviews in Fisheries Science* 14 (2007), pp. 1–11.

[15] NSK Ship Design. *NSK - 3417 HAVFARM*. Available from: https://www.nskshipdesign.com/designs/aquaculture/fish-farm-2/fish-farm/.

[16] Nordlaks. *Havfarmene*. Available from: https://www.nordlaks.no/havfarm.

[17] Aker Solutions and Norway Royal Salmon. *Arctic Offshore Farming*. Available from: https://www.arcticoffshorefarming.no/english.

[18] Norway Royal Salmon. *Arctic Offshore Farming granted development licenses*. Available from: https://norwayroyalsalmon.com/en/Home/News/Norway-Royal-Salmon-ASA-NRS-Arctic-Offshore-Farming-granted-development-licenses.

[19] Hauge Aqua. *Technology for sustainable growth in Aquaculture*. Available from: http://www.haugeaqua.com/Technology/.

[20] SalMar. *Ocean Farm 1 towing [Image on the internet]*. Available from: https://www.salmar.no/en/gallery/.

[21] Ministry of Trade, Industry and Fisheries. *Forskrift om krav til teknisk standard for flytende akvakulturanlegg (NYTEK-forskriften)*. FOR-2014-12-15-1831. 2015.

[22] NS 9415. *Marine fish farms - Requirements for site survey, risk analyses, design, dimensioning, production, installation and operation*. 2009.

[23] Exposed Aquaculture Operations. *Annual Report 2017*. Available from: https://exposedaquaculture.no/arsrapport-2017/. 2017.

[24] Det Norske Veritas. *Reccomended practice DNV-RP-C205: Environmental Conditions and Environmental Loads*. 2010.

[25] Pettersen, B. *Marin Teknikk 3: Hydrodynamikk*. (in Norwegian). Department of Marine Technology, NTNU, 2007.

[26] Myrhaug, D. *Marin Dynamikk (uregelmessige bølger og bølgestatistikk)*. (in Norwegian). Akademika Forlag, 2004.

[27] Faltinsen, O.M. *Sea Loads on Ships and Offshore Structures*. Cambridge University Press, 1993.

[28] Wallis, G.B. *Added mass*. Available from: http://www.thermopedia.com/content/289/. 2011.

[29] Langen, I. and Sigbjørnsson, R. *Dynamic Analysis of Structures*. Tapir, 1979.

[30] SINTEF Ocean. *RIFLEX 4.10.1 Theory Manual*. 2017.

[31] Kristiansen, T. and Faltinsen, O.M. "Modelling of current loads on aquaculture net cages". In: *Journal of Fluids and Structures* 34 (2012), pp. 218–235.

[32] Løland, G. "Current Forces On and Flow Through Fish Farms". Dr.ing dissertation. Division of Marine Hydrodynamics, The Norwegian Institute of Technology, 1991.

[33] Løland, G. "Current forces on, and water flow through and around, floating fish farms". In: *Aquaculture International* 1 (1993), pp. 72–89.

[34] Moan, T. *TMR 4190 Finie Element Modelling and Analysis of Marine Structures*. Department of Marine Technology, NTNU, 2003.

[35] Min, L.Y. OT5204 Lecture notes: Dynamic Analysis. Lecture presented at: National University of Singapore, 2018.

[36] Kongsberg. *Offshore fish farming: Food for thought*. Available from: https://www.kongsberg.com/maritime/about-us/news-and-media/our-stories/offshore-fish-farming-food-for-thought/.

[37] Larsen, C.M. *Marine Dynamics*. Department of Marine Technology, NTNU, 2015.

[38] Ong, P.P.A. and Pellegrino, S. "Modelling of seabed interaction in frequency domain analysis of mooring cables". In: *ASME 2003 22nd International Conference on Offshore Mechanics and Arctic Engineering*. American Society of Mechanical Engineers. 2003.

[39] AKVA group. *EcoNet [Image on the internet]*. Available from: https://www.akvagroup.com/pen-based-aquaculture/pens-nets/nets-/econet.

[40] DNV GL. *Sesam user manual, GeniE*. 2016.

[41] DNV GL. *Sesam user manual, HydroD*. 2017.

[42] DNV GL. *Sesam user manual, Wadam*. 2018.

[43] Molland, A.F. *The Maritime Engineering Reference Book*. Elsevier Science & Technology, 2008.

[44] SINTEF Ocean. *SIMO 4.10.1 User Guide*. 2017.

[45] SINTEF Ocean. *RIFLEX 4.10.1 User Guide*. 2017.

[46] DNV GL. *Offshore Standard DNVGL-OS-E301, Position mooring*. 2015.

[47] Orcaflex. *Chain Properties*. Available from: https://www.orcina.com/SoftwareProducts/OrcaFlex/Documentation/Help/Content/html/Chain.htm.

[48] Høiland, A.V. "Dynamic Analysis of a Vessel-shaped Fish Farm for Open Sea". Master Thesis. Department of Marine- and Subsea Technology, Universitetet i Stavanger, 2017.

[49] F. Le Bris and D Marichal. "Numerical and experimental study of submerged supple nets: Applications to fish farms". In: *Journal of Marine Science and Technology* 3.4 (1998), pp. 161–170.

[50] Autodesk Help. *Section 21: Modal or Natural Frequency Analysis*. Available from: https://knowledge.autodesk.com/support/inventor-nastran/getting-started/caas/CloudHelp/cloudhelp/2018/ENU/NINCAD-SelfTraining/files/GUID-978425AB-D2FA-491B-8D39-BD1A757F3BBD-htm.html. 2018.

Appendix A

Structural Drawings

A.1 Top view

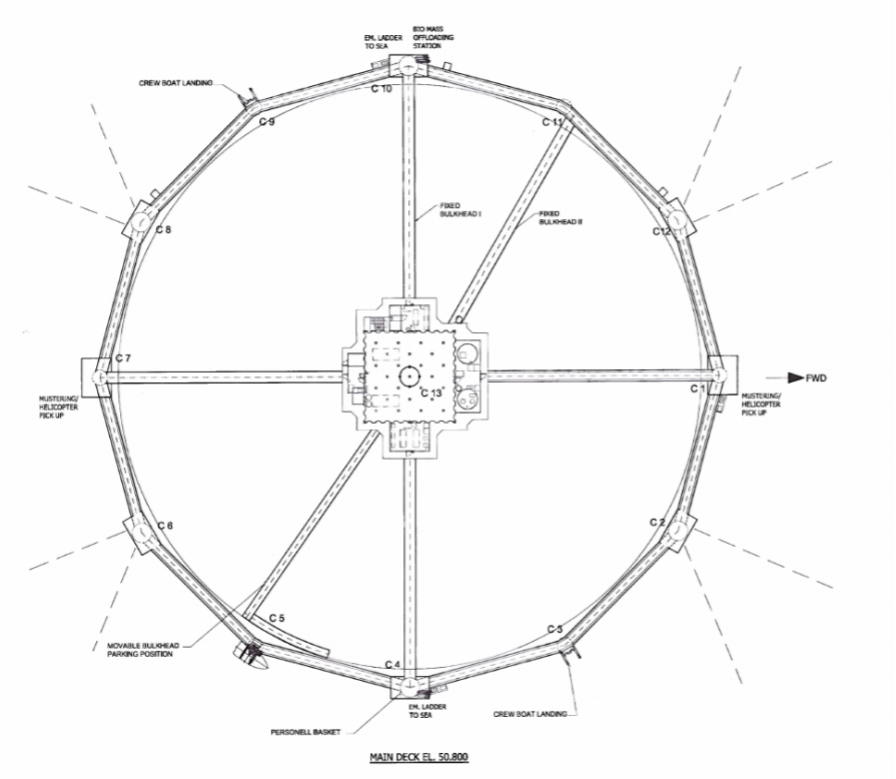

A.2 Top view: Bulkheads highlighted

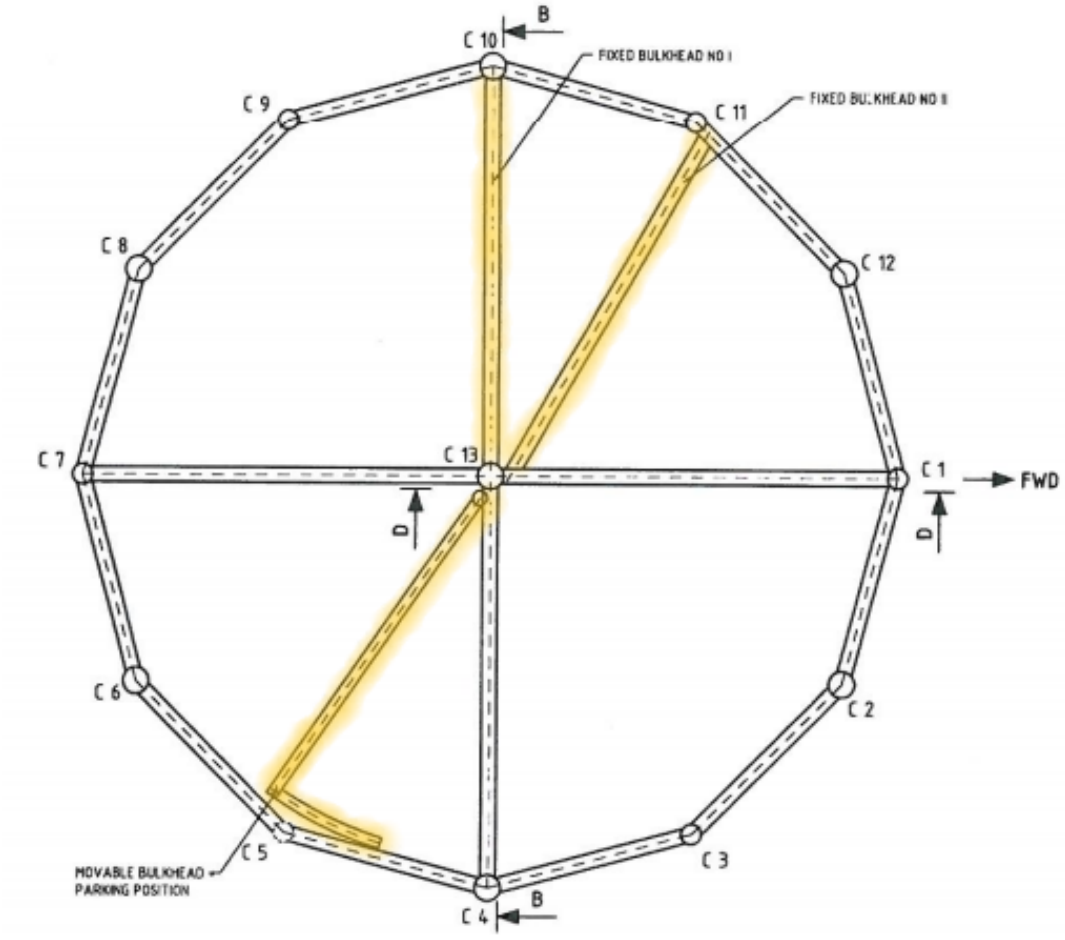

A.3 Plan view

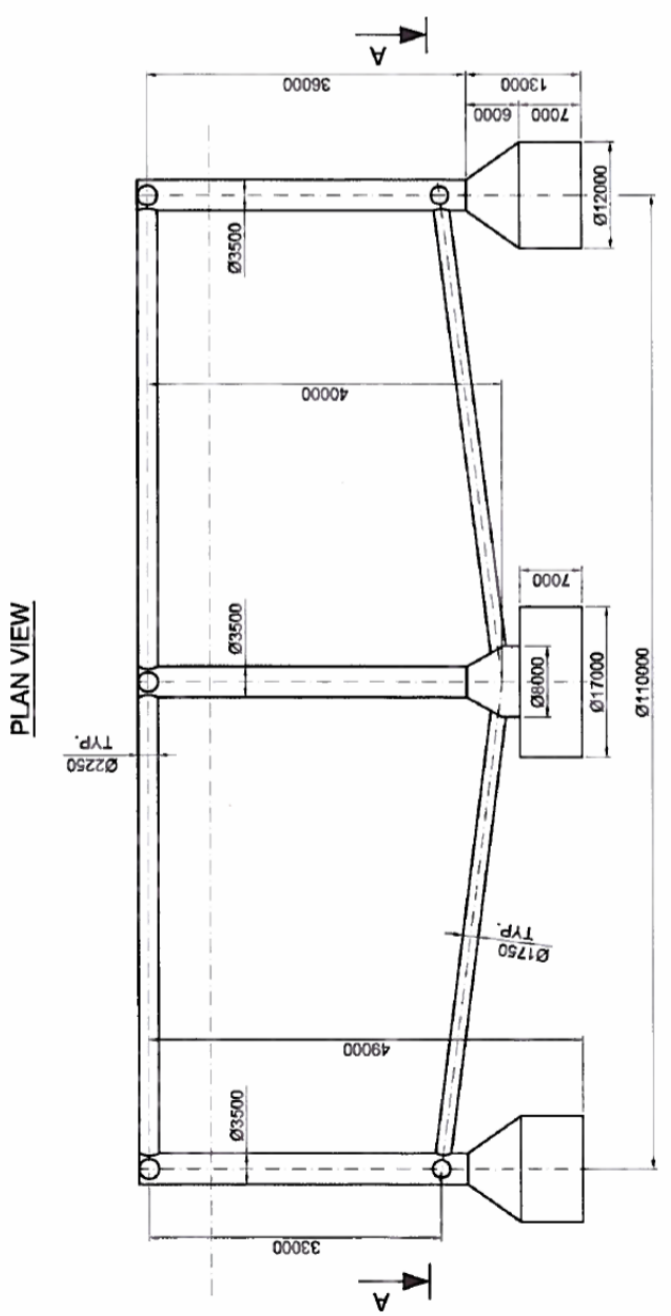
PLAN VIEW
A
A
36000
13000
7000
6000
Ø12000
Ø3500
40000
7000
Ø3500
Ø8000
Ø17000
Ø110000
Ø2250
TYP.
Ø1750
TYP.
49000
Ø3500
33000

Appendix B

Hydrodynamic Results for the Pontoons

B.1 Periphery Pontoons

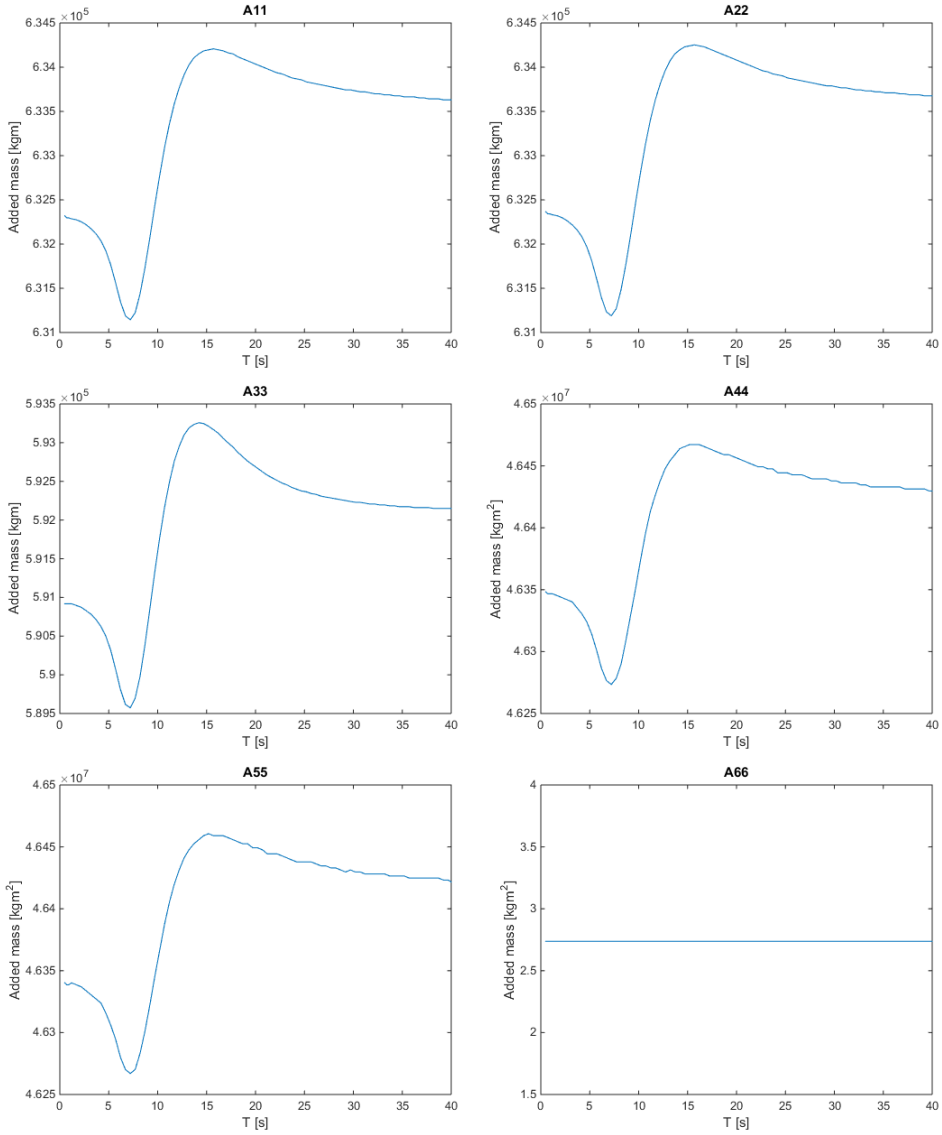

Figure B.1: Added mass at mesh size 0.5 m x 0.5 m

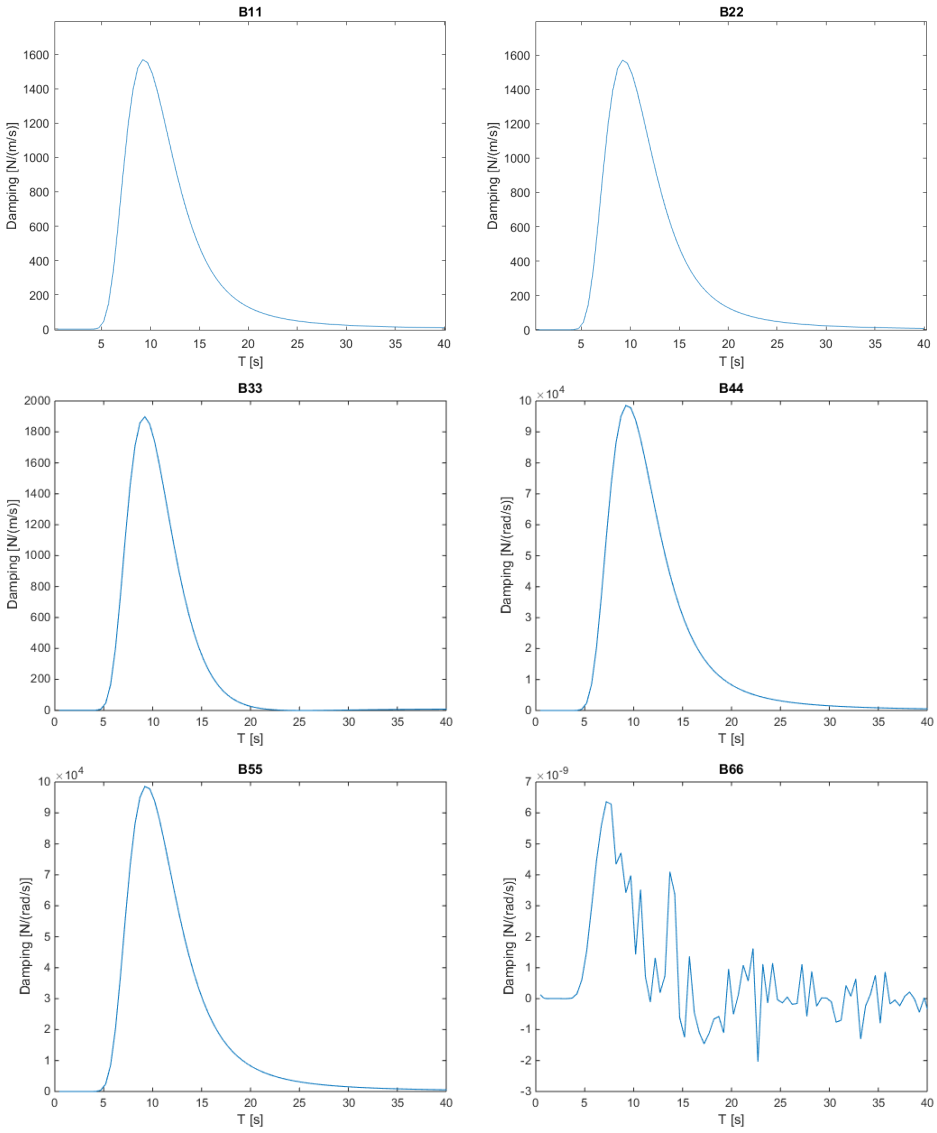

Figure B.2: Radiation damping at mesh size 0.5 m x 0.5 m

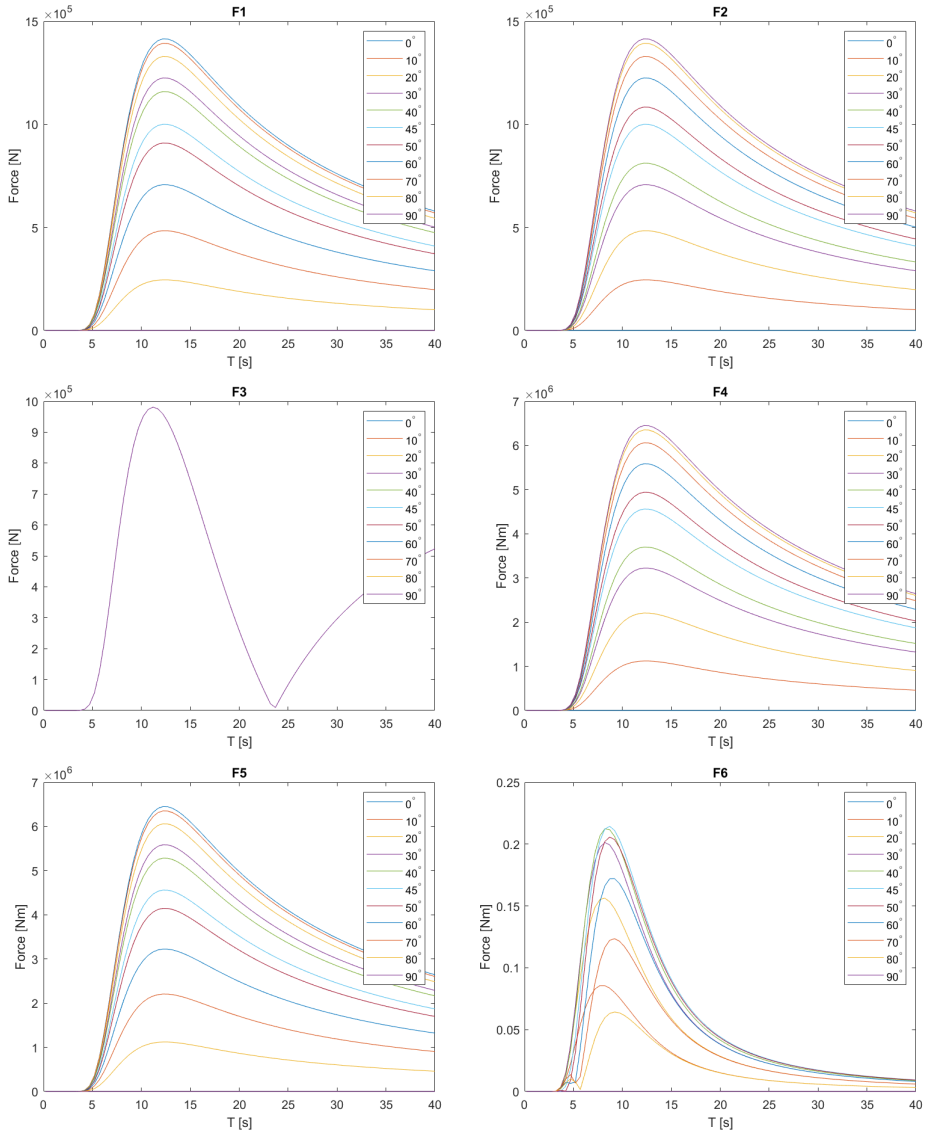

Figure B.3: First order wave force transfer functions for mesh size 0.5 m x 0.5 m. Incoming wave direction varying between 0°-90°.

B.2 Centre Pontoon

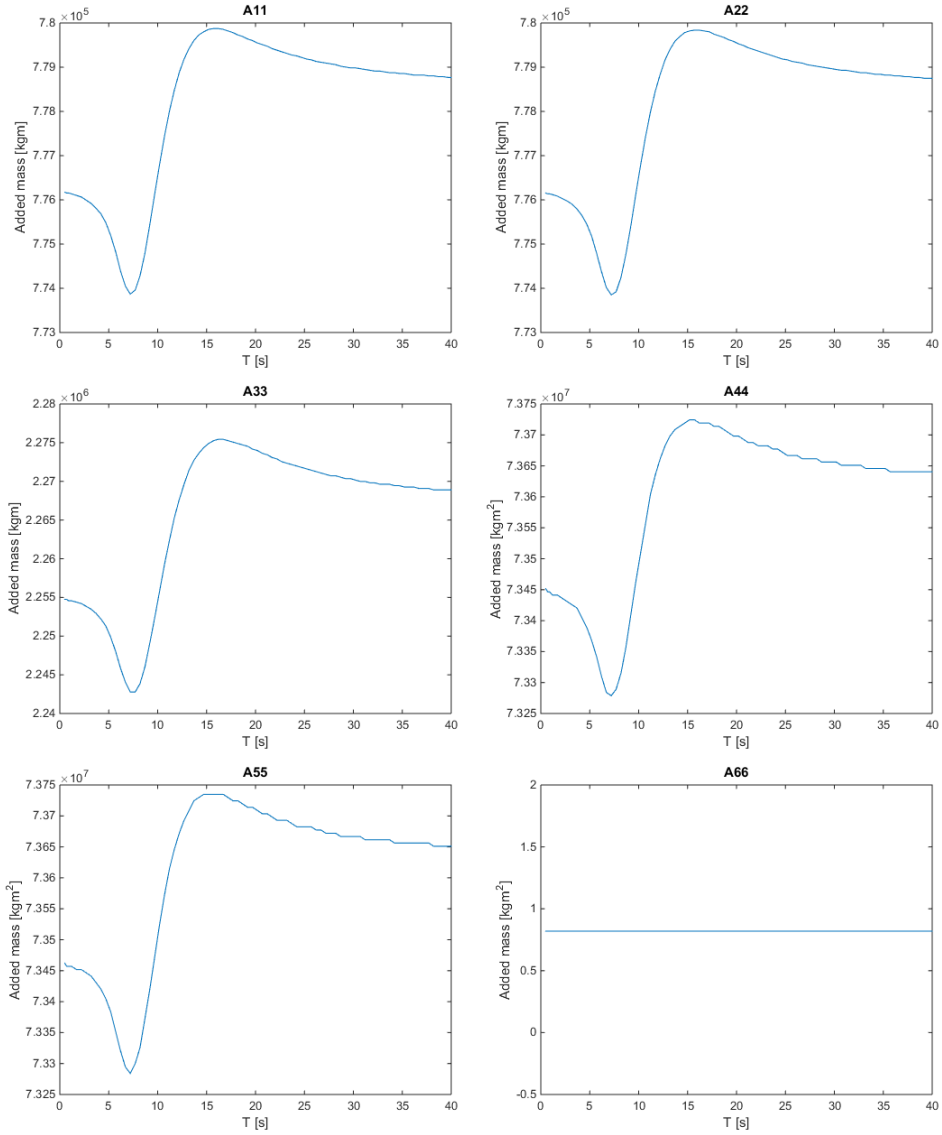

Figure B.4: Added mass at mesh size 0.5 m x 0.5 m

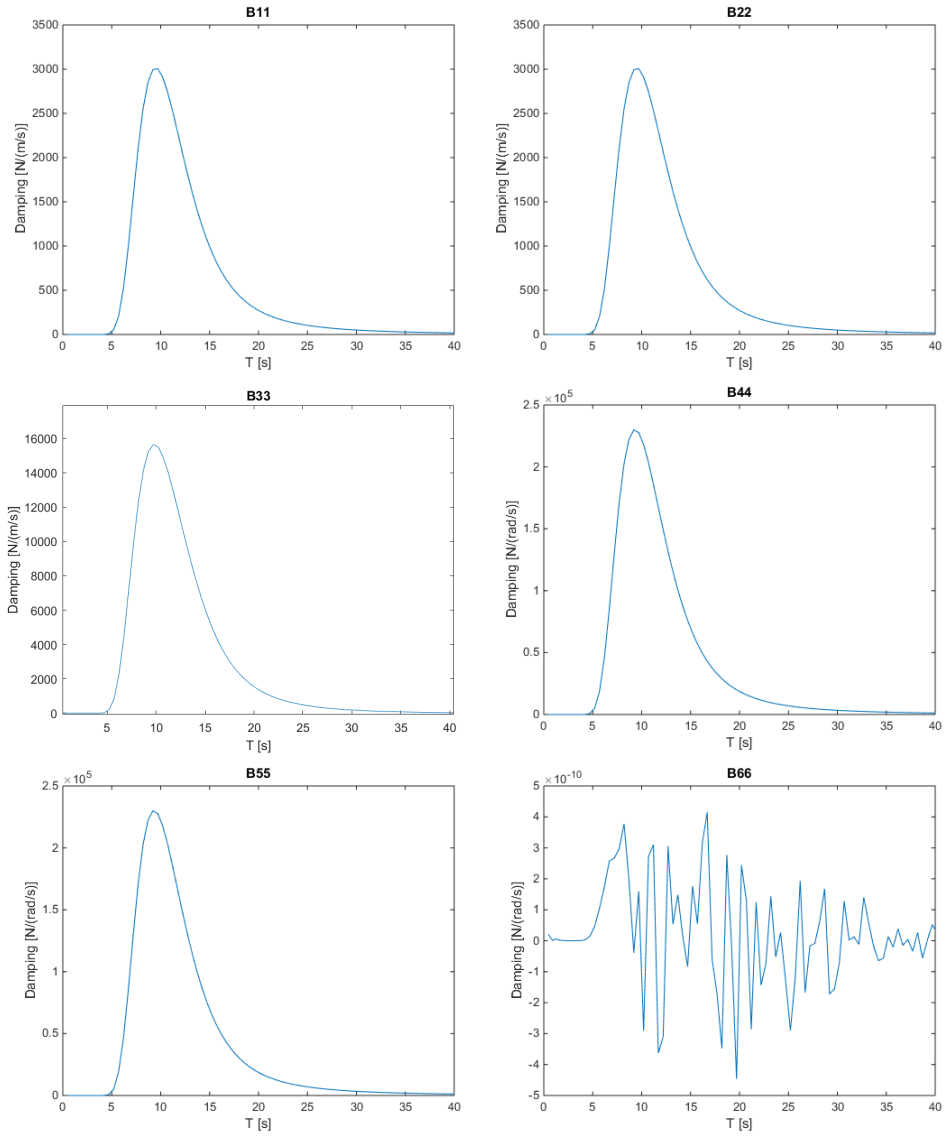

Figure B.5: Radiation damping at mesh size 0.5 m x 0.5 m

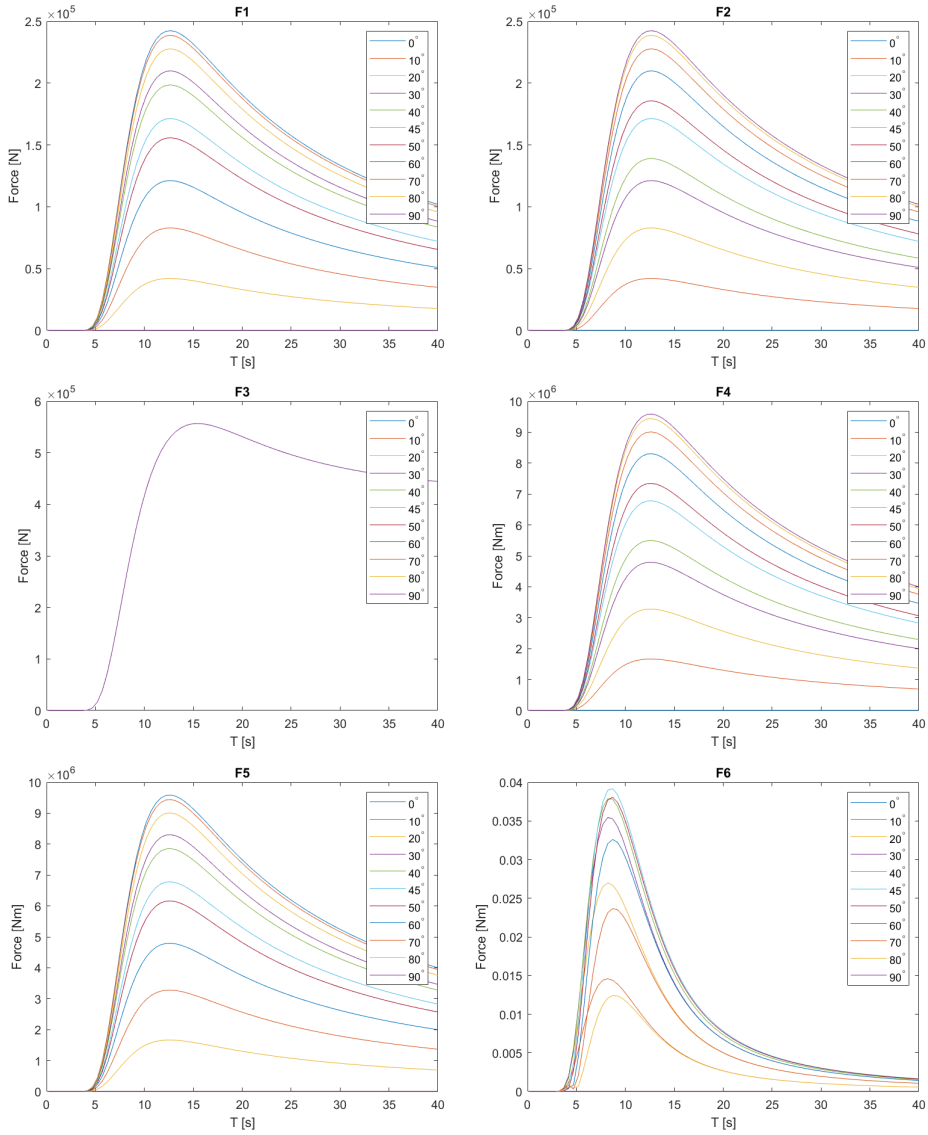

Figure B.6: First order wave force transfer functions for mesh size 0.5 m x 0.5 m. Incoming wave direction varying between 0°-90°.

Appendix C

Eigenvalue Analysis

C.1 Eigenvalues

Mode	Frequency [Hz]	Period [s]	Angular frequency [rad/s]
1	0.0039	259.4	0.0245
2	0.0072	138.9	0.0452
3	0.0075	133.3	0.0471
4	0.0088	113.6	0.0553
5	0.0088	113.6	0.0553
6	0.0106	94.34	0.0667
7	0.0000	-	0.0000
8	0.0000	-	0.0000
9	0.0163	61.35	0.1024
10	0.0164	61.0	0.1030
11	0.0165	60.61	0.1037
12	0.0166	60.24	0.1043
13	0.0203	49.26	0.1275
14	0.0231	43.29	0.1451
15	0.0241	41.49	0.1514
16	0.0241	41.49	0.1514
17	0.0259	38.61	0.1627
18	0.0266	37.59	0.1671
19	0.0305	32.79	0.1916
20	0.0307	32.57	0.1929
21	0.0320	31.25	0.2011
22	0.0321	31.15	0.2017
23	0.0322	31.06	0.2023
24	0.0325	30.77	0.2042

Mode	Frequency [Hz]	Period [s]	Angular frequency [rad/s]
25	0.0327	30.58	0.2055
26	0.0328	30.49	0.2061
27	0.0390	25.64	0.2450
28	0.0390	25.64	0.2450
29	0.0462	21.65	0.2903
30	0.0463	21.60	0.2909
31	0.0465	21.51	0.2922
32	0.0470	21.28	0.2953
33	0.0481	20.79	0.3022
34	0.0486	20.58	0.3054
35	0.0488	20.49	0.3066
36	0.0491	20.37	0.3085
37	0.0533	18.76	0.3349
38	0.0534	18.73	0.3355
39	0.0601	16.64	0.3776
40	0.0602	16.61	0.3782
41	0.0642	16.13	0.4034
42	0.0646	15.48	0.4059
43	0.0648	15.43	0.4072
44	0.0656	15.24	0.4122
45	0.0664	15.06	0.4172
46	0.0665	15.04	0.4178
47	0.0699	14.31	0.4392
48	0.0707	14.14	0.4442
49	0.0724	13.81	0.4549
50	0.0725	13.79	0.4555
51	0.0792	12.63	0.4976
52	0.0793	12.61	0.4983
53	0.0805	12.42	0.5058
54	0.0810	12.35	0.5089
55	0.0813	12.30	0.5108
56	0.0822	12.17	0.5165
57	0.0865	11.56	0.5435
58	0.0867	11.53	0.5448
59	0.0935	10.70	0.5875
60	0.0943	10.60	0.5925
61	0.0944	10.59	0.5931
62	0.0945	10.58	0.5938
63	0.0970	10.31	0.6095
64	0.0975	10.26	0.6126
65	0.0979	10.21	0.6151
66	0.0991	10.09	0.6227
67	0.1023	9.78	0.6428
68	0.1024	9.77	0.6434

Mode	Frequency [Hz]	Period [s]	Angular frequency [rad/s]
69	0.1105	9.05	0.6943
70	0.1106	9.04	0.6949
71	0.1137	8.80	0.7144
72	0.1143	8.75	0.7182
73	0.1147	8.72	0.7207
74	0.1161	8.61	0.7295
75	0.1174	8.52	0.7376
76	0.1187	8.42	0.7458
77	0.1188	8.42	0.7464
78	0.1189	8.41	0.7471
79	0.1272	7.86	0.7992
80	0.1274	7.85	0.8005
81	0.1305	7.66	0.8200
82	0.1311	7.63	0.8237
83	0.1316	7.60	0.8269
84	0.1332	7.51	0.8369
85	0.1358	7.36	0.8533
86	0.1360	7.35	0.8545
87	0.1416	7.06	0.8897
88	0.1432	6.98	0.8998
89	0.1445	6.92	0.9079
90	0.1447	6.91	0.9092
91	0.1473	6.79	0.9255
92	0.1480	6.76	0.9299
93	0.1486	6.73	0.9337
94	0.1505	6.64	0.9456
95	0.1534	6.52	0.9638
96	0.1535	6.51	0.9645
97	0.1623	6.16	1.0198
98	0.1625	6.15	1.0210
99	0.1642	6.09	1.0317
100	0.1650	6.06	1.0367

C.2 Mode Shapes: Mooring Line 4

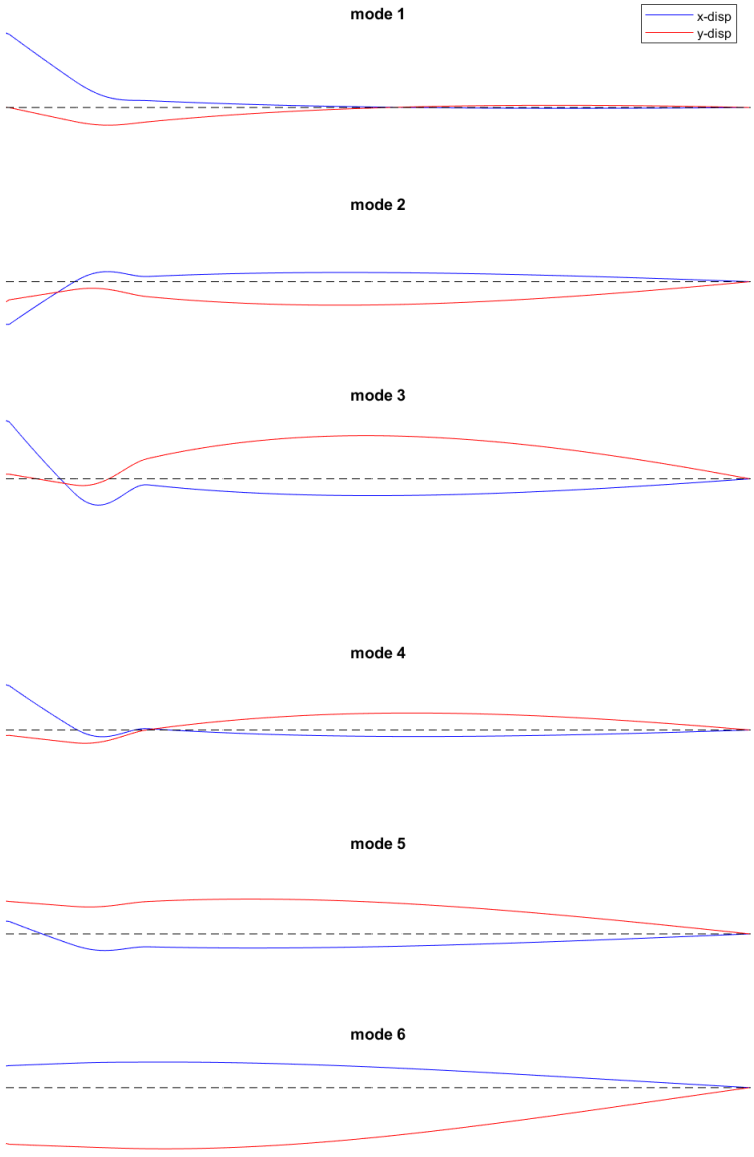

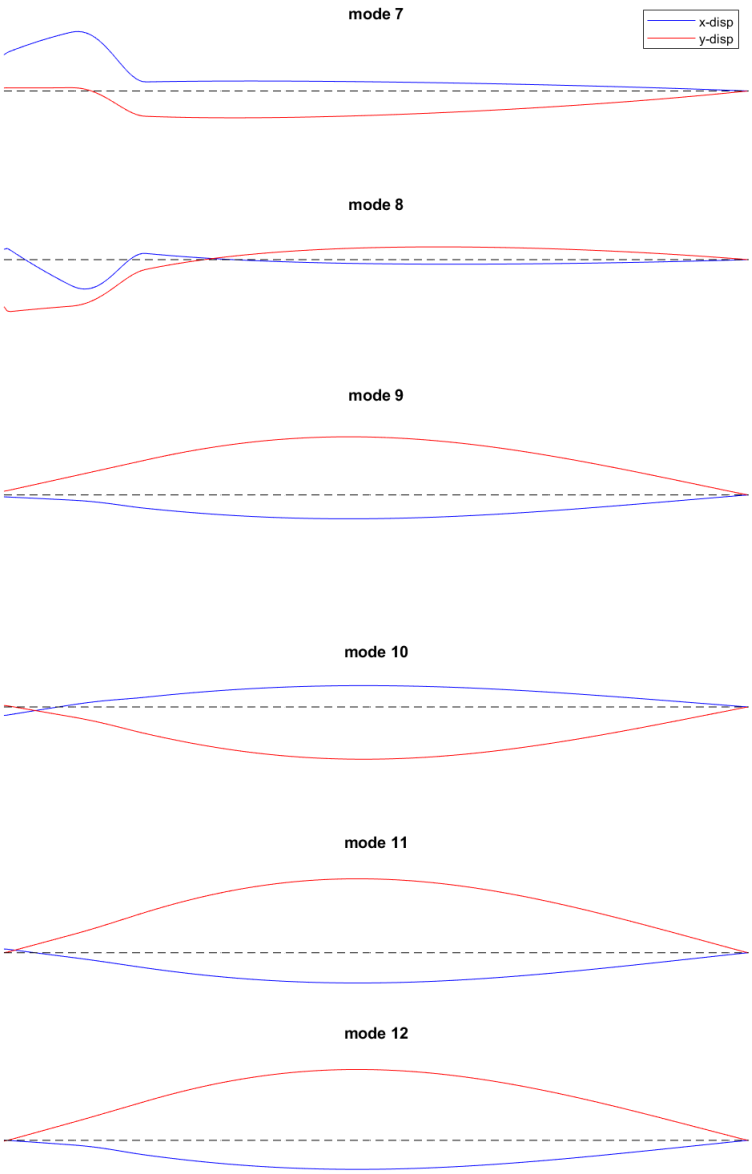
mode 7
x-disp
y-disp
mode 8
mode 9
mode 10
mode 11
mode 12

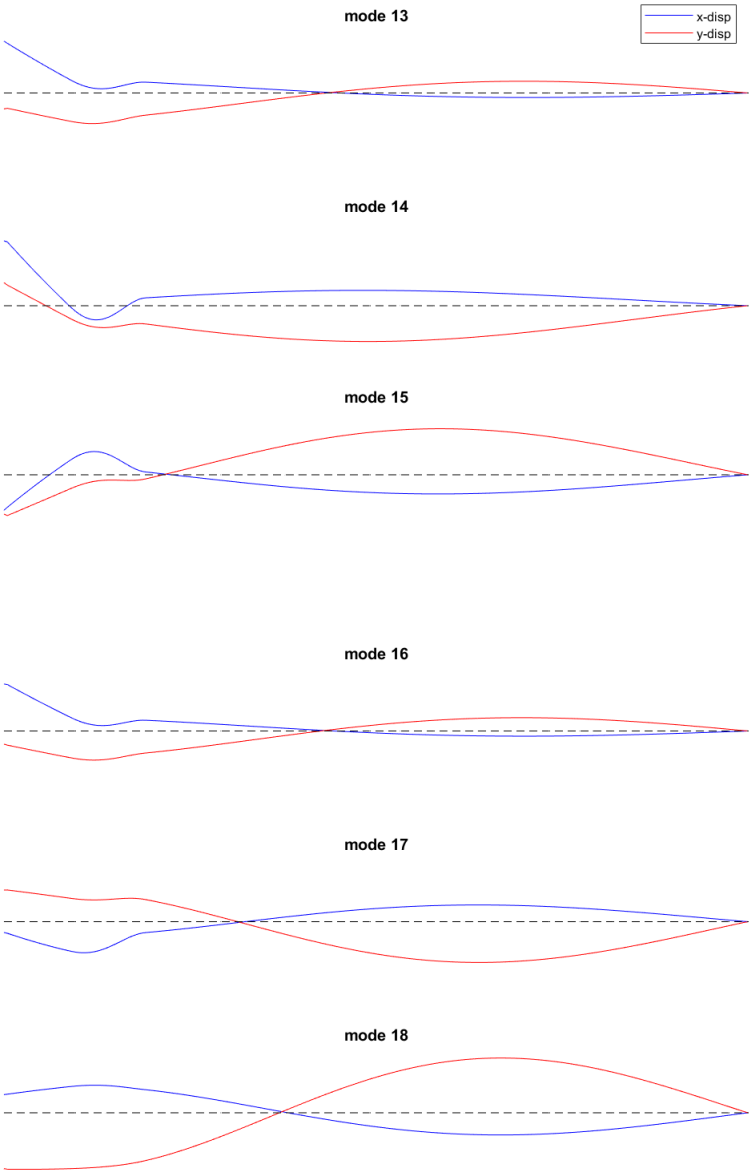
mode 13
x-disp
y-disp
mode 14
mode 15
mode 16
mode 17
mode 18

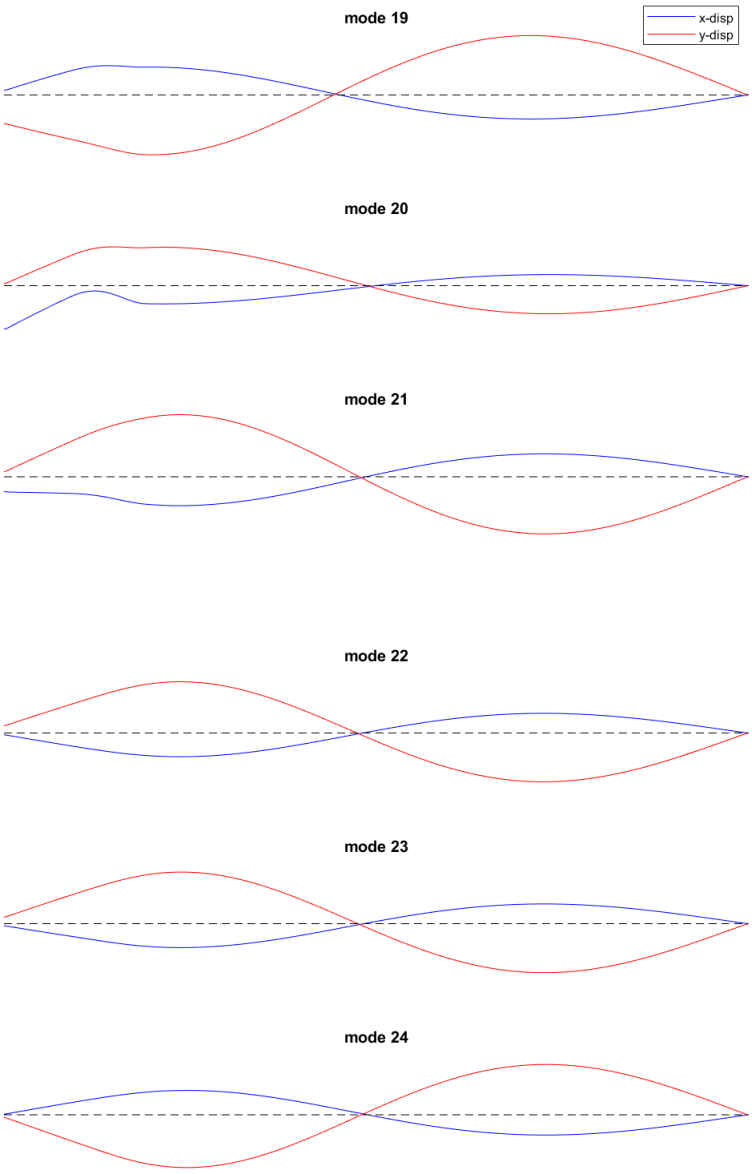
mode 19
x-disp
y-disp
mode 20
mode 21
mode 22
mode 23
mode 24

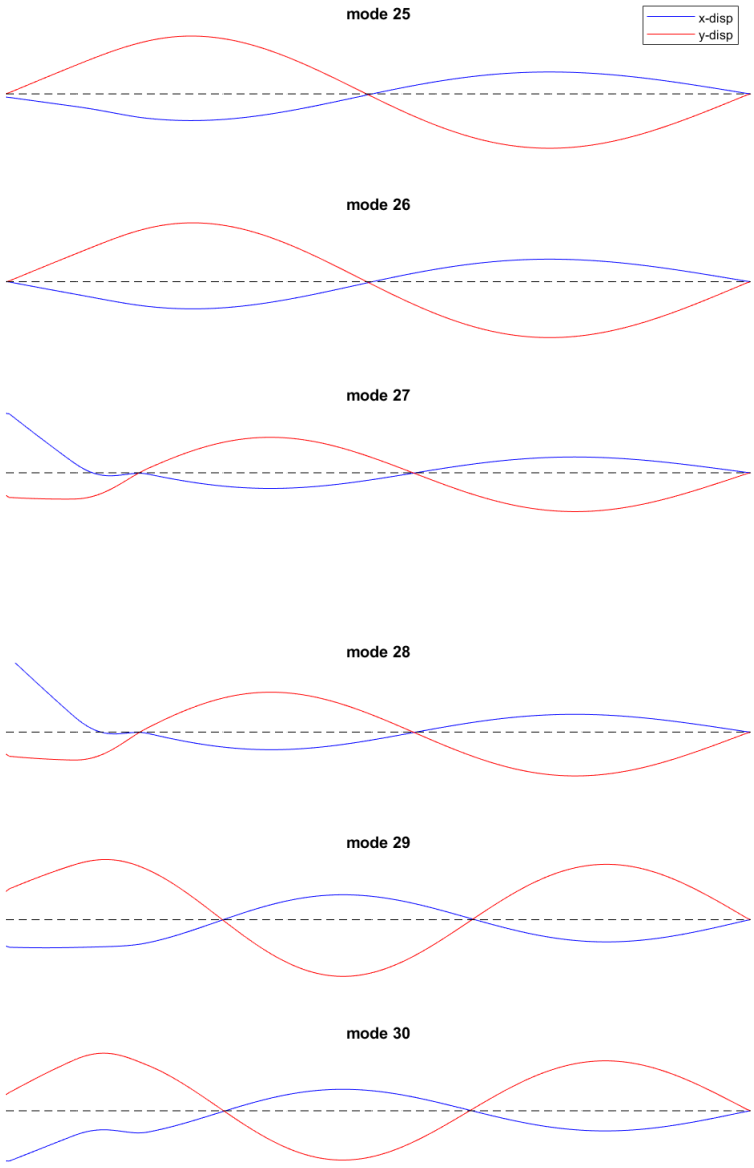
mode 25
x-disp
y-disp
mode 26
mode 27
mode 28
mode 29
mode 30

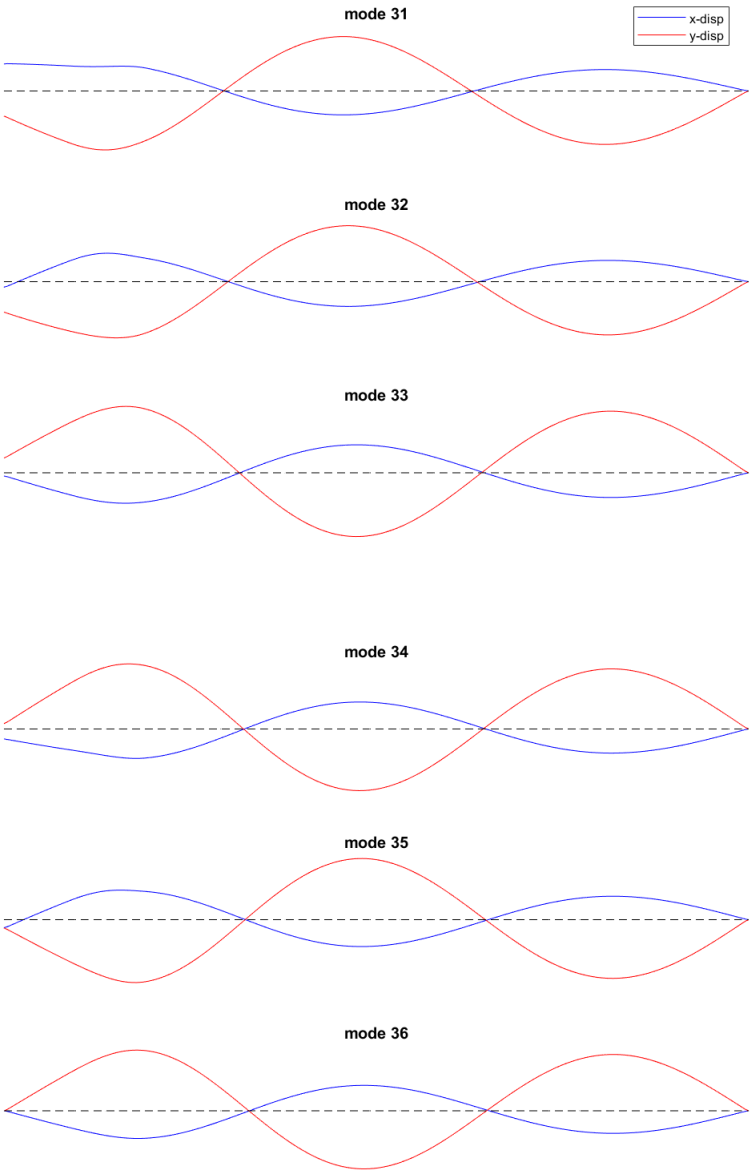
mode 31
x-disp
y-disp
mode 32
mode 33
mode 34
mode 35
mode 36

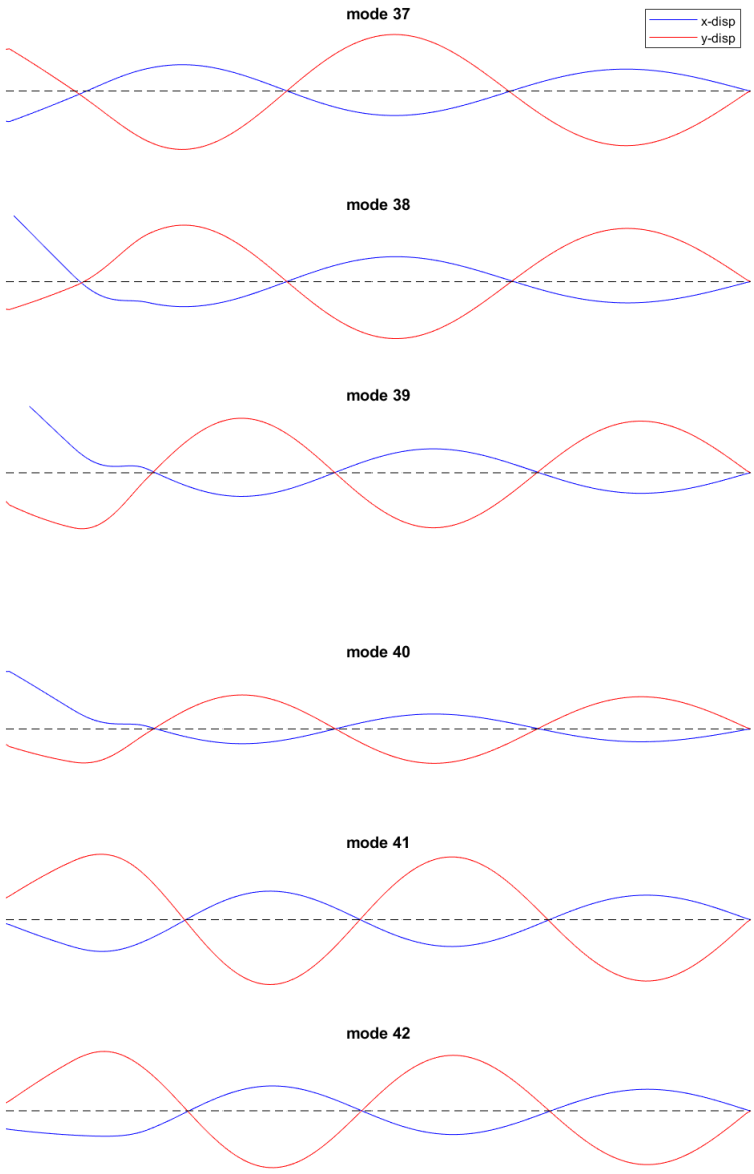
mode 37
x-disp
y-disp
mode 38
mode 39
mode 40
mode 41
mode 42

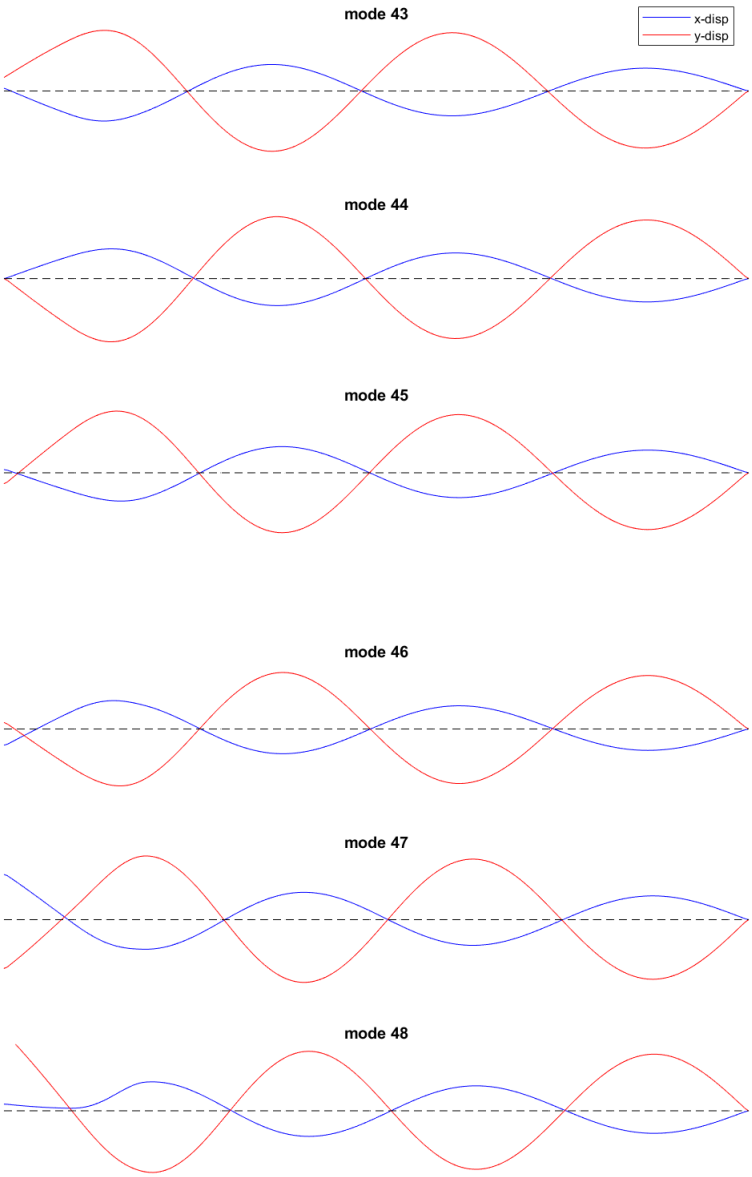
mode 43
x-disp
y-disp
mode 44
mode 45
mode 46
mode 47
mode 48

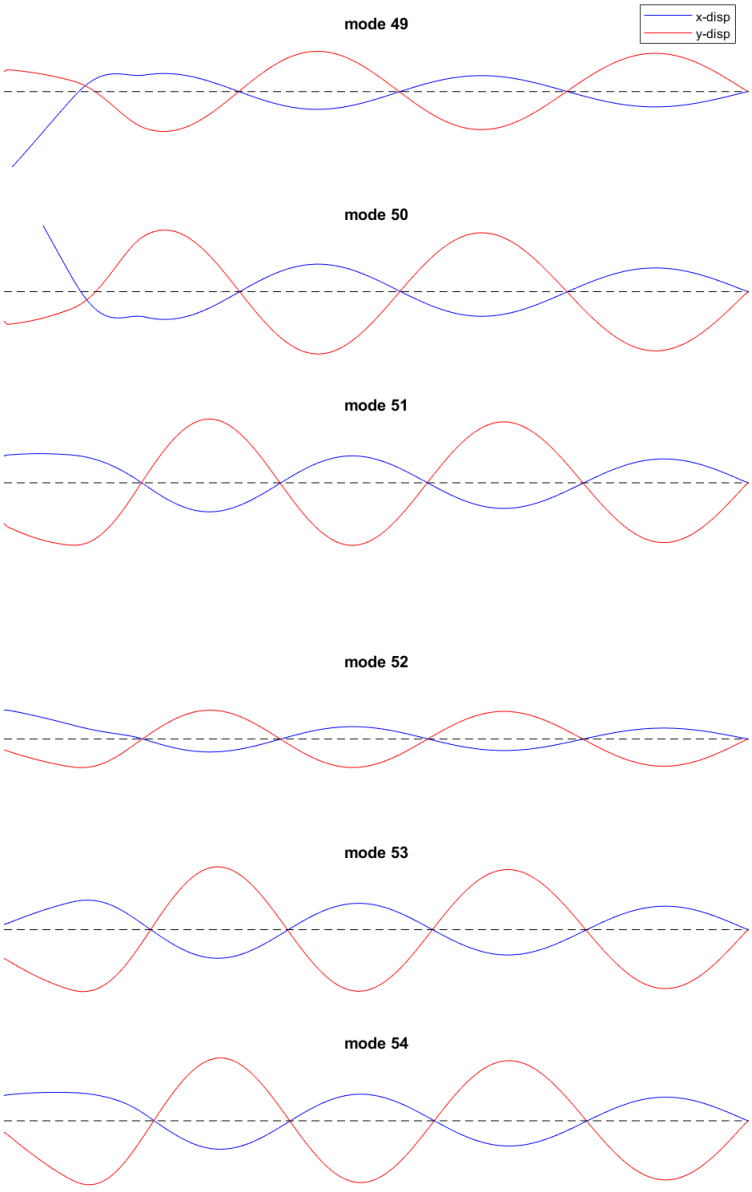
mode 49
x-disp
y-disp
mode 50
mode 51
mode 52
mode 53
mode 54

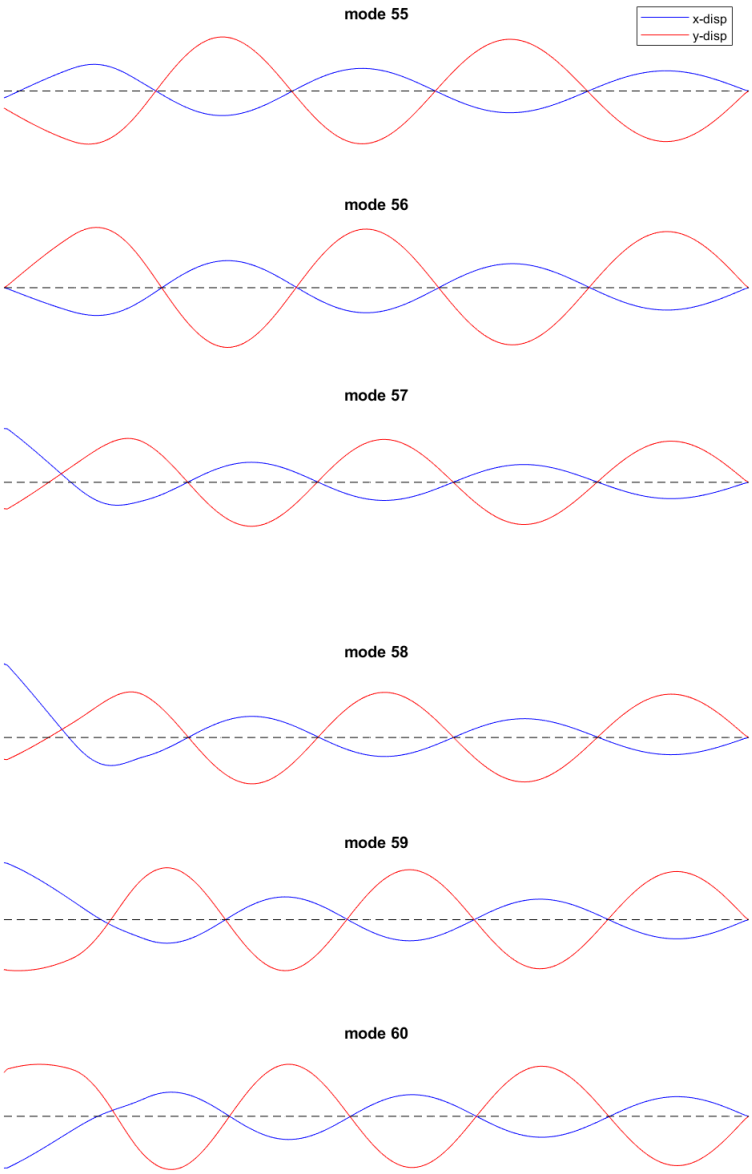
mode 55
x-disp
y-disp
mode 56
mode 57
mode 58
mode 59
mode 60

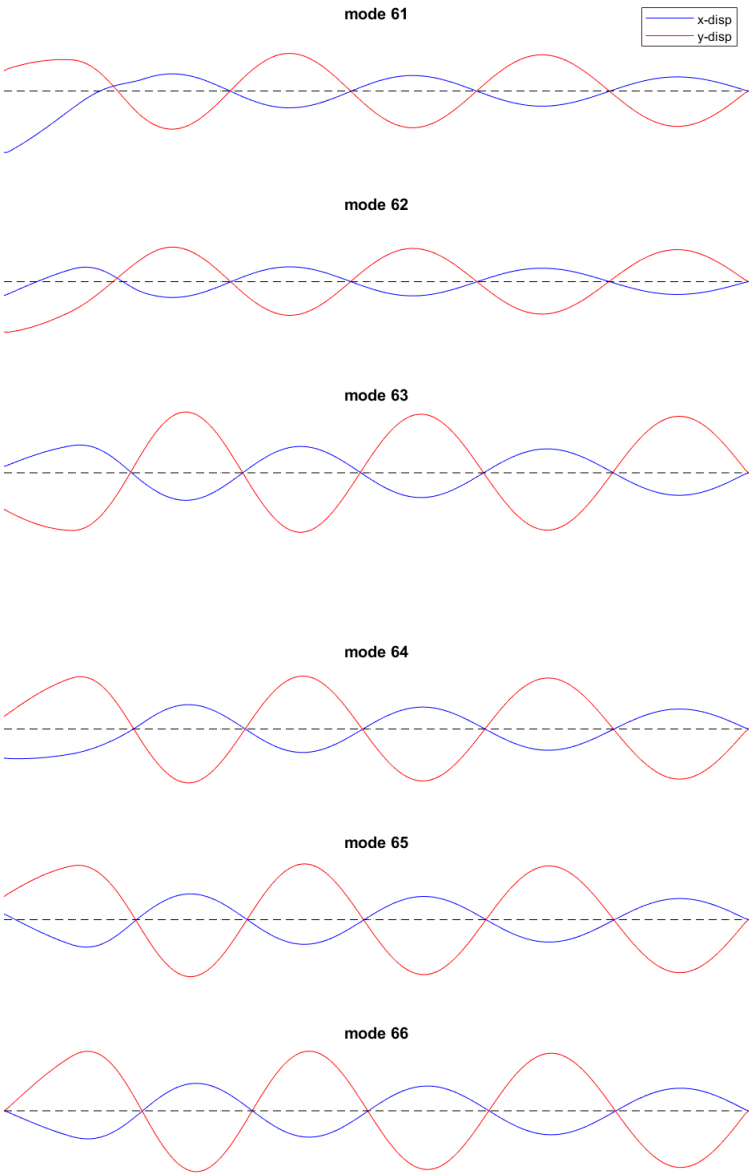
mode 61
x-disp
y-disp
mode 62
mode 63
mode 64
mode 65
mode 66

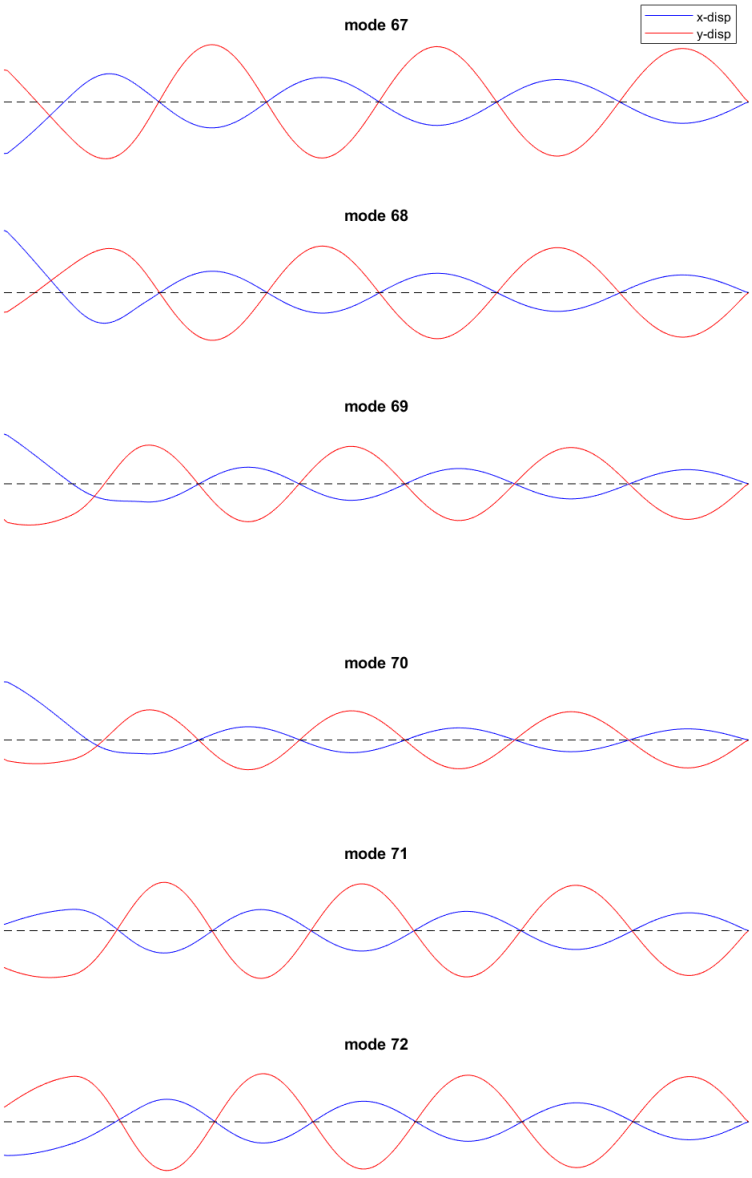
mode 67
x-disp
y-disp
mode 68
mode 69
mode 70
mode 71
mode 72

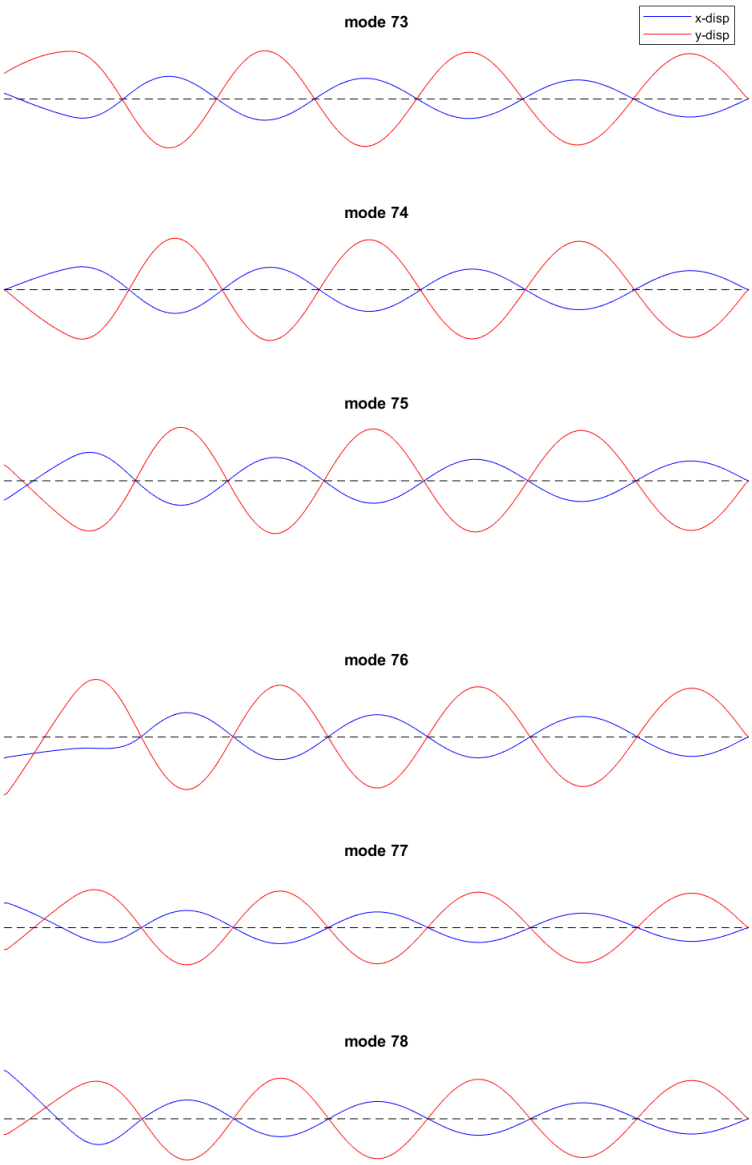
mode 73
x-disp
y-disp
mode 74
mode 75
mode 76
mode 77
mode 78

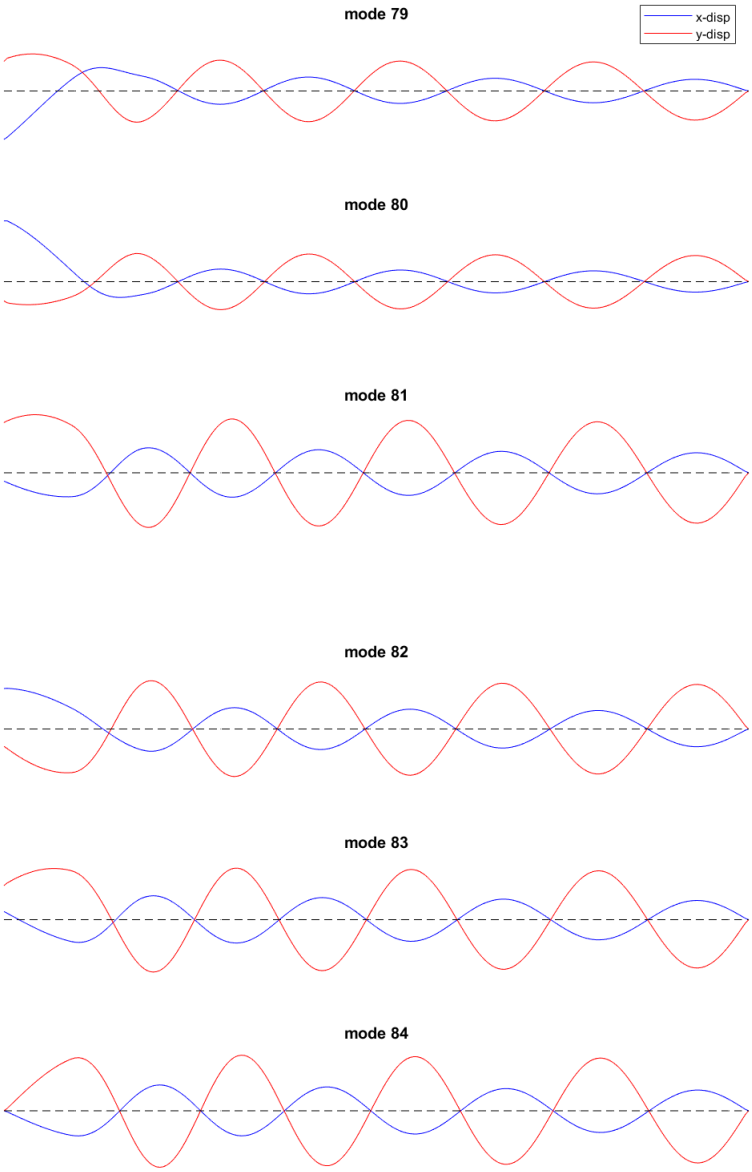
mode 79
x-disp
y-disp
mode 80
mode 81
mode 82
mode 83
mode 84

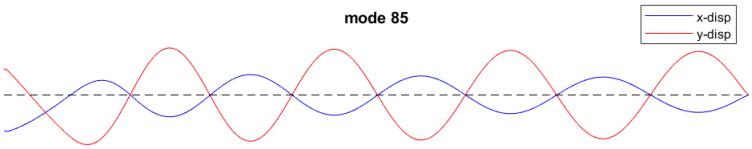
mode 85
x-disp
y-disp

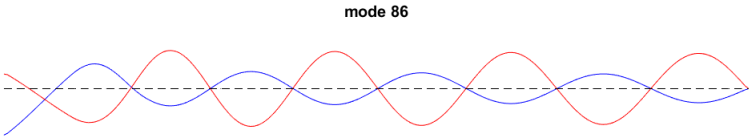
mode 86

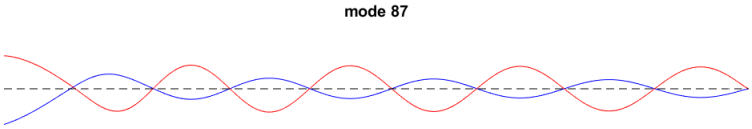
mode 87

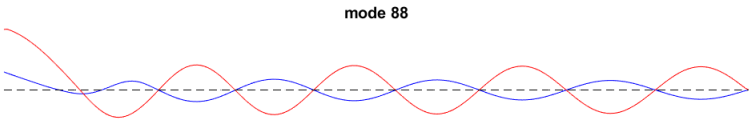
mode 88

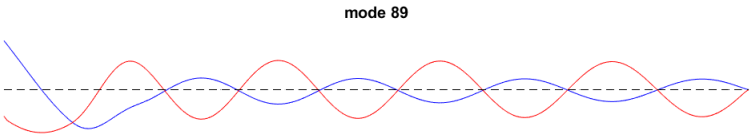
mode 89

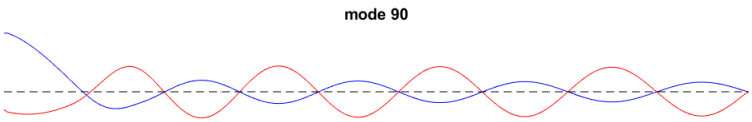
mode 90

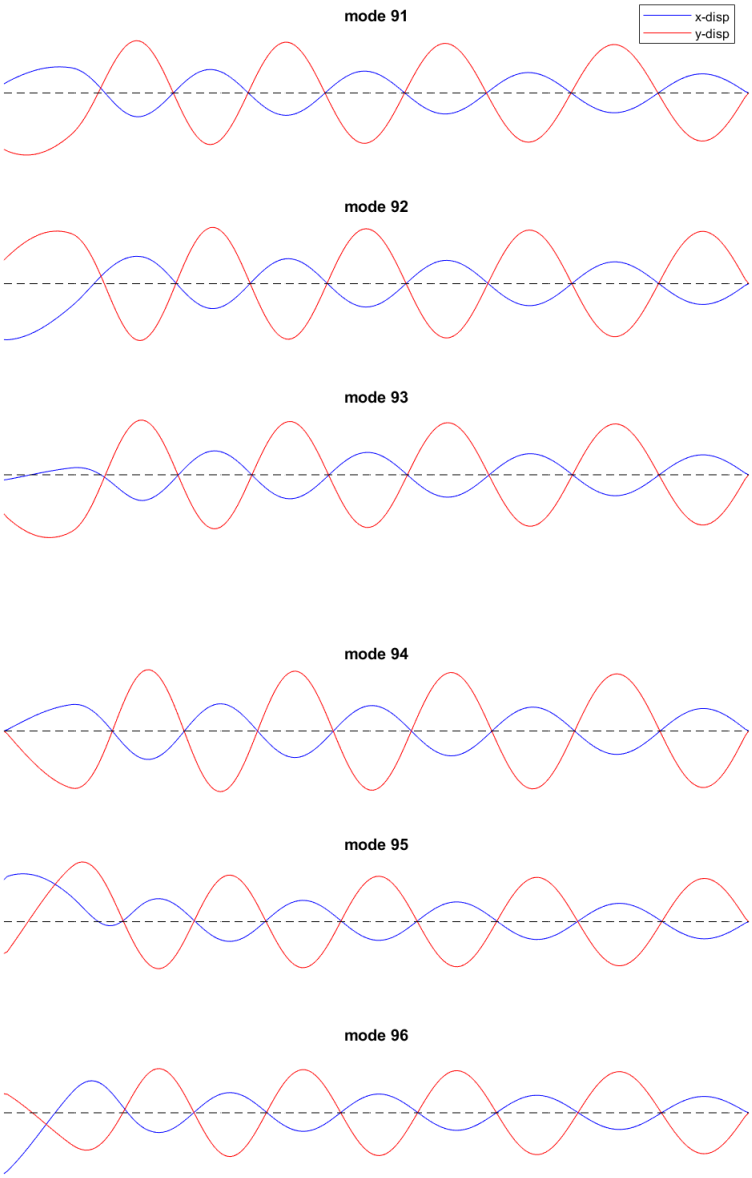
mode 91
x-disp
y-disp
mode 92
mode 93
mode 94
mode 95
mode 96

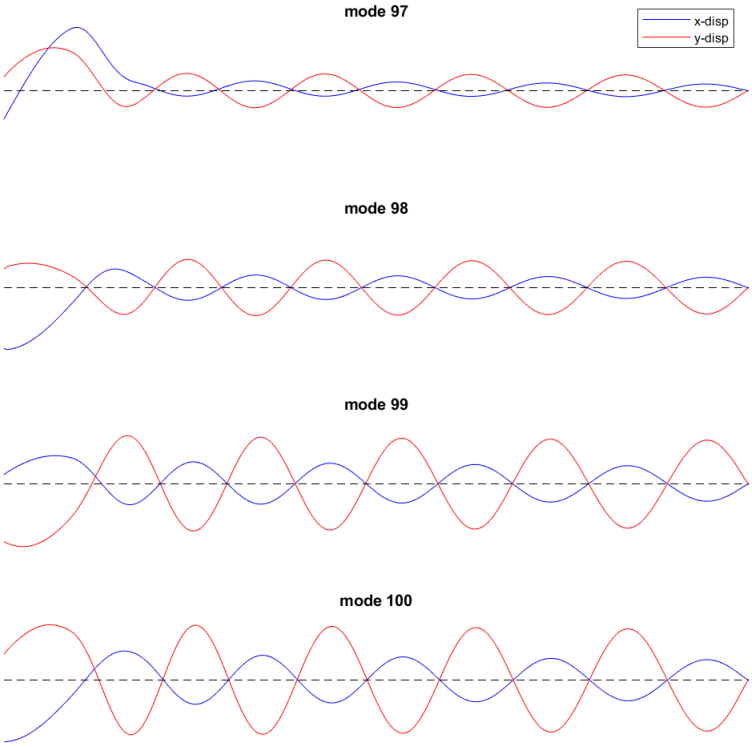
mode 97
x-disp
y-disp
mode 98
mode 99
mode 100

Ina Anda

Static and Dynamic Response Analysis of Salmar Offshore Aquaculture Cage

NTNU
Kunnskap for en bedre verden